



Trick  
2  
8002

This is to certify that the

dissertation entitled

SURFACE-INITIATED LIVING POLYMERIZATIONS ON  
GOLD: SYNTHESIS AND CHARACTERIZATION OF  
NANO-THIN POLYMER FILMS

presented by

Jong-Bum Kim

has been accepted towards fulfillment  
of the requirements for

Ph.D. degree in Chemistry

  
Major professor

Date 3 May 2002

*MSU is an Affirmative Action/Equal Opportunity Institution*

O-12771

LIBRARY  
Michigan State  
University



SURFACE-INITIATED LIVING POLYMERIZATIONS ON  
GOLD: SYNTHESIS AND CHARACTERIZATION OF  
NANOMETER THICK POLYMER FILMS

By

Jong-Bum Kim

A Dissertation

Submitted to  
Michigan State University  
in partial fulfillment of the requirements  
for the degree of

DOCTOR OF PHILOSOPHY

Department of Chemistry

2002

## ABSTRACT

### SURFACE-INITIATED LIVING POLYMERIZATIONS ON GOLD: SYNTHESIS AND CHARACTERIZATION OF NANOMETER THICK POLYMER FILMS

By

Jong-Bum Kim

We successfully synthesized polymer brushes on gold surfaces by surface-initiated atom transfer radical polymerization (ATRP) of (meth)acrylates at room temperature. The temperature used in this polymer brush synthesis is the lowest reported for surface-initiated radical polymerizations, and we report the direct measurement of the molecular weight of polymer brushes grown on a flat surface. The molecular weight of the polymer brushes suggests a high grafting density of poly(methyl methacrylate) (PMMA) on gold surfaces. Little polymer forms in solution, and a simple solvent rinse can clean the polymer brushes on the surface.

We also elucidated the termination mechanism of surface-initiated ATRP. To demonstrate the dependence of film growth on radical concentration, polymer brushes were synthesized using different catalyst concentrations. The surface-initiated ATRP of methyl methacrylate (MMA) with no addition of  $\text{Cu(II)Br}_2$  revealed a rapid initial increase in thickness, but early termination of film growth. In contrast, polymerization with initial addition of  $\text{Cu(II)Br}_2$  showed less deviation from ideal linear growth with time. There exists an optimum catalyst concentration to yield maximum film thickness of polymer after a certain period of reaction time.

ATRP from a surface is especially useful for synthesis and characterization of triblock copolymer brushes. Surface-tethered triblock copolymers composed of poly(methyl acrylate), PMAA, and poly(2-hydroxyethyl methacrylate) (PHEMA) were grown from gold surfaces by a series of atom transfer radical polymerizations at ambient temperature. GPC determinations of the molecular weights of model PMMA-*b*-PMMA-*b*-PMMA triblock polymer brushes demonstrate that this method can yield relatively homogeneous polymer brushes (polydispersity around 1.5). Between the synthesis of different blocks, films were exposed to a large excess of Cu(II)Br<sub>2</sub> to quench polymerization prior to washing and reinitiation.

We also examined surface-initiated ring-opening polymerization (ROP) of lactide on PHEMA surfaces to synthesize biodegradable polylactide (PLA) thin films. Using the dual living polymerization system of ATRP and ROP, we successfully synthesized PHEMA-*g*-PLA on gold and controlled the thickness of PLA by varying polymerization time. The growth of PLA on PHEMA followed 1st order kinetics as evidenced by a linear increase in PLA thickness with polymerization time. This suggests living polymerization. Degradation of PLA film was tracked by surface reflectance FTIR. Changes in surface morphology were also studied by optical microscopy during hydrolytic degradation.

**To My Family**

## ACKNOWLEDGMENTS

First, I would like to thank my advisor, Professor Gregory Baker, for his kind guidance to help me to achieve my goals at Michigan State University. He has been an excellent research advisor as well as a mentor for me. What I have learned from him will be invaluable to my success at the next level. I wish to express my deep appreciation to my committee members. Working with Professor Merlin Bruening was very good luck for me because I learned his sincere approach to science with critical insights. I also learned good organic chemistry and surface science from Professor Babak Borhan, Simon Garrett and Gary Blanchard, which are crucial parts of my knowledge. I would like to thank Professor Ned Jackson and Rob Maleczka for their guidance during my first year at MSU.

I would like to give my thanks to all Baker group members: Sue, Cory, Yiyan, Micah, Chun, Gao, Tara, Mao, Kirk, Erin, Fadi, Tianqi, Ying, Bao, Xuwei, Feng, Leslie, and Ping for making my life as a Baker Group member a memorable one. I also enjoyed working with Wenxi, Milind, Matt, Skanth, and Anagi. We were such an excellent research team. Special thanks to Lisa Dillingham for her being kind to me during my stay in Chemistry Department. She has been always a big help for me.

Finally, I want to thank my family. They have always been supportive of pursuit my dreams. My wife Seonmee and daughter Yerin, they deserve my biggest thanks and love. My life would not have been the same without their love. Thank you for everything.

## TABLE OF CONTENTS

	<b>Page</b>
List of Abbreviations.....	x
List of Schemes .....	xii
List of Tables.....	xiv
List of Figures.....	xv
<b>Chapter 1. Introduction.....</b>	<b>1</b>
<b>I. Atom Transfer Radical Polymerization (ATRP).....</b>	<b>1</b>
I-1. Comparison of ATRP with Conventional Radical polymerization .....	1
I-2. Mechanism.....	3
I-3. Kinetics .....	5
I-4. Catalyst and Initiating Systems.....	9
I-5. Ligands.....	14
I-6. Solvents and Other Factors .....	18
<b>II. Surface-initiated Polymerizations .....</b>	<b>20</b>
II-1. Preparation of Polymer Brushes .....	20
II-2. Surface-initiated Free Radical Polymerization .....	22
II-3. Surface-initiated ATRP .....	29
II-4. Surface-initiated Cationic Polymerizations .....	35
II-5. Surface-initiated Anionic Polymerizations.....	37
II-6. Surface-initiated Ring-opening Metathesis Polymerization .....	40
II-7. Electropolymerization and Plasma Polymerization on Surfaces .....	41
II-8. Application of Surface-initiated Polymerization .....	42
<b>III. References.....</b>	<b>48</b>

<b>Chapter 2. Surface-initiated ATRP on Gold at Ambient Temperature</b>	.....55
I. Introduction.....	55
II. Surface-initiated ATRP with Me <sub>6</sub> TREN.....	58
III. Control Experiment.....	61
IV. Molecular Weight Determination.....	63
V. Conclusion.....	64
VI. References .....	67
<b>Chapter 3. Kinetic Study of Surface-initiated Atom Transfer Radical Polymerization from Flat Surfaces.....</b>	<b>69</b>
I. Introduction.....	69
II. Dependence of Polymer Film Growth on Radical Concentration.....	72
III. Dependence of Polymer Film Growth on Stirring .....	87
IV. Conclusions .....	89
V. References.....	90
<b>Chapter 4. Synthesis of Triblock Copolymer Brushes by Surface- Initiated Atom Transfer Radical Polymerization .....</b>	<b>92</b>
I. Introduction.....	92
II. Synthesis of Tethered PMA- <i>b</i> -PMMA- <i>b</i> -PHEMA Brushes on Gold.....	97
III. Molecular Weights of Triblock Homopolymer Brushes .....	102
IV. Quantification of the Efficiency of Q& R .....	104
V. Comparison of Cu(II)Br <sub>2</sub> Quenching with Simple Solvent Washing .....	110
VI. Conclusions .....	112
VII. References .....	115

<b>Chapter 5. Controlled Growth and Degradation of Biodegradable Nanometer-Thick Films of PLA from PHEMA Surfaces ..</b>	<b>118</b>
I. Introduction.....	118
II. Synthesis of PHEMA- <i>g</i> -PLA .....	120
III. Kinetics of Lactide Polymerization from PHEMA Surface .....	124
IV. Control Experiments Without Surface –OH Groups .....	124
V. Degradation of PLA Film .....	129
VI. Surface Morphology Study of PLA Film During Degradation.....	134
VII. Conclusions .....	140
VIII. References.....	141
<b>Chapter 6. Experimental.....</b>	<b>144</b>
I. General Details .....	144
I-1. Materials .....	144
I-2. Synthesis of Me <sub>6</sub> TREN.....	144
I-3. Synthesis of dnNbpy .....	145
I-4. Analytical Methods.....	146
II. Kinetic Studies of ATRP .....	147
II-1. General Procedures for Surface-initiated Polymerization .....	147
II-2. Preparation of Monomer/Catalyst Solution.....	147
II-3. Polymerization for Kinetic Study .....	148
II-4. Solution Polymerization Procedures .....	149
II-5. Polymerization With or Without Stirring .....	150
II-6. Simulation of Polymer Brush Growth at Different Catalyst Concentration.....	150
III. Synthesis of Triblock Copolymer Brushes .....	151

III-1. Preparation of Substrate Immobilized with Initiator .....	151
III-2. Procedures for Block Formation .....	152
III-3. Quenching Procedure .....	153
III-4. Detachment of Polymer Brushes from Gold Surfaces.....	153
VI. Synthesis of Biodegradable Nanometer-Thick Films of PLA.....	154
VI-1. Preparation of Monomer Solution and Substrates .....	154
VI-2. Ring-opening Polymerization from PHEMA Surface .....	155
VI-3. Hydrolytic Degradation of PLA film .....	156
VI-4. Observation of PHEMA- <i>g</i> -PLA Films During Hydrolytic Degradation .....	156
VII. References .....	157

## LIST OF ABBREVIATIONS

AIBN	2,2'-Azobisisobutyronitrile
AFM	Atomic Force microscopy
ATRP	Atom transfer radical polymerization
2-BPB	2-Bromopropionyl bromide
BPMOA	N,N- <i>bis</i> (2-pyridylmethyl)octylamine
bpy	Bipyridine
dHbpy	4,4'-diheptyl-2,2'-bipyridine
DMF	N,N-dimethylformamide
dNbpy	4,4'-di(5-nonyl)-2,2'-bipyridine
EXAFS	Extended X-ray absorption fine structure
FTIR	Fourier transform infrared
GC	Gas chromatography
GPC	Gel permeation chromatography
HEMA	2-hydroxyethyl methacrylate
HMTETA	1,1,4,7,10,10-hexamethyltriethylenetetramine
LB	Langmuir-Blodgett
LCP	Liquid crystalline polymer
MA	Methyl acrylate
MAA	Methacrylic acid
$\mu$ CP	Microcontact printing
MeHQ	Methyl hydroquinone
Me <sub>6</sub> TREN	<i>tris</i> [2-(dimethylamino)ethyl]amine
MMA	Methyl methacrylate
$M_n$	Number average molecular weight
MUD	Mercaptoundecanol
$M_w$	Weight average molecular weight
NMR	Nuclear Magnetic Resonance
OEGMA	Oligo(ethylene glycol) methacrylate
OTf	Triflate
PDI	Polydispersity index calculated as $M_w/M_n$
PDMAEMA	Poly(dimethylaminoethyl methacrylate)
PGMA	Poly(glycidyl methacrylate)
PHEMA	Poly(2-hydroxyethyl methacrylate)
PMMA	Poly(methyl methacrylate)
PMDETA	N,N,N',N',N''-pentamethyldiethylenetriamine
PPEI	Poly(N-propionylethylenimine)
PS	Polystyrene
PTBA	Poly( <i>tert</i> -butyl acrylate)
ROMP	Ring-opening metathesis polymerization
$R_p$	Rate of polymerization

<b>SAM</b>	Self-assembled monolayer
<b>SEM</b>	Scanning electron microscopy
<b>TEMPO</b>	2,2,6,6-tetramethylpiperidinyloxy
<b>TMEDA</b>	Tetramethylethylenediamine
<b>TPMA</b>	<i>tris</i> [(2-pyridyl)methyl]amine
<b>T-triazine</b>	1,3,5-tris[(dimethylamino)propyl]hexahydro-triazine
<b>UV</b>	Ultraviolet
<b>X<sub>n</sub></b>	Degree of polymerization

## LIST OF SCHEMES

<b>Scheme</b>	<b>Page</b>
Scheme 1.1. Radical generation steps in conventional and atom transfer radical polymerization.....	2
Scheme 1.2. Example of an atom transfer radical addition .....	3
Scheme 1.3. Mechanism of ATRP of methyl methacrylate.....	4
Scheme 1.4. Unit reactions in ATRP of styrene .....	7
Scheme 1.5. ATRP initiators .....	11
Scheme 1.6. Possible structures of CuX/dNbpy catalysts.....	13
Scheme 1.7. Proposed structures of the Cu(I)(bpy) <sub>2</sub> and Cu(II)(bpy) <sub>2</sub> catalysts in ATRP.....	14
Scheme 1.8. Ligands used for copper-mediated ATRP .....	16
Scheme 1.9. Polymer brushes on a flat solid substrate .....	21
Scheme 1.10. Synthesis of polystyrene brushes on silica and cleavage of the polymers from the surface .....	25
Scheme 1.11. Surface-immobilized initiators: (a) TEMPO-based and (b) iniferter .....	29
Scheme 1.12. Synthesis of a polystyrene- <i>b</i> -poly(methyl methacrylate) brush by sequential carbocationic polymerization and ATRP .....	32
Scheme 1.13. Cationic polymerization of hexyl isocyanate on gold nanoparticles .....	37
Scheme 1.14. Surface-initiated anionic polymerization of styrene on gold.....	38
Scheme 1.15. Surface-initiated anionic polymerization of styrene on clay .....	39
Scheme 1.16. Surface-initiated ROMP of norbornene-based chiral monomers .....	40
Scheme 1.17. Surface patterning by microcontact printing, surface-initiated ATRP, and etching .....	43

<b>Scheme 1.18.</b>	<b>Surface-initiated ROMP from SiO<sub>2</sub>/Si surface.....</b>	<b>44</b>
<b>Scheme 2.1.</b>	<b>Surface-initiated ATRP of MMA with Me<sub>6</sub>TREN at RT.....</b>	<b>59</b>
<b>Scheme 3.1.</b>	<b>Surface-initiated ATRP of (meth)acrylates on gold.....</b>	<b>73</b>
<b>Scheme 3.2.</b>	<b>Kinetic scheme for ATRP: pathways for radical generation and consumption .....</b>	<b>74</b>
<b>Scheme 4.1.</b>	<b>Possible reaction pathways of a polymeric radical in ATRP of MMA.....</b>	<b>96</b>
<b>Scheme 4.2.</b>	<b>Synthesis of PMA-<i>b</i>-PMMA-<i>b</i>-PHEMA triblock copolymer brushes.....</b>	<b>98</b>
<b>Scheme 5.1.</b>	<b>Synthetic pathway for PHEMA-<i>g</i>-PLA.....</b>	<b>122</b>

## LIST OF TABLES

<b>Table</b>		<b>Page</b>
Table 2.1.	Molecular weight of PMMA brushes .....	63
Table 4.1.	GPC data for PMMA standards and polymers grown from surfaces using ATRP .....	105

## LIST OF FIGURES

<b>Figure</b>		<b>Page</b>
Figure 1.1.	Rate of methacrylic acid polymerization initiated by UV irradiation of a xanthate system as a function of (a) fraction of xanthate in the monolayer and (b) pH.....	23
Figure 1.2.	Time-dependent properties of polymer chains grown by surface-initiated free radical polymerization of styrene: (a) molecular weight $M_n$ , (b) grafting densities $\delta(\text{PS})$ , and (c) polydispersity of the covalently attached polymers .....	27
Figure 1.3.	Schematic illustration of ATRP initiator immobilization on Si by the LB technique.....	31
Figure 1.4.	AFM images of polyacrylamide films prepared by (a) surface-initiated ATRP and (b) surface-initiated free radical polymerization .....	34
Figure 1.5.	Surface-initiated cationic polymerization of 2-oxazolines.....	36
Figure 1.6.	Sequential surface derivatization of PET films.....	41
Figure 1.7.	Optical micrographs of patterned surfaces .....	42
Figure 1.8.	Surface patterning by surface-initiated ROMP .....	45
Figure 1.9.	Schematic depiction of an LC brush swollen in a low molecular weight nematic .....	47
Figure 2.1.	Differences in the radical generation mechanism for surface-initiated free radical polymerization and surface-initiated ATRP.....	56
Figure 2.2.	Reflectance FTIR spectra of (a) a SAM of MUD (4), (b) initiator immobilized on a MUD SAM (5), and (c) a grafted PMMA layer on the initiator surface (6) .....	60

Figure 2.3.	Reflectance FTIR spectra of (a) a SAM of MUD (4), (b) propionyl group anchored MUD SAM (7), and (c) after surface polymerization.....	62
Figure 2.4.	Detachment of polymer brushes from gold by I <sub>2</sub> treatment followed by molecular weight determination by GPC .....	65
Figure 2.5.	Tapping mode AFM images of (a) a bare gold surface and (b) PMMA brushes on gold .....	66
Figure 3.1.	Dependence of PMMA film growth on the presence of Cu(II)Br <sub>2</sub> : (a) without initial addition of Cu(II)Br <sub>2</sub> and (b) with initial addition of Cu(II)Br <sub>2</sub> .....	75
Figure 3.2.	Dependence of additional PMA film growth on the amounts of remaining surface-initiating sites .....	78
Figure 3.3.	Solution phase ATRP results: (a) first order kinetic plot of MMA polymerization and (b) molecular weight and distribution of polymers. ....	79
Figure 3.4.	Growth of PMA layer thickness vs polymerization time .....	82
Figure 3.5.	Optimum catalyst concentration that yields the thickest PMA film after 4 hr of polymerization.....	84
Figure 3.6.	Simulation of surface-tethered radical concentrations as a function of catalyst concentration.....	85
Figure 3.7.	Influence of radical concentrations on the probability of recombination.....	86
Figure 3.8	Growth of PMMA layer thickness vs polymerization time: (a) polymerization without stirring; (b) polymerization with stirring.....	88
Figure 3.9.	Digital images of the glass reactor used for polymerization with stirring .....	89

Figure 4.1.	Reflectance FTIR spectra of (a) a layer of initiator immobilized on gold (1), (b) a grafted PMA layer on the initiator surface (2), (c) a grafted PMA- <i>b</i> -PMMA diblock copolymer (3), and (d) a grafted PMA- <i>b</i> -PMMA- <i>b</i> -PHEMA triblock copolymer (4).....	100
Figure 4.2.	Tapping mode AFM images of PMA(58Å)- <i>b</i> -PMMA(111Å)- <i>b</i> -PHEMA(75Å) .....	101
Figure 4.3.	Ellipsometric thickness of PMMA films vs polymerization time.....	107
Figure 4.4.	Thickness of multiblock PMMA films vs polymerization time.....	113
Figure 4.5.	Thickness of multiblock PMA films vs polymerization time .....	114
Figure 5.1.	Reflectance FTIR spectra of (a) 2: a grafted PHEMA layer (174 nm) on gold, (b) 3: a grafted PHEMA(170 nm)- <i>g</i> -PLA(29 nm) layer after 90 min of lactide polymerization, (c) 3: a grafted PHEMA(173 nm)- <i>g</i> -PLA(127 nm) layer after 180 min of lactide polymerization, (d) 3: a grafted PHEMA(178 nm)- <i>g</i> -PLA(179 nm) layer after 240 min of lactide polymerization, and (e) 3: a grafted PHEMA(178 nm)- <i>g</i> -PLA(409 nm) layer after 480 min of lactide polymerization.....	123
Figure 5.2.	Plot of PLA thickness increase vs polymerization time.....	125
Figure 5.3.	Reflectance FTIR spectra of (a) a surface grafted PHEMA layer on gold, (b) after lactide polymerization from PHEMA, (c) a surface grafted acetylated-PHEMA layer, and (d) after attempted lactide polymerization from acetylated-PHEMA.....	126
Figure 5.4.	Reflectance FTIR spectra of (a) a surface grafted PMMA layer on gold, (b) after attempted lactide polymerization from PMMA, (c) a surface grafted PHEMA layer, and (d) after lactide polymerization initiated from PHEMA .....	127

**Figure 5.5.** Reflectance FTIR spectra of (a) PHEMA (174 nm) before PLA growth, (b) PHEMA (174 nm)-g-PLA(464 nm) before degradation, and (c)–(l) PHEMA-g-PLA films at various times during hydrolytic degradation ..... 131

**Figure 5.6.** Plot of PLA carbonyl peak area vs degradation time ..... 133

**Figure 5.7.** Surface images of PHEMA(177 nm)-g-PLA(353 nm) obtained by optical microscopy during hydrolytic degradation ..... 135

**Figure 5.8.** Evolution of surface domains during degradation..... 137

**Figure 5.9.** Differences in the optical microscopic images of domains as a function of changes in focal length ..... 138

**Figure 5.10.** Evolution in surface morphology during the drying of water-swollen films ..... 139

**Figure 6.1.** Digital images of five stacked initiator-immobilized samples in a reaction vial ..... 149

# **Chapter 1. Introduction**

## **I. Atom Transfer Radical Polymerization (ATRP)**

### **I-1. Comparison of ATRP with Conventional Radical Polymerization**

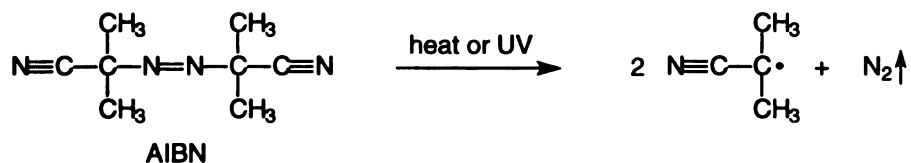
Radical polymerization is one of the most useful and practical synthetic methods for forming polymers because of its applicability to a wide range of monomers, relatively simple reaction conditions, and compatibility with solution, bulk, suspension, and emulsion polymerization. Free radical polymerization, however, is limited by the fast irreversible termination of growing radicals by coupling, disproportionation, and chain transfer reactions. This termination leads to poor control over molecular weight and polymer structure, and thus much effort has been devoted to developing controlled radical polymerizations that produce well-defined polymers with narrow molecular weight distributions. Since Matyjaszewski<sup>1</sup> and Sawamoto<sup>2</sup> independently reported Atom Transfer Radical Polymerization (ATRP) in 1995, ATRP has become one of prevailing polymerization methods for minimizing termination reactions in radical polymerizations.<sup>3</sup>

ATRP is a versatile method for polymerizing acrylates, methacrylates, and styrene. Using ATRP, the molecular weights of these polymers can be controlled easily by varying monomer/initiator ratios and polymerization times. Molecular weight distributions are narrower than for polymers prepared by conventional free radical polymerizations. The improved control over polymerization afforded by ATRP can be ascribed to a different mechanism for radical generation. In conventional free radical polymerization, a propagating radical is irreversibly generated by photochemical or

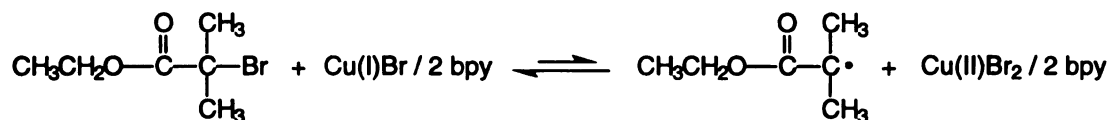
thermal processes, while in ATRP, metal-catalyzed atom transfer leads to “reversible” radical generation. This reversibility keeps the radical concentration low, which minimizes radical termination by recombination. **Scheme 1.1** shows the radical generation steps in conventional and atom transfer radical polymerization.

**Scheme 1.1.** Radical generation steps in conventional and atom transfer radical polymerization

i) Conventional Free Radical Polymerization



ii) Atom Transfer Radical Polymerization



Ethyl 2-bromoisobutyrate

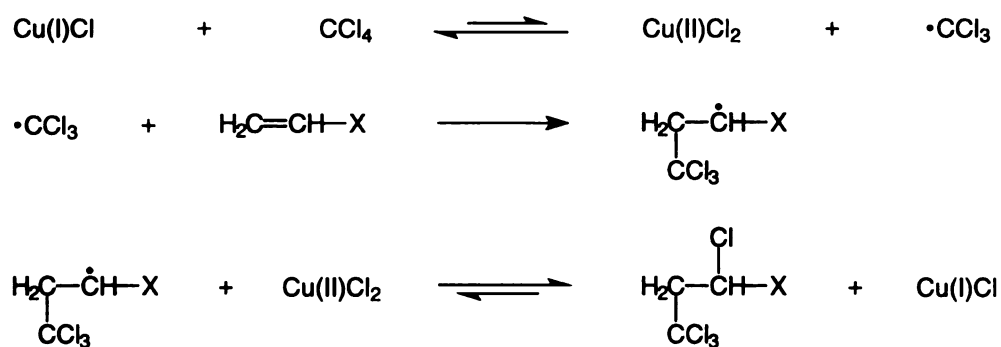
ATRP is considered to be a “living” polymerization, a chain-growth polymerization without irreversible termination and chain transfer reactions. Thus, once chains are initiated, they propagate until the supply of monomer is exhausted or until an equilibrium is established between propagation and depropagation reactions. The chain ends remain active until terminating agents are intentionally introduced. In practice a true

living radical polymerization is rarely achieved because free radicals are so reactive that it is not possible to prevent some active chain ends from participating in termination and chain transfer reactions. In certain cases, however, these side reactions occur so infrequently that well-defined polymers can be prepared. These polymerizations are termed “controlled” polymerizations.<sup>4</sup> ATRP exhibits many characteristics of living polymerizations, but most polymer chemists prefer to describe them as “controlled”/living polymerizations because termination is unavoidable in radical polymerization.

## I-2. Mechanism

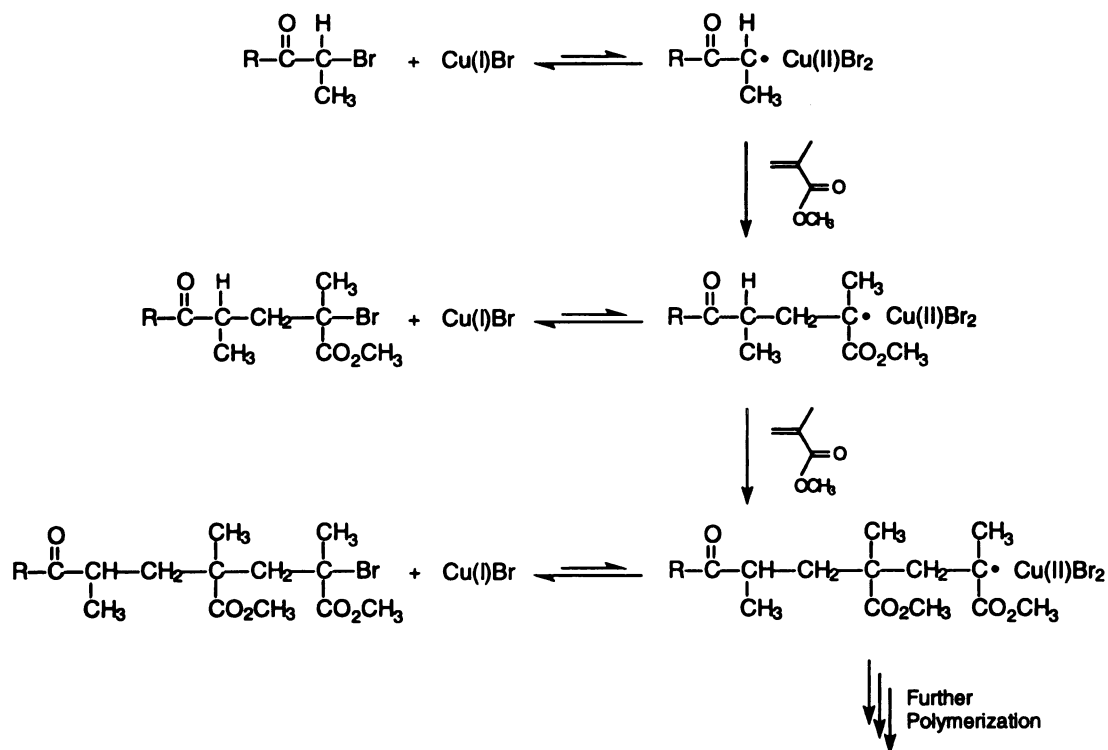
ATRP is a multistep repetition of atom transfer radical addition reactions (Scheme 1.2).<sup>5,6</sup> An organic radical is first generated by transferring a halogen atom from an organic halide to a transition metal complex. Addition of the radical to an alkene followed by transfer of the halogen atom to the resulting radical completes the reaction.

**Scheme 1.2.** Example of an atom transfer radical addition



In ATRP systems, reversible termination is used to reduce the steady state concentration of growing radicals and suppress radical termination reactions. Once a radical is generated from a dormant initiator, it can either add monomer or deactivate by reacting with a metal complex to regenerate the dormant initiator and a metal in a lower oxidation state. A series of similar activation/deactivation reactions occurs during reinitiation and propagation. **Scheme 1.3** shows the ATRP of methyl methacrylate (MMA), including the reversible radical generation steps that occur after the addition of each monomer.

**Scheme 1.3.** Mechanism of ATRP of methyl methacrylate



Even though the steady state concentration of active radicals in ATRP has not yet been directly measured by spectroscopy, solving the rate expressions for ATRP implies a radical concentration of  $\sim 10^{-7}$  to  $10^{-8}$  M. Since the radical concentration is low, deactivation is several orders of magnitude faster than recombination between two radicals, and thus irreversible termination is suppressed. However, some early termination invariably occurs during the initial formation of Cu(II) species, which are needed for control via the persistent radical effect.<sup>7,8</sup> Electron paramagnetic resonance studies of the bulk ATRP of styrene at 110 °C showed that after 20 min, the Cu(II) concentration was nearly steady state, corresponding to 4–6 mol % of the initial Cu(I) species.<sup>9</sup> Since the polymerization used 1-phenylethyl bromide and CuBr(dNbpy)<sub>2</sub> (dNbpy = 4,4'-di(5-nonyl)-2,2'-bipyridine) as the initiating system with no added Cu(II) species, the Cu(II) concentration built up *in situ*.

### I-3. Kinetics

ATRP provides well-defined polymers with low polydispersities ( $1.05 < M_w/M_n < 1.5$ ). The number average degree of polymerization ( $X_n$ ) is determined by the ratio of the concentrations of consumed monomer to initial initiator:  $X_n = \Delta[M]/[I]_0$ .<sup>10</sup> As shown in equation 1, ATRP usually follows first-order kinetics with respect to monomer, initiator, and catalyst (Cu(I)) concentration, while the rate of polymerization is inversely proportional to the deactivator (Cu(II)). Equation 2 describes the evolution of the polydispersity ( $M_w/M_n$ ) with conversion ( $p$ ).<sup>11</sup>

$$R_p = k_p \frac{k_{act}}{k_{deact}} [M][I]_0 \frac{[Cu^I]}{[XCu^{II}]} \quad \text{eq. 1}$$

$$\frac{M_w}{M_n} = 1 + \left( \frac{k_p [I]_0}{k_{deact} [XCu^{II}]} \right) \left( \frac{2}{p} - 1 \right) \quad \text{eq. 2}$$

The two equations show the trade-off between polymerization rate and control over molecular weight. A high  $k_{act}/k_{deact}$  ratio leads to a high radical concentration and a corresponding high rate of polymerization. At the same time, a relatively low  $k_{deact}$  leads to an increase in the polydispersity, probably through irreversible termination. In the limit where  $k_{act} \gg k_{deact}$ , the polymerization rate is very high but the reaction yields a polydisperse polymer. This case is best described as a conventional redox-initiated radical polymerization process. The equations show that adding Cu(II) favors the deactivation of radicals, slows the polymerization rate, and provides a lower polydispersity. Equation 2 also indicates that  $M_w/M_n$  decreases with conversion, a characteristic of living polymerizations. Thus, an ATRP process with a low  $k_p/k_{deact}$  ratio and a high concentration of deactivator will provide a narrow molecular weight distribution at high degrees of polymerization.<sup>11</sup>

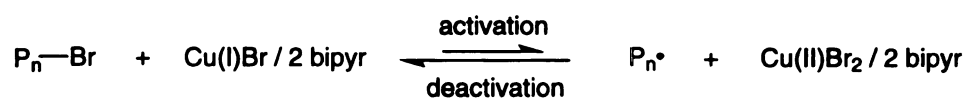
ATRP successfully polymerizes styrene, acrylates, and methacrylates. Matyjaszewski and coworkers investigated the ATRP kinetics for methyl acrylate (MA), MMA, and styrene. For the homogeneous polymerization of MA using CuBr(dNbpy)<sub>2</sub>,<sup>12</sup> plots of the evolution of molecular weight vs conversion and  $\ln([M]_0/[M])$  vs time were linear, confirming 1st order kinetics. The equilibrium constant for reversible radical formation at 90 °C,  $K_{eq} = 1.2 \times 10^{-9}$ , is much smaller than in the ATRP of styrene or

MMA. For comparison,  $K_{eq}$  for the ATRP of MMA with CuCl at 90 °C is  $7.0 \times 10^{-7}$ , and  $K_{eq}$  for the ATRP of styrene with CuBr is  $2 \times 10^{-8}$ . The differences in  $K_{eq}$  are probably due to different radical stabilities or the differences in the C–halogen bond strength.

ATRP of styrene at 110 °C (1 mol % initiator and catalyst) has been studied in detail.<sup>13</sup> The characteristic time intervals for the various steps in ATRP can be estimated from the reciprocal of the product of the bimolecular rate constants and the reagent concentration ( $\tau = 1/k_2[R]$ ). **Scheme 1.4** shows the characteristic times for the individual steps in the ATRP of styrene, activation, deactivation, propagation, and termination.

**Scheme 1.4.** Unit reactions in ATRP of styrene

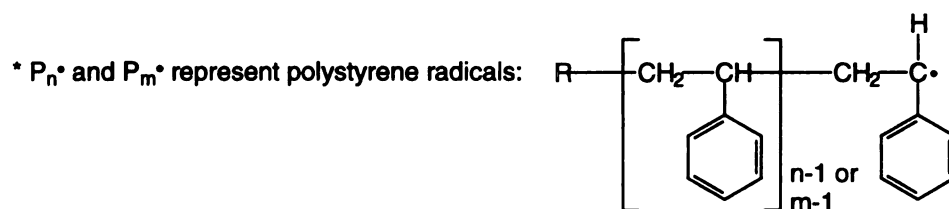
i) activation ( $\tau_a = 22$  s); deactivation ( $\tau_d = 0.018$  ms)



ii) propagation ( $\tau_p = 0.12$  s)



iii) termination ( $\tau_t = 0.1$  s)



The calculated periodicities shown in **Scheme 1.4** lead to a plausible kinetic scenario for styrene polymerization.<sup>13</sup> Early in the polymerization, a high concentration of radicals is generated and their rapid recombination leads to ~5 % loss of chain ends and the *in situ* production of ~5 % of Cu(II) species from the Cu(I) catalyst. The Cu(II) species deactivate growing radicals, decrease their concentration, and suppress termination. At 30 % conversion, an average chain is activated to a radical every 22 sec, and then is deactivated after 0.018 msec. Since the deactivation rate is seven times faster than propagation ( $\tau = 12$  msec), addition of one monomer to a polymer chain requires seven activation/deactivation cycles (2.5 min), and 4 h to prepare a polymer chain with a degree of polymerization of 100. Termination is 830 times slower than propagation ( $\tau = 12$  msec), leading to good control over the polydispersity. For the ATRP of MA, similar characteristic time estimates predict that 14 monomers are added to a growing radical during each activation/deactivation cycle. The number of monomer units ( $n$ ) added during each activation step can be expressed as

$$n = k_p[M]/k_{\text{deact}}[D] \quad \text{eq. 3}$$

where  $[M]$  and  $[D]$  are the concentration of monomer and deactivator respectively.

The above kinetic description is simplified because it fails to take into account chain transfer reactions and termination by processes other than bimolecular coupling or disproportionation. ATRP kinetics vary with the kind and concentration of catalyst, ligand, monomer, solvent, and temperature. In the next sections, these factors and their influence on ATRP are explored in more detail.

#### I-4. Catalyst and Initiating Systems

In ATRP, the catalyst plays an important role in determining the rate of the polymerization and the molecular weight distribution of the resulting polymers. The catalyst activity can be adjusted by changing the ligand, counterion, or transition metal ion. A variety of metal catalysts have been developed to initiate and control ATRP, including copper,<sup>14,15</sup> ruthenium,<sup>2,16</sup> nickel,<sup>17,18</sup> iron,<sup>19,20</sup> and rhodium complexes.<sup>21</sup> The copper halide systems are the most popular because of their versatility with vinyl and (meth)acrylate monomers.<sup>22</sup> Since copper-based ATRP was used for this research, this discussion emphasizes copper catalysts.

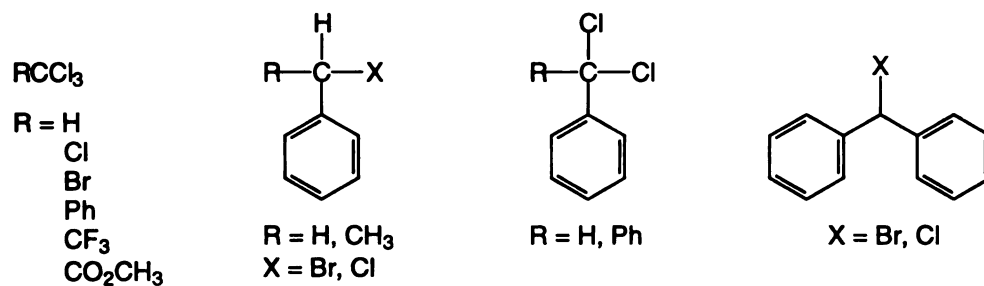
The halogen atoms in the radical generation step play important roles in defining the position of the equilibrium.<sup>23</sup> The C-Cl bond energy in benzyl chloride is ~ 284.7 kJ/mol while the C-Br bond energy in benzyl bromide is 213.5 kJ/mol.<sup>24</sup> Thus, initiation of C-Br is faster than C-Cl, reflecting the difference in the carbon-halogen bond energy. The partial ionic character of the Cu-X bonds in a ligated complex such as  $\text{Cu}(\text{bpy})_2^+\text{X}^-$  may also be a factor in determining the equilibrium position. **Scheme 1.5** shows various initiators used in ATRP. Besides those listed in the scheme,  $\alpha$ -haloketones also have been used as ATRP initiators. Radicals generated  $\alpha$  to functional groups are stabilized in the order  $\text{CN} > \text{C}(=\text{O})\text{R} > \text{C}(=\text{O})\text{OR} > \text{Ph} > \text{Cl} > \text{Me}$ . Tertiary alkyl halides are better initiators than secondary and primary alkyl halides because of the higher stability of substituted radicals. Alkyl chlorides should be the least efficient initiators because the order of bond strength in alkyl halides is  $\text{R-Cl} > \text{R-Br} > \text{R-I}$ . Chlorosulfonylphenyl groups ( $-\text{Ph-SO}_2\text{Cl}$ ) are also good ATRP initiators because the Cl atom can be easily abstracted by copper catalysts, producing  $-\text{Ph-SO}_2$  radicals.

Control experiments on halide-free catalysts show that the ions coordinating with copper have little effect on the deactivation step. The halides of Cu bipyridine complexes were replaced by triflates ( $L_2Cu(OTf)_2$ , or  $L_2Cu(OTf)$ ,  $L$  = a substituted bipyridine) and the complexes were added to model free radical polymerizations initiated by AIBN.  $L_2Cu(OTf)_2$  had no effect on MA and styrene polymerizations, while  $L_2Cu(OTf)$  reduced the polymerization rate of MA, but had no effect on styrene polymerization. Thus, the control seen in ATRP does not come from the interactions of growing radicals with copper complexes but in the reversible halogen atom transfer.<sup>25</sup>

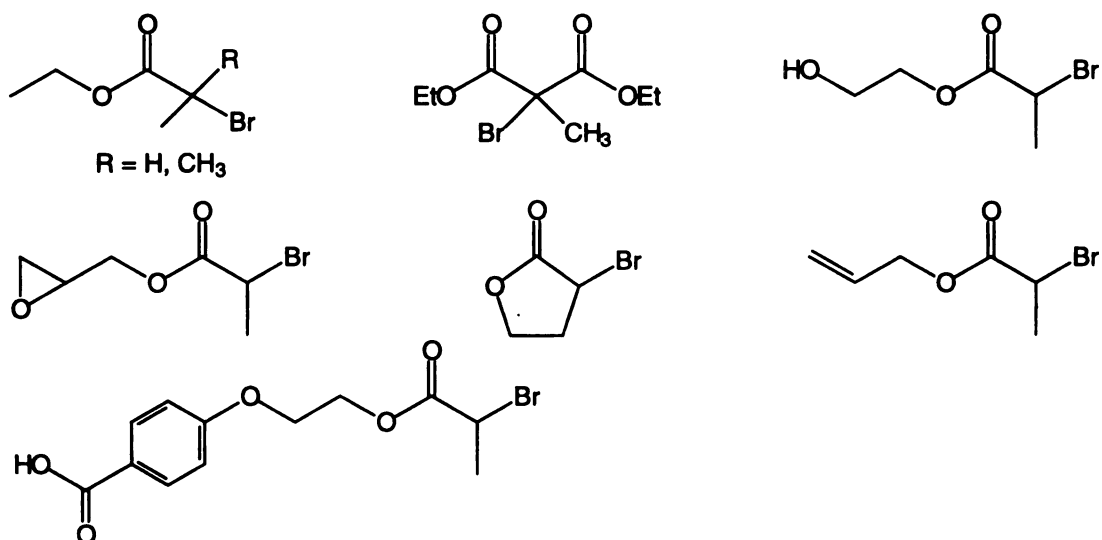
Mixed halide systems (R-Br/CuCl) slow the polymerization rate and reduce the rate of termination.<sup>26</sup> As a result, control over polymerization is improved, and polydispersity is reduced. To better understand halogen exchange between initiator and CuCl, model studies<sup>27,28</sup> were run at 90 °C using several initiators (R-Br = benzyl bromide, 1-phenylethyl bromide, methyl-2-bromopropionate, and ethyl-2-bromoisobutyrate) with CuCl. NMR and GC results show that within 30 min, 80–90 mole% of the R-X groups are R-Cl formed by the back transfer of Cl from CuBrCl to R•.<sup>28</sup> For R-Cl/CuBr systems, R-Cl is also the dominant alkyl halide at steady state. Thus for mixed halide systems, the rate of halogen exchange is rapid and alkyl chlorides are preferentially formed over alkyl bromides. These results also suggest that the mixed halide system should give fast initiation.

### Scheme 1.5. ATRP initiators

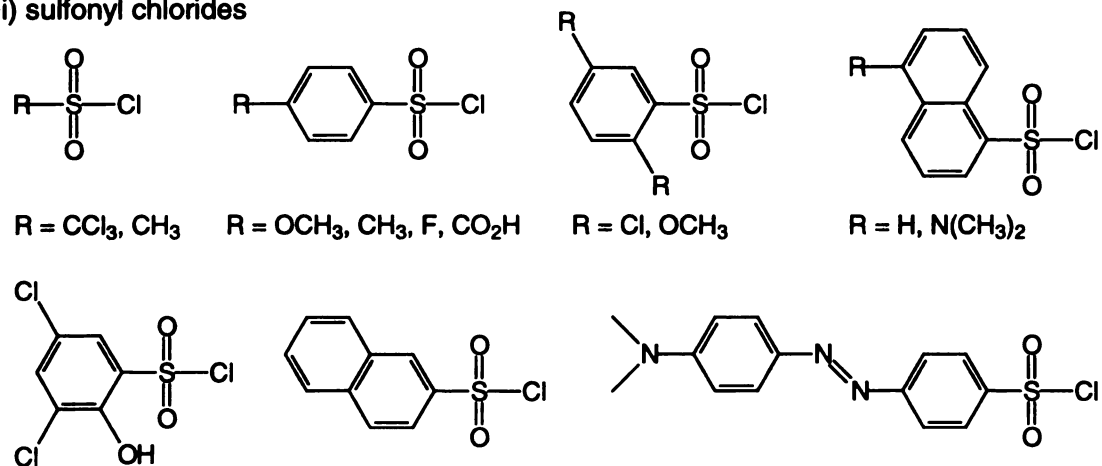
#### i) halogenated alkanes and benzylic halides



#### ii) $\alpha$ -bromoesters



#### iii) sulfonyl chlorides

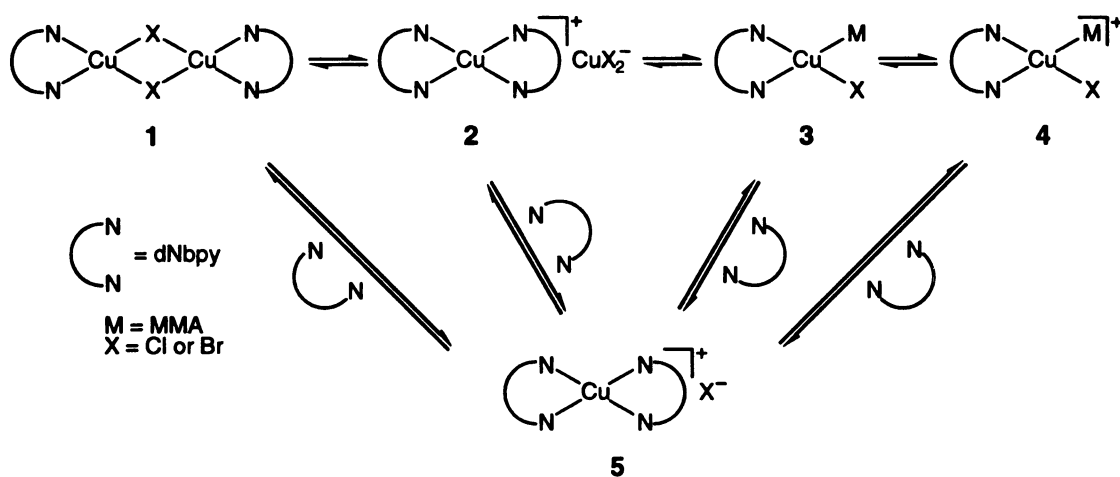


To have good control over the polymerization kinetics and polymer molecular weight distribution in ATRP, a few major criteria should be fulfilled. First, fast initiation is required to generate significant numbers of polymer chains and ensure that all chain ends start to grow polymer at the same time. Second, the equilibrium position in the radical generation step should strongly favor the dormant species. Fast deactivation of active radicals to dormant chain ends is indispensable for minimizing chain termination reactions that broaden the polymer molecular weight distribution. Third, all initiators must grow polymers for the molecular weight of the final polymer to be defined by the [monomer]/[initiator] ratio. In terms of the above three requirements, the mixed halogen initiation system, R-Br/CuCl is possibly more advantageous than the R-Br/CuBr or R-Cl/CuCl because R-Br/CuCl allows faster initiation than the R-Cl/CuCl system and faster deactivation than R-Br/CuBr. The experimental data show that mixed halide systems provide better control over ATRP. For example, the ATRP of MMA using a R-Br/CuCl system showed lower polydispersity than polymerization with R-Br/CuBr.<sup>28</sup>

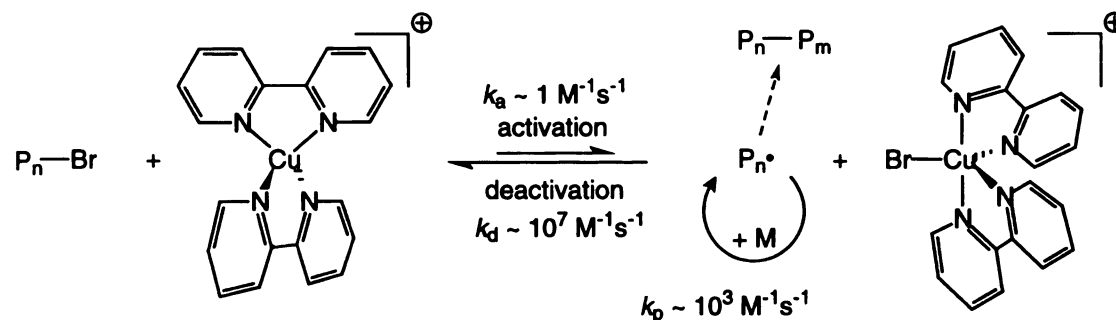
To date, the exact structure of the catalysts in solution is unclear, and even the structure of the widely studied Cu/bpy system is uncertain. <sup>1</sup>H NMR studies suggest that the Cu(I) and Cu(II) complexes are labile with fast exchange between coordinated and free bpy.<sup>29</sup> Temperature-dependent color changes of catalyst solutions have been interpreted as a structural change from a monomeric Cu(I) species to a dimeric halogen bridged species.<sup>26</sup> Based on literature data on the coordination chemistry of copper complexes in polar solvents, Matyjaszewski proposed the structures shown in **Scheme 1.6** as possible forms of CuX/dNbpy during the polymerization.<sup>3</sup> There are three types of complexes that can have a 1:1 Cu(I)X to bidentate ligand ratio, the halogen bridged dimer

1, complexes 2 and 5 which have two bidentate ligands coordinated to Cu(I) and either a halide or dihalocuprate counter-anion,<sup>30,31</sup> and complexes 3 and 4, where monomer acts as a ligand. The structure of the CuX/bpy complex depends on the solvent polarity,<sup>32</sup> and the monomeric form 5 should dominate in polar solvents, while bridged dimer 1 could exist in less polar media. More complex structures also may be possible. The maximum rates of polymerization for styrene and MA were observed when the ratio of dNbpy to CuX was 1:2,<sup>12,20</sup> suggesting 5 as the active catalyst. X-ray and EXAFS data point to a cationic bipyramidal structure  $[X-Cu(II)(bpy)_2]^+$  for the solid catalyst isolated from nonpolar media, however, a neutral distorted square planar structure  $(X_2Cu(II)/bpy)$  may be preferred in solution.<sup>33</sup> It was also proposed that the active Cu/bpy complexes involved in the ATRP are tetrahedral  $Cu(I)(bpy)_2$  and trigonal bipyramidal  $X-Cu(II)(bpy)_2$  complexes (Scheme 1.7).<sup>34,35</sup>

**Scheme 1.6.** Possible structures of CuX/dNbpy catalysts.



**Scheme 1.7.** Proposed structures of the Cu(I)(bpy)<sub>2</sub> and Cu(II)(bpy)<sub>2</sub> catalysts in ATRP.



### I-5. Ligands

While the metal catalyst controls the polymerization reaction by mediating the atom transfer equilibrium, the ligands play critical roles in solubilizing the catalyst in organic media and tuning the rates of the activation and deactivation steps. Extensive research has focused on finding new ligands that are readily available and whose structures can easily be varied for tuning ATRP. Common ligands for copper halides are multidentate aliphatic amines,<sup>36</sup> aromatic amines,<sup>12,20,37-39</sup> and imines.<sup>40,41</sup> Recently, Matyjaszewski *et al.* investigated the structure-activity relationship for Cu catalysts with the multidentate ligands shown in **Scheme 1.8**.<sup>11</sup>

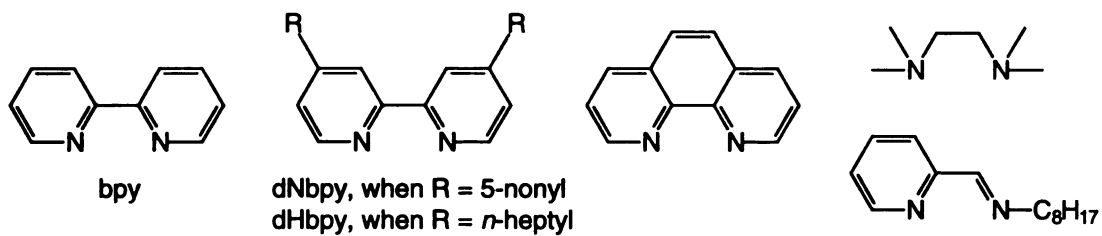
According to kinetic and electrochemical studies, catalyst activity increases as the ligand stabilizes the Cu(II) state of the catalyst. In general, the activity of ligands decreases in the order: alkyl amine  $\approx$  pyridine > alkyl imine  $\gg$  aryl imine > aryl amine. A sufficiently high deactivation rate is required to obtain good control over polymerization because the molecular weight distribution is influenced by the rate of

deactivation. In terms of the rates of the activation and deactivation, N,N,N',N',N''-pentamethyldiethylenetriamine (PMDETA) and N,N-bis(2-pyridylmethyl)octylamine (BPMOA) are suitable ligands for Cu-based ATRP of a wide range of acrylates, methacrylates, and styrenic monomers.

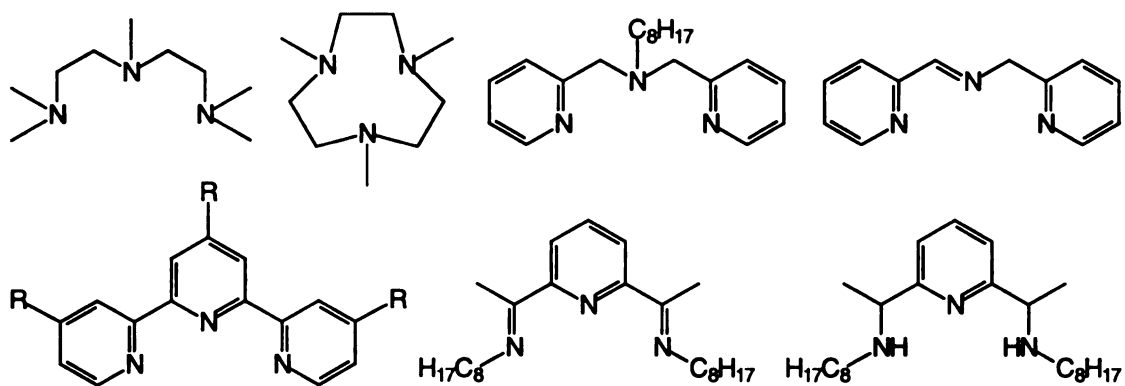
Initially bpy was used as the ligand in copper-mediated ATRP of styrene and (meth)acrylate monomers.<sup>1,37</sup> The Cu/bpy catalyst has limited solubility, and a poorly soluble Cu(II) complex will suppress the deactivation step and compromise control over the polymerization. To improve the solubility of the catalyst, bpy was replaced with 4,4'-diheptyl-2,2'-bipyridine (dHbpy) and dNbpy and ATRP was better controlled.<sup>20,42</sup> Besides controlling solubility, ligands also lead to steric effects in ATRP. ATRP with 4,4'-di-*tert*-butyl-2,2'-bipyridine produced polymers with a narrow molecular weight distribution, while ATRP using 6,6'-disubstituted 2,2'-bipyridine as the ligand failed to yield polymers.<sup>43</sup> The bulky substituted groups presumably hindered coordination of ligands to the copper catalyst.

### Scheme 1.8. Ligands used for copper-mediated ATRP

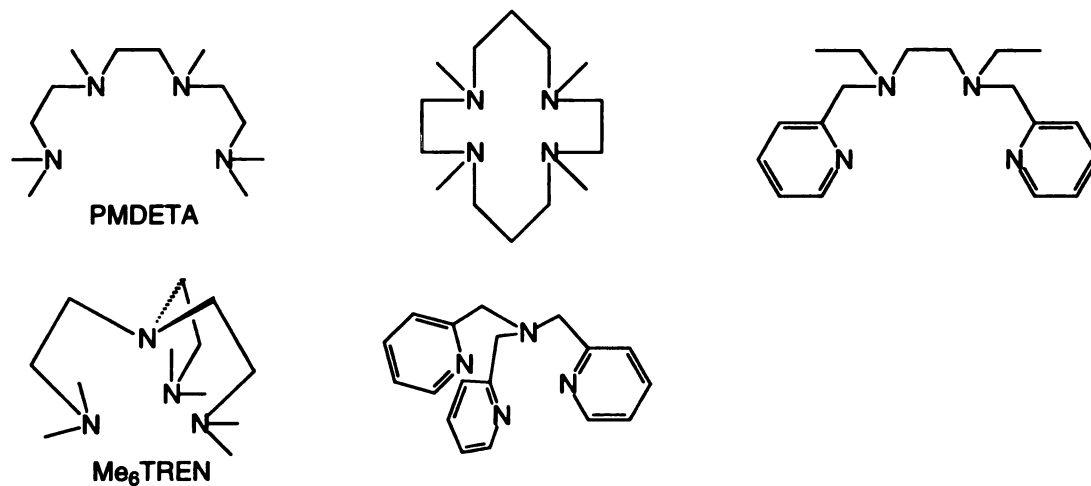
#### i) bidentate ligands



#### ii) tridentate ligands



#### iii) tetradentate ligands



Catalysts containing multidentate amines such as PMDETA and 1,1,4,7,10,10-hexamethyltriethylenetetramine (HMTETA) have faster polymerization rates than those using bpy as the ligand.<sup>36</sup> One possible explanation is that the copper-amine complexes have lower redox potentials than copper-bpy complexes,<sup>44</sup> shifting the equilibrium from dormant species towards radicals, which results in a higher polymerization rate. In some cases, polymerizations using copper catalysts with multidentate amine ligands showed significant deviations from first-order kinetics. For example, first order kinetic plots of the ATRP of MMA are curved when PMDETA is used as the ligand, and styrene polymerizations using tetramethylethylenediamine (TMEDA) significantly deviate from first-order kinetics at high conversions. Both results are consistent with either an increase in the concentration of growing radicals or loss of initiating sites during polymerization.<sup>36</sup>

The increased activity of catalysts with multidentate ligands makes ATRP possible at room temperature. ATRP of MA proceeded at ambient temperature with *tris*[2-(dimethylamino)ethyl]amine (Me<sub>6</sub>TREN) as a ligand,<sup>38</sup> while the use of dNbpy required 90 °C.<sup>12</sup> Currently, the most popular ligands for ATRP are 1,3,5-tris[(dimethylamino)propyl]hexahydro-triazine (T-triazine),<sup>23</sup> Me<sub>6</sub>TREN,<sup>38</sup> N,N-bis(2-pyridylmethyl)octylamine (BPMOA),<sup>45</sup> *tris*[(2-pyridyl)methyl]amine (TPMA),<sup>45</sup> N-(*n*-pentyl)-2-pyridylmethanimine,<sup>40</sup> PMDETA,<sup>36</sup> and HMTETA.<sup>36</sup>

In conclusion, ligands serve two purposes. They fine-tune the equilibrium constant that governs atom transfer between active radicals and dormant initiators, and they control the solubility and stability of catalytic complexes in various monomers and solvents at different temperatures.

## I-6. Solvents and Other Factors

In addition to the catalyst concentration and activity, several other experimental parameters such as temperature, use of zero-valent metals, and the solubility of the catalyst affect the rates of polymerization and termination. For some catalysts, the Cu(II) complexes have limited solubility and have been observed to precipitate from nonpolar solvents.<sup>23</sup> Loss of Cu(II) often leads to non-first-order kinetics and a loss of control over polydispersity. ATRP of *n*-butyl acrylate with CuBr/bpy was poorly controlled in benzene ( $M_w/M_n = 2.4$ ), while the same polymerization using the more soluble CuBr/dNbpy afforded well-defined polymer with the expected molecular weight and a low polydispersity ( $M_w/M_n = 1.1$ ).<sup>10</sup> In ethylene carbonate, the same polymerizations catalyzed by CuBr/bpy provided good control over molecular weight, a low PDI, and a rate of polymerization that was faster than a bulk polymerization of *n*-butyl acrylate.<sup>10</sup> The authors speculated that the rate increase is due to the formation of a monomeric copper species with dissociated anions.

In general, the use of polar solvents improves the solubility of Cu(II) complexes and leads to homogeneous, well-controlled ATRP. Polar solvents reported to be compatible with ATRP include  $\gamma$ -butyrolactone,<sup>23</sup> DMF,<sup>10</sup> carbonates (ethylene, dimethyl, and propylene carbonate),<sup>10</sup> and ethers (anisole, diphenyl ether, 1,4-dioxane, 1,4-dimethoxybenzene, and THF).<sup>10</sup> Mixed solvent systems have also been investigated, such as the ATRP of 2-hydroxyethyl methacrylate (HEMA)<sup>10</sup> in a mixture of methyl ethyl ketone and 1-propanol, and in methanol/water mixtures. Recently, a room temperature ionic liquid, 1-butyl-3-methylimidazolium hexafluorophosphate was shown to be a good solvent for copper-mediated ATRP of MMA.<sup>46</sup>

While most ionic and coordination polymerizations cannot be carried out in the presence of water, radical polymerizations are compatible with water and carbonyl groups. Recently, Armes reported ATRP of methoxy-capped oligo(ethylene glycol) methacrylate (OEGMA) in aqueous media using a Cu(I)/bpy catalyst.<sup>47</sup> Both OEGMA and the catalyst are water soluble. The rate of aqueous ATRP at 20 °C is faster than ATRP run in organic solvents at elevated temperatures. Due to its polarity, water is believed to promote the formation of  $[\text{Cu}(\text{bpy})_2]^+$  a very active mononuclear catalyst. Although compatible with water, ATRP is like normal free radical polymerizations in terms of its sensitivity to oxygen, which must be excluded to limit formation of unreactive peroxy radicals.<sup>48</sup>

Monomer structure is one of the major factors that determine the propagation rate ( $k_p$ ) of polymerization since it defines the stability of the radical formed after its addition to growing chain ends. The polymerization rate of acrylate and methacrylate is different because the propagating radical of MMA is more stable and thus chains grow more slowly.<sup>10</sup>

Because of its tolerance to many organic functional groups, ATRP is useful for the synthesis of polymers with complex architectures. Using ATRP, polyhedral oligomeric silsesquioxane acrylates were polymerized to give hybrid polymers with previously unattainable compositions and low polydispersities.<sup>49</sup> In addition, ATRP and a second polymerization mechanism can be combined to yield well-defined block copolymers. For example, ATRP of MMA and the ring-opening metathesis polymerization (ROMP) of 1,5-cyclooctadiene were initiated simultaneously from a single ruthenium complex.<sup>50</sup>

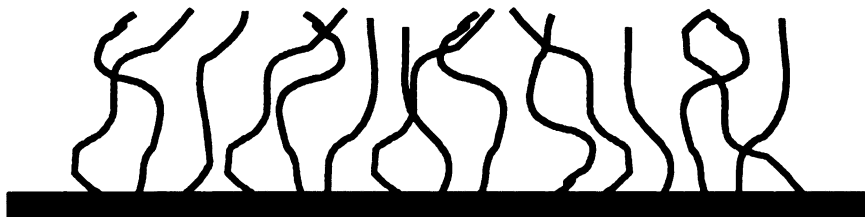
Even though ATRP normally gives well-defined final polymers, there are several problems that must be overcome before it gains widespread applicability in industry. In a typical ATRP, the catalyst concentration is 0.1–1 mol % relative to monomer, and the residual catalyst colors the final polymer. Extra steps must be taken to remove catalyst after polymerization. Potential solutions include the use of supported catalysts<sup>51</sup> and promoters. ATRP of MMA was reported for a CuBr-HMTETA catalyst system supported on silica gel,<sup>52,53</sup> and both visible light and methyl hydroquinone (MeHQ) were shown to accelerate ATRP<sup>54</sup> and improve its living character at low catalyst levels. In the case of MeHQ, the activation energy for MMA polymerization was reduced from 60.3 to 44.9 kJ/mol.<sup>40</sup> This suggests that MeHQ may act as a coordinating ligand for copper and thus affect the position of the Cu(I)/Cu(II) equilibrium.

## **II. Surface-initiated Polymerizations**

### **II-1. Preparation of Polymer Brushes**

The preparation of polymer brushes on solid surfaces has been of great interest because of their potential as sensing layers, anti-corrosion layers, for controlling the wetting of surfaces, and for nanostructuring surfaces. More than two decades ago, DeGennes developed a model for understanding polymer brush systems and suggested the synthesis of polymer brushes from surface-immobilized initiators.<sup>55</sup> According to Milner's definition, polymer brushes are long-chain polymer molecules attached by one end to a surface or interface by some means, with a density of attachment points high enough so that the chains are obliged to stretch away from the interface, sometimes much farther than the typical unstretched size of a chain.<sup>56</sup>

**Scheme 1.9.** Polymer brushes on a flat solid substrate

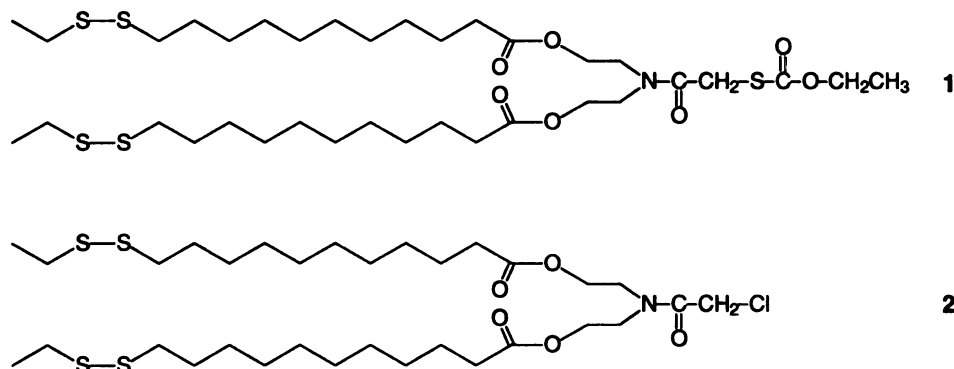


The physical properties of polymer brushes largely depend on the chain length, grafting density, backbone flexibility, and excluded volume. Due to their confinement to a surface, polymer brushes respond to stimuli in a collective and uniform way, and usually these responses trigger changes in surface properties. Since these polymer chains are covalently bound to the surface, adhesion between the polymers and the substrate is much stronger than can be achieved from simple physisorption. However, due to limited access of catalyst and monomer to areas close to the interface, polymers grown from surfaces may be less uniform than those grown under homogeneous conditions.

To obtain homogeneous polymer brushes, the grafting density must be high and uniform, the PDI of the polymers should be near 1,<sup>57</sup> and all chains must be terminally grafted onto surfaces. Strategies for attaching polymer brushes to surfaces include the "grafting to" technique,<sup>58</sup> tethering preformed polymer chains from solution to a surface, and the "grafting from" technique pioneered by Sogah,<sup>59</sup> polymerization from surface-anchored initiators. The former results in a lower density of polymer brushes than the "grafting from" technique because steric hindrance eventually prevents incoming polymer chains from diffusing through the film to surface reaction sites. This section will focus on the "grafting from" technique, i.e. surface-initiated polymerizations.

## II-2. Surface-initiated Free Radical Polymerization

Niwa used UV light to photoinitiate the polymerization of methacrylic acid (MAA) from a self-assembled monolayer (SAM) of xanthate derivatives on gold.<sup>60</sup> Both the formation of the xanthate SAM and the photopolymerization process were monitored using a quartz crystal microbalance. The SAM was a mixed monolayer prepared from double-chained xanthate **1**, and the xanthate-free analog **2**. The polymerization rate was strongly dependent on the mole fraction of **1** ( $f_1$ ) in the SAM and reached a maximum at  $f_1 = 0.2$ . The reaction also was pH-dependent, with almost no polymerization at pH 7, and a rapid increase as the pH was lowered to 2.3, the lowest pH tested (**Figure 1.1**). The reason for this dependence is unclear, although one possibility is that increasing electrostatic repulsion at high pH between incoming MAA and PMAA decreases the monomer diffusion rate and turns off the polymerization. The surface properties of the PMAA brushes were characterized by their interaction with cytochrome c, a typical redox protein with a surface covered with positively charged lysine residues at neutral pH. The rapid adsorption of cytochrome c on PMAA was monitored using a quartz crystal microbalance.



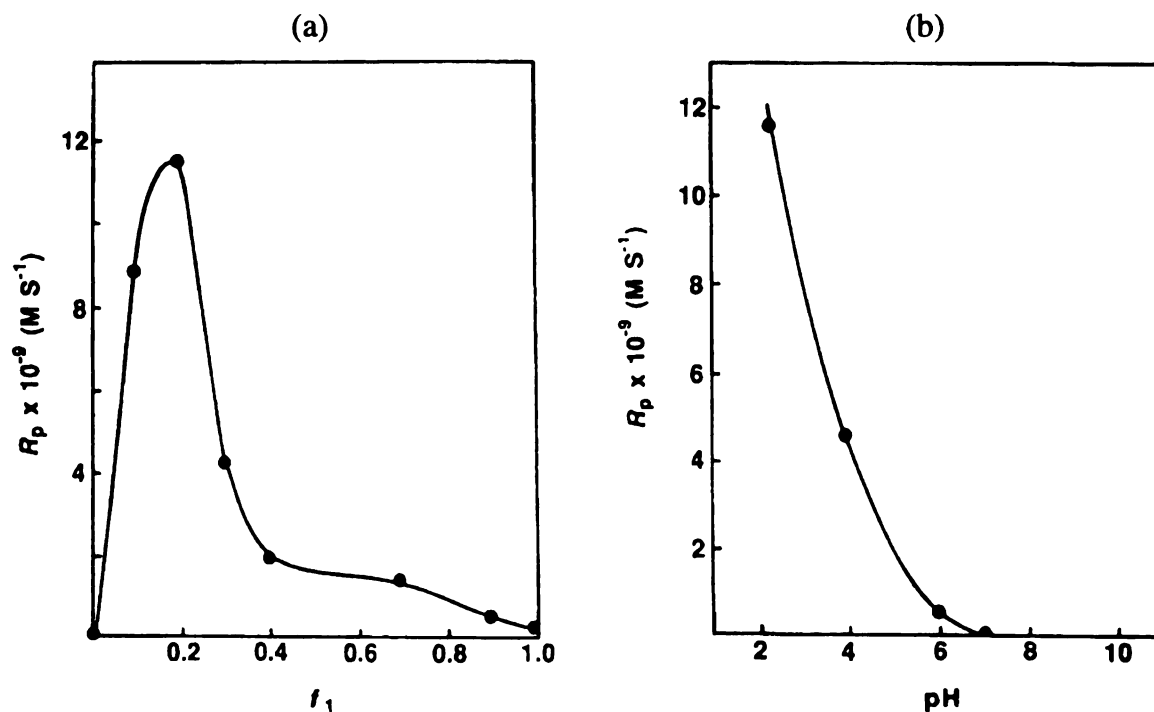


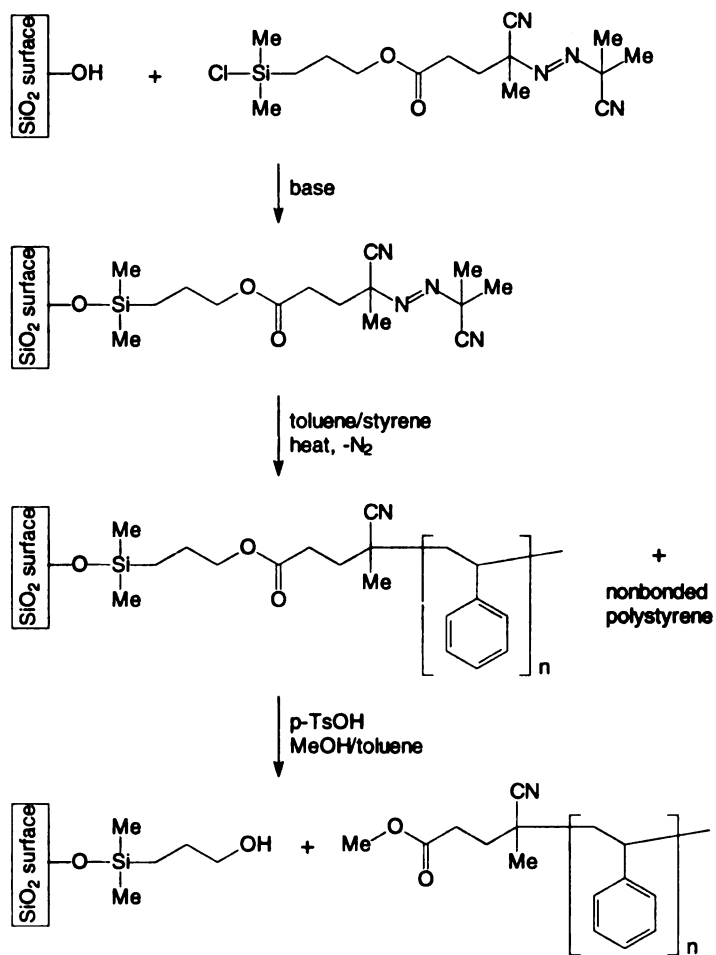
**Figure 1.1.** Rate of methacrylic acid polymerization initiated by UV irradiation of a xanthate system as a function of (a) fraction of xanthate in the monolayer and (b) pH. Reprinted with permission from *Macromolecules* 1996, 29, 3681-3685. Copyright 1996 American Chemical Society.

Prucker and Ruhe reported surface-initiated free radical polymerization of styrene from a self-assembled monolayer of azo initiators covalently bound to high surface area silica gels.<sup>61</sup> **Scheme 1.10** shows the polymerization reaction and the scheme for detachment of the polymer chains from the silica gel. The initiators have three important functionalities: (1) an azo group that generates free radicals upon heating or UV irradiation, (2) a chlorosilane that allows the initiator to be anchored to the surface through reaction with silanol groups of the silica substrate, and (3) an ester that can be hydrolyzed to detach the polymer brushes from the surface. After polymerization of

styrene, the ester bonds that connected the polystyrene (PS) to the surface were cleaved and the molecular weights of the polymers were determined to allow comparison between free radical polymerization in solution and at a surface. Irradiation of selected areas of surfaces allowed preparation of microstructured thin polymer layers by surface-initiated free radical polymerization.<sup>62</sup> Velten *et al.* attached cation-bearing peroxides to mica surfaces via ion exchange. Initiation of styrene polymerization from the initiators gave the surface-bound polymers.<sup>63</sup> When treated with a poor solvent (methanol), the polystyrene chains appeared as distinct molecular droplets in SEM images.

Prucker and Ruhe also investigated the kinetics and mechanism of surface-initiated free radical polymerization from a monolayer of azo initiators attached to the surface of silica particles.<sup>64</sup> The rate of decomposition of the surface-immobilized initiator was monitored by DSC and by a volumetric method that quantifies the amount of nitrogen generated during decomposition. Dilatometry was used to follow the kinetics of polymer brush formation. The polymer chains were detached from the surface and the molecular weights of the degrafted polymers and their distribution were studied as a function of the reaction parameters during polymerization.

**Scheme 1.10.** Synthesis of polystyrene brushes on silica and cleavage of the polymers from the surface



Wittmer *et al.* predicted strong differences between polymer brushes grown from surfaces and polymers generated in solution.<sup>65</sup> They assumed that long chains are more efficient at adding monomers than short chains because they are more mobile and easily accessible to monomers, and thus polymer brushes formed at the surface should have a higher polydispersity compared to the same reaction occurring in solution. In fact, the PDI of the detached polymer brushes prepared by Prucker and Rhe ranged from 1.5 to 2, which is close to the PDI of free radical polymerizations in solution. Consequently, it can be concluded that surface immobilization does not cause excessive broadening of the molecular weight distribution. **Figure 1.2** shows the molecular weights and polydispersities of the detached polymer brushes.

Minko *et al.* used *in situ* ellipsometry to study the kinetics of the surface-initiated free radical polymerization of styrene from a silica surface with either immobilized azo-initiators or a physisorbed hydroperoxide macroinitiator.<sup>66</sup> The kinetics of the grafting process could be described by classical treatments of free radical polymerization, taking into account the termination of growing chain ends by disproportionation and coupling, or by chain transfer reactions. Such behavior resulted in a linear dependence of the polymerization rate on the surface concentration of the initiator and an inverse square root dependence on the initiator concentration in solution. The amount of grafted polymer approached a constant value with extended polymerization time, with the saturation value dependent on the polymerization rate. Using the same polymerization technique, they prepared grafted polymer coatings of styrene and MMA on titanium dioxide powder.<sup>67</sup>

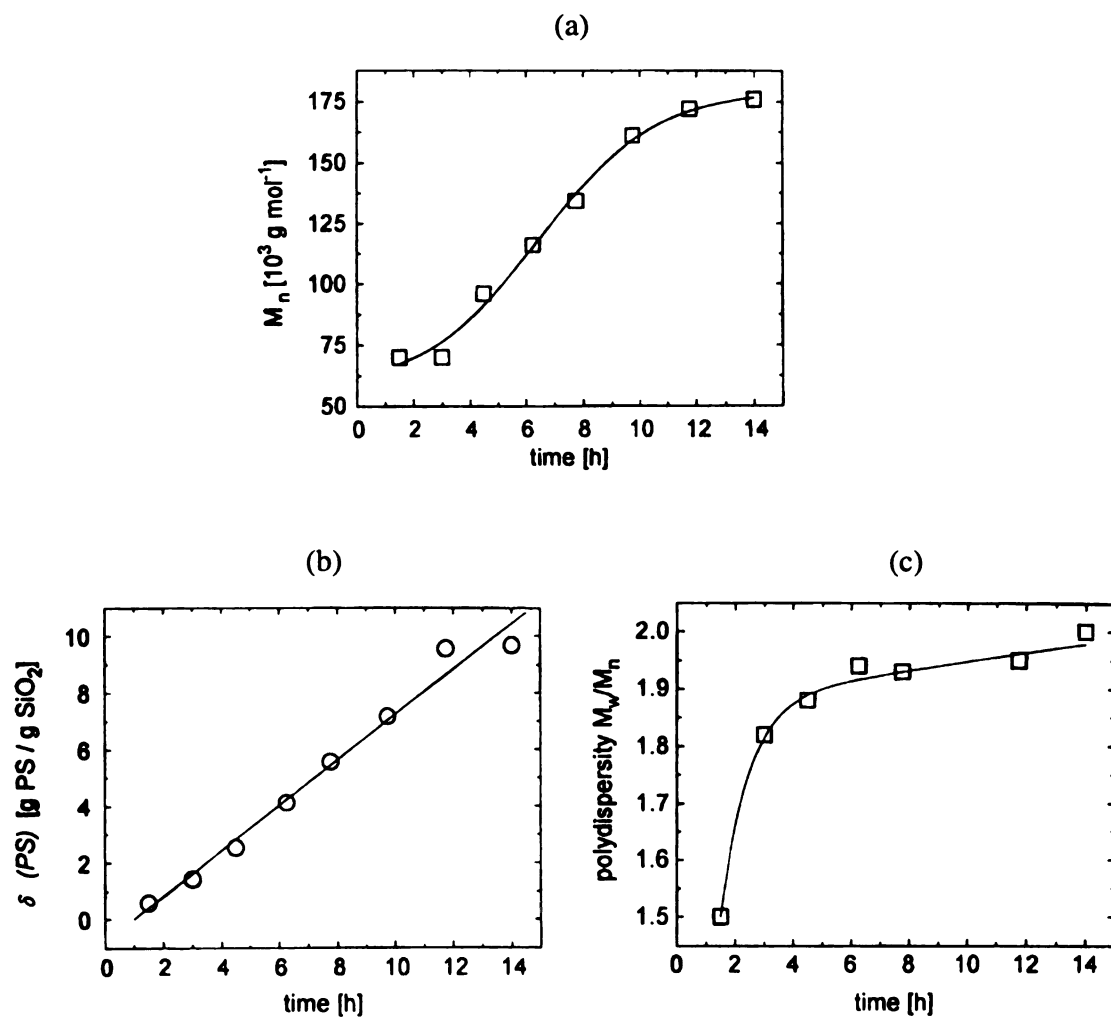


**Figure 1.2.** Time-dependent properties of polymer chains grown by surface-initiated free radical polymerization of styrene: (a) molecular weight  $M_n$ , (b) grafting densities  $\delta(\text{PS})$ , and (c) polydispersity of the covalently attached polymers. Reprinted with permission from *Macromolecules* **1998**, *31*, 602-613. Copyright 1998 American Chemical Society.

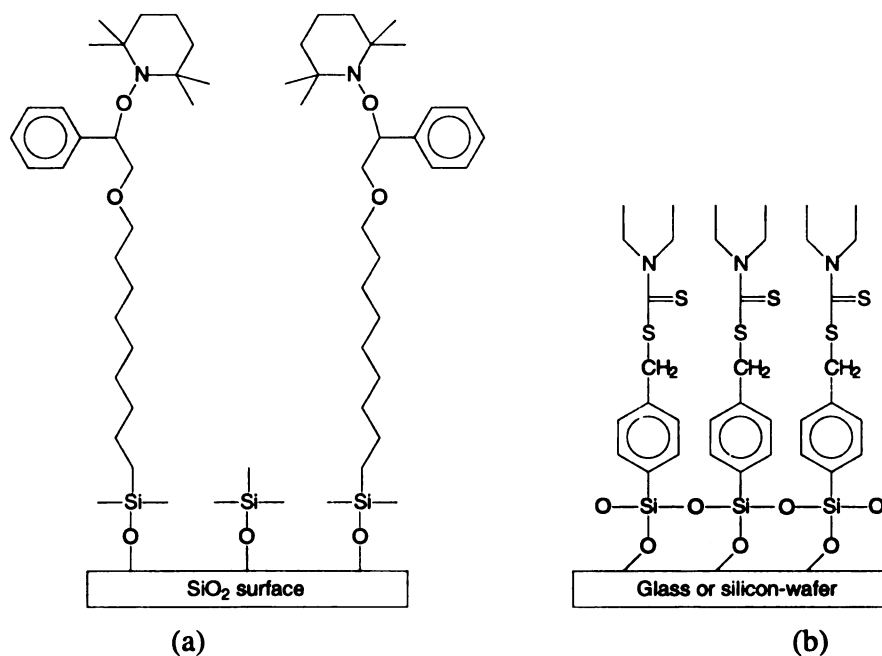
Prucker and R  he's approach was extended to the formation of block copolymers. A poly( $\epsilon$ -caprolactone) macroinitiator containing azo groups was physisorbed on a silicon oxide surface. Initiation of polymerization from the macroinitiator gave the block copolymer.<sup>68</sup> The principal advantage of this approach is that a simple physisorbed macroinitiator system allows the creation of hydrophobic layers on hydrophilic surfaces.

Despite the success of Prucker and R  he's approach, traditional free radical polymerization cannot provide well-defined polymer structures or block copolymer brushes. Hawker *et al.* used 2,2,6,6-tetramethylpiperidinyloxy (TEMPO) (**Scheme 1.11a**) as a persistent radical to achieve living free radical polymerization from a surface. The initiator contains a benzyl radical trapped with TEMPO and a site for linking the initiator to SiO<sub>2</sub> surfaces. Hawker was able to grow well-defined polymer brushes with a PDI of 1.14 and controlled molecular weight.<sup>69</sup> However, it was necessary to add predetermined amounts of free alkoxyamine initiator to the reaction mixture to control polymer growth from the surface bound initiators. The free initiator establishes a concentration of nitroxide radicals in the polymerization mixture that is high enough to control chain growth from initiators on the surface and in solution. The calculated grafting density was  $\sim 200 \text{ \AA}^2$  per polymer chain for molecular weights  $> 20,000 \text{ g/mol}$ .

Besides nitroxide-mediated polymerization, ATRP and polymerization with iniferters have been used to carry out "living" radical polymerizations from surfaces. The term, iniferter originates from *initiator*, chain *transfer* agent, and *termination* species because iniferters act in all three roles. Using the photoiniferter technique, de Boer *et al.* synthesized polymer films grafted from iniferter monolayers on glass or silicon wafers (**Scheme 1.11b**).<sup>70</sup> The ability to control the thickness of the grafted polymer and prepare

well-defined diblock copolymer brushes affirmed the living character of the process. The use of ATRP for surface-initiated polymerization is described in detail in the next section.

**Scheme 1.11.** Surface-immobilized initiators: (a) TEMPO-based and (b) iniferter



### II-3. Surface-initiated ATRP

Ejaz *et al.* deposited Langmuir-Blodgett (LB) films of ATRP initiators onto oxidized silicon substrates (Figure 1.3).<sup>71</sup> The initiator, 2-(4-chlorosulfonylphenyl)ethyl trimethoxysilane (CTS) was heated to attach the initiator to the substrate, and then the polymerization was started by the addition of MMA and a Cu(I) catalyst. The polymerization was not controlled, but the addition of *p*-toluenesulfonyl chloride as a free initiator resulted in a well-controlled polymerization. The role of the free initiator is to

increase the Cu(II) concentration, thus increasing the rate of the deactivation process. AFM showed the formation of a homogeneous polymer layer on the substrate. von Werne and Patten immobilized initiators on silica nanoparticles and showed that structurally well-defined polymer-nanoparticle hybrids could be prepared by surface-initiated ATRP.<sup>72</sup> The addition of a small amount of free initiator to the polymerization gave control over the molecular weight, but the addition of 5-15 mol% of deactivator (a Cu(II) complex) failed to give controlled polymerization. This suggests that significant amounts of a Cu(II) complex are needed to establish equilibrium in the radical generation step.

Zhao reported the first synthesis of diblock copolymer brushes, PS-*b*-PMMA, by sequential carbocationic polymerization and ATRP.<sup>73</sup> **Scheme 1.12** shows the synthetic pathway for growing grafted diblock copolymer from silicate surfaces. The authors stated that the addition of free initiator during ATRP was necessary to ensure a sufficient concentration of deactivating Cu(II) species, otherwise the polymerization was not controlled.

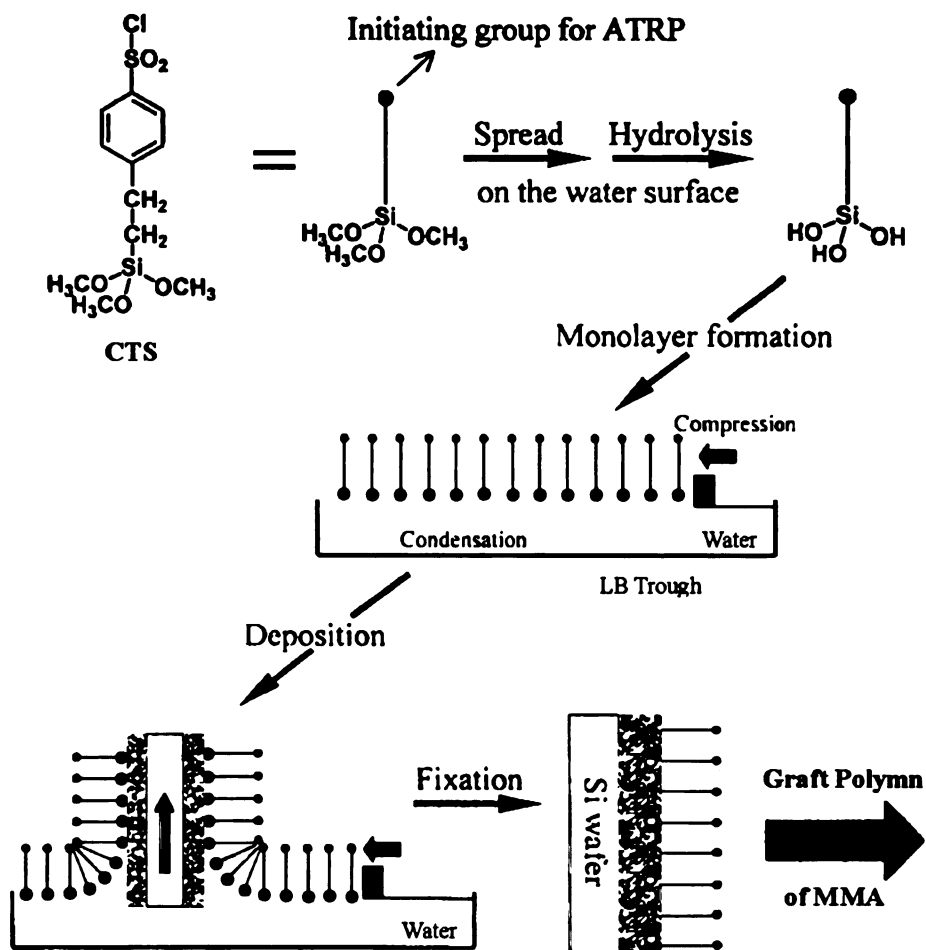
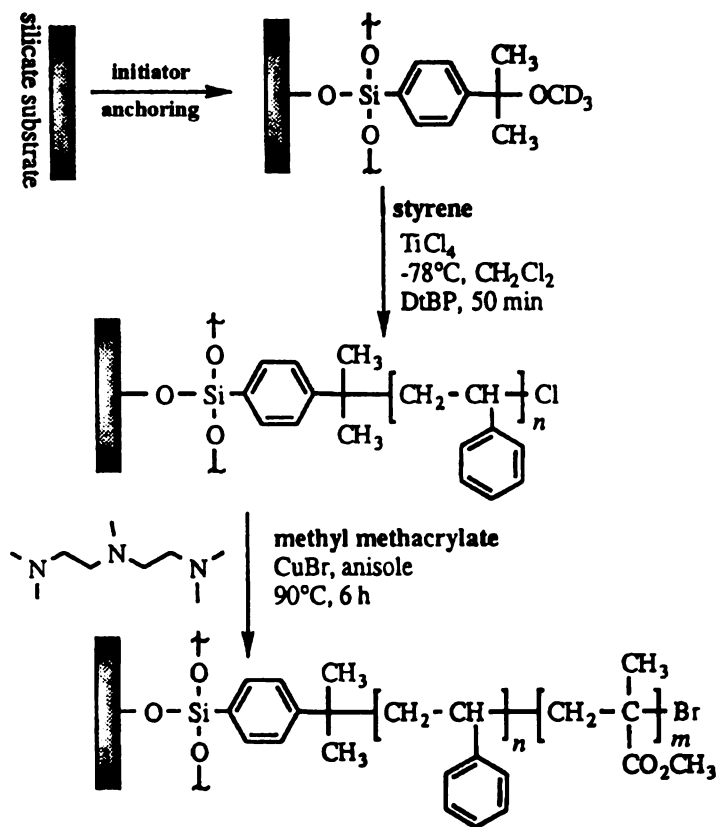
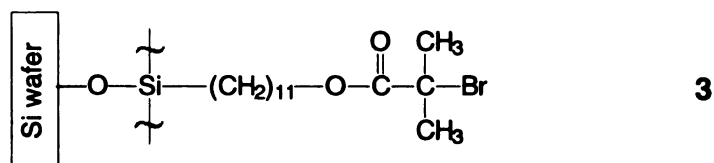


**Figure 1.3.** Schematic illustration of ATRP initiator immobilization on Si by the LB technique. Reprinted with permission from *Macromolecules* 1998, 31, 5934-5936. Copyright 1998 American Chemical Society.

**Scheme 1.12.** Synthesis of a polystyrene-*b*-poly(methyl methacrylate) brush by sequential carbocationic polymerization and ATRP (Reprinted with permission from *J. Am. Chem. Soc.* **1999**, *121*, 3557-3558. Copyright 1999 American Chemical Society)



In another study, styrene and methyl acrylate were polymerized from an initiator layer of 2-bromoisobutyrate immobilized on silicon wafers (3). The polymerizations showed a linear increase in the polymer thickness with reaction time.<sup>74</sup> Controlled growth was achieved by the addition of a deactivating Cu(II) species, but more importantly, control was achieved without a sacrificial initiator in solution. Shah *et al.* also used surface-initiated ATRP of acrylates and methacrylates to prepare a variety of polymer brushes.<sup>75</sup>



ATRP is reported to be very tolerant of functional groups, impurities, and water. Water accelerates ATRP and allows polymerization to take place at room temperature. Huang *et al.* synthesized crosslinked polymer films on gold surface<sup>76</sup> and Jones *et al.* grew poly(glycidyl methacrylate) (PGMA) brushes and PMMA-*b*-PHEMA copolymer brushes from Si surfaces.<sup>77</sup> Both groups used aqueous ATRP to obtain controlled growth of polymer films from surfaces. Wirth reported that the surface topography of polyacrylamide films grown by ATRP is quite different from films grown from surface-immobilized azo initiator by free radical polymerization.<sup>78</sup> **Figure 1.4** shows AFM images of the polymer surface. The surface roughness was 0.5 nm for the film prepared by ATRP and 3.1 nm for the film formed by conventional radical polymerization methods.

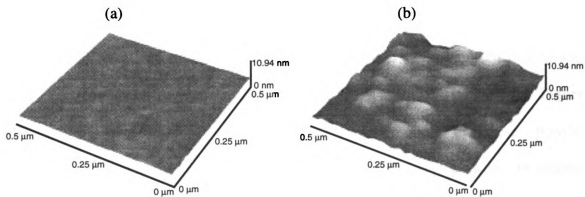


**Figure 1.4.** AFM images of polyacrylamide films prepared by (a) surface-initiated ATRP and (b) surface-initiated free radical polymerization. Reprinted with permission from *Anal. Chem.* **1998**, *70*, 4023-4029. Copyright 1998 American Chemical Society.

Surface initiated ATRP can be applied to curved as well as flat surfaces. Recently, Ejaz *et al.* anchored 2-(4-chlorosulfonylphenyl) groups to a porous glass filter and polymerized MMA from the surface.<sup>79</sup> The polymer brushes were cleaved from the glass by treatment with HF, and GPC measurements showed that  $M_n$  increased linearly with monomer conversion, in good agreement with the theoretical value. The polydispersity of the polymer brushes was low ( $1.1 \leq \text{PDI} \leq 1.2$ ), confirming that graft polymerization from curved surfaces also is controlled.

Surface-initiated ATRP provides several advantages over conventional radical polymerizations including good control over the molecular weight of the polymers and hence the thickness of polymer brushes, the ability to tailor surface properties through the polymerization of a wide spectrum of commercially available vinyl monomers, tolerance to water and impurities, and the option of carrying out polymerizations at relatively low temperatures with active catalytic systems.

#### II-4. Surface-initiated Cationic Polymerizations

Ulman *et al.* reported surface-initiated cationic polymerization of 2-oxazolines as a novel and efficient approach to immobilization of poly(2-ethyl-2-oxazolines).<sup>80</sup> **Figure 1.5** outlines the reaction pathway for the preparation of these poly(N-propionylethylenimine) (PPEI) brushes. The polymer chains were grown from triflates immobilized on SAM, and after several days, the chain ends were functionalized with a dialkyl amine to terminate the polymerization and form amphiphilic polymer brushes. The resulting PPEI film was uniform in thickness and was stable to exhaustive Soxhlet extraction with a good solvent. The formation of the polymer layers was confirmed by ellipsometry, contact angle measurements, and external reflectance FTIR.

Even though controlled radical polymerization methods can provide a broad range of polymers, this approach is restricted to polyolefins that typically have flexible backbones. Seery *et al.* used surface-initiated cationic polymerization of isocyanates at room temperature to prepare polymer brushes on silica or gold nanoparticles (**Scheme 1.13**).<sup>81</sup> The use of a nanoparticle system allows for characterization of brushes by NMR spectroscopy and transmission FTIR because the particles have a high surface area to volume ratio and are easily suspended in solution. The kinetics of the polymerization of hexyl isocyanate from the surface of gold nanoparticles was studied by real time IR spectroscopy.<sup>82</sup> Surprisingly, the kinetic plots were consistent with a second-order process after a short induction period, while analogous homogeneous polymerizations showed the expected first-order dependence on monomer concentration.<sup>83</sup> The exact interpretation of the kinetic results and the observation of an induction time are not currently understood.

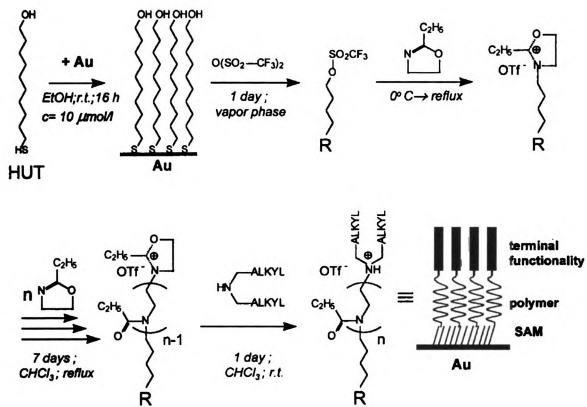
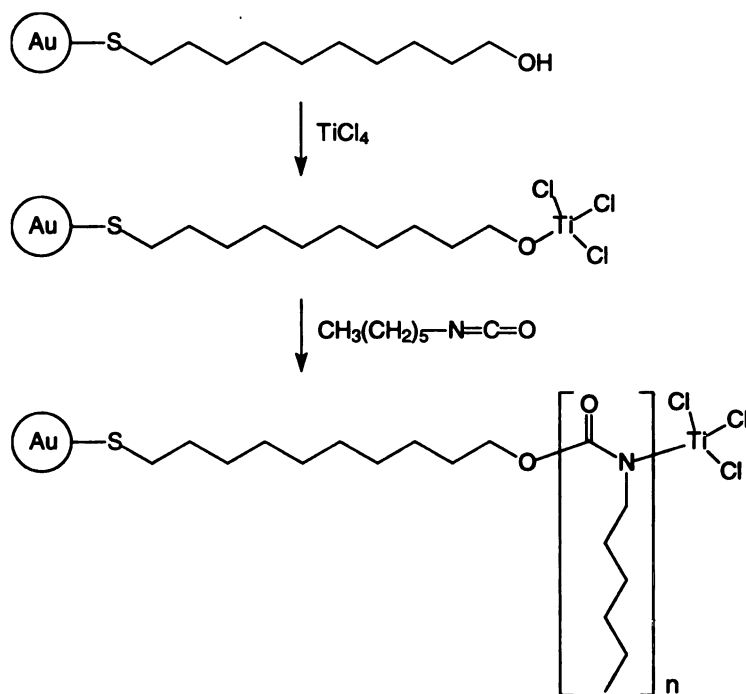


**Figure 1.5.** Surface-initiated cationic polymerization of 2-oxazolines. Reprinted with permission from *J. Am. Chem. Soc.* **1998**, *120*, 243-247. Copyright 1998 American Chemical Society.

**Scheme 1.13.** Cationic polymerization of hexyl isocyanate on gold nanoparticles



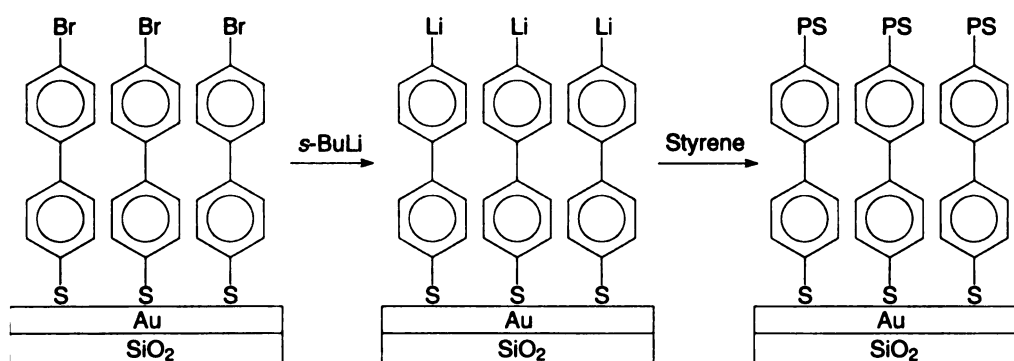
## II-5. Surface-initiated Anionic Polymerizations

Jordan *et al.* reported surface-initiated anionic polymerization of styrene from a SAM of 4'-bromo-4-mercaptobiphenyl on a gold surface.<sup>84</sup> The bromo-functionalized SAM was metalated with *sec*-BuLi to generate 4'-lithio-4-mercaptobiphenyl, the initiator for the anionic polymerization (Scheme 1.14). The grafting density for this polystyrene brush was 320–360  $\text{\AA}^2/\text{chain}$ . Based on  $\sim 20 \text{ \AA}^2$  per organic molecule in the SAM, one out of 16–18 biphenyl thiols initiates the growth of a polymer chain from the surface. Polarized infrared spectroscopy was used to study the conformation of the polymer chains. Since only vertical components of vibrating dipoles are detectable, reflection

absorption IR spectroscopy is especially sensitive to the chain orientation with respect to the reflecting surface. The spectrum of the polystyrene brush was compared to that of bulk film, and differences in the ratios of  $\nu\text{CH}_2(\text{as})/\nu\text{CH}_2(\text{s})$  in the spectra of bulk films and polymer brushes indicate that the average orientation of the polymer brushes is different from that of chains in bulk films, and that the polymer brushes are considerably elongated due to the high grafting density.

Qingye *et al.* also reported styrene polymerization from surfaces. They prepared 1,1-diphenylethylene (DPE) derivatives with quaternary ammonium tethers, and then immobilized the initiator by cation exchange (Scheme 1.15).<sup>85</sup> There was a linear relationship between the monomer concentration and the  $M_n$  of the cleaved polymers, which is consistent with a living anionic polymerization mechanism.

**Scheme 1.14.** Surface-initiated anionic polymerization of styrene on gold

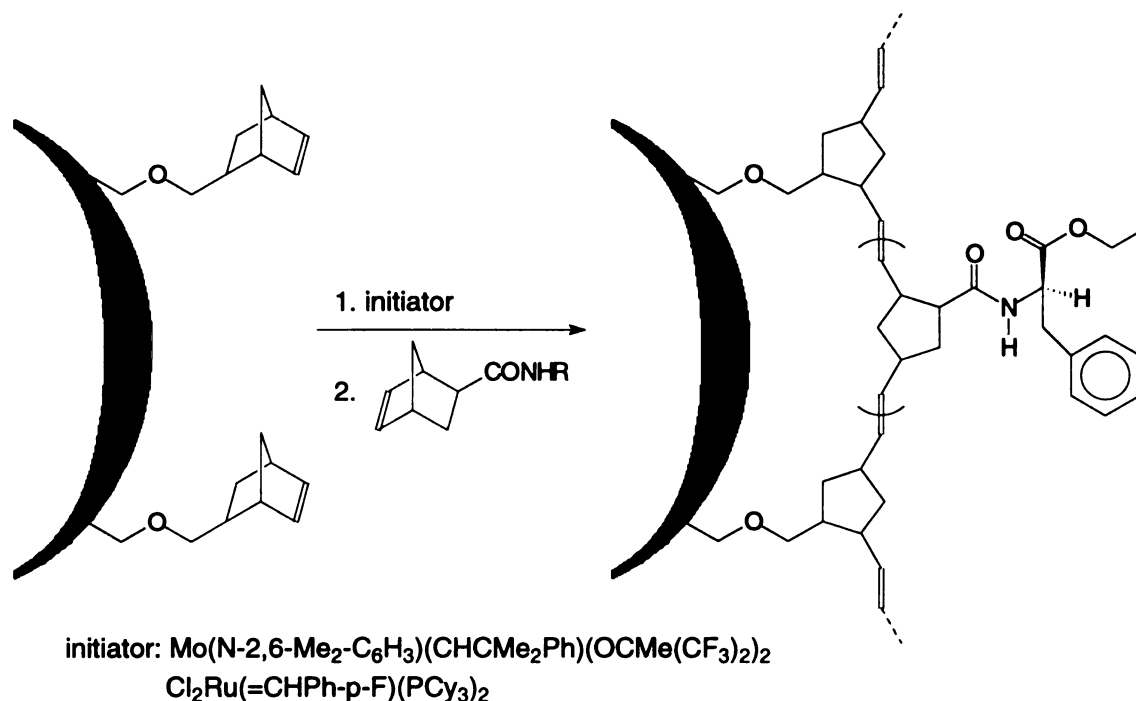




## II-6. Surface-initiated Ring-opening Metathesis Polymerization

As shown in **Scheme 1.16**, Buchmeiser *et al.* prepared surface-grafted polymer supports by surface-initiated ring-opening metathesis polymerization (ROMP) of norbornene-based chiral monomers containing L-valine and L-phenylalanine.<sup>86</sup> The chiral monomers could be polymerized at room temperature using molybdenum and ruthenium initiators, and the thickness of the films could be varied over a wide range (up to 1  $\mu\text{m}$ ).<sup>87</sup> The film thickness increased with monomer concentration, but the polymer growth stopped after ~30 min, presumably due to deactivation of the immobilized catalyst.

**Scheme 1.16.** Surface-initiated ROMP of norbornene-based chiral monomers



## II-7. Electropolymerization and Plasma Polymerization on Surfaces

Crispin *et al.* grafted poly(acrylonitrile) and poly(ethyl acrylate) on transition metal surfaces by electropolymerization.<sup>88</sup> Because this method yields a very stable polymer/metal interface, the deposited polymer film adheres to the metal surface even after washing with solvent. The strong adhesion was attributed to the formation of metal-carbon chemical bonds. Cohn *et al.* used the plasma polymerization of tetrafluoroethylene to generate a highly cross-linked fluorinated polymer layer on poly(ethylene terephthalate) (PET).<sup>89</sup> Exposing the fluoropolymer film to an ammonia plasma introduced amines on the fluoropolymer surface, which were then used as anchoring sites for further derivatization via diisocyanate spacers. (Figure 1.6).

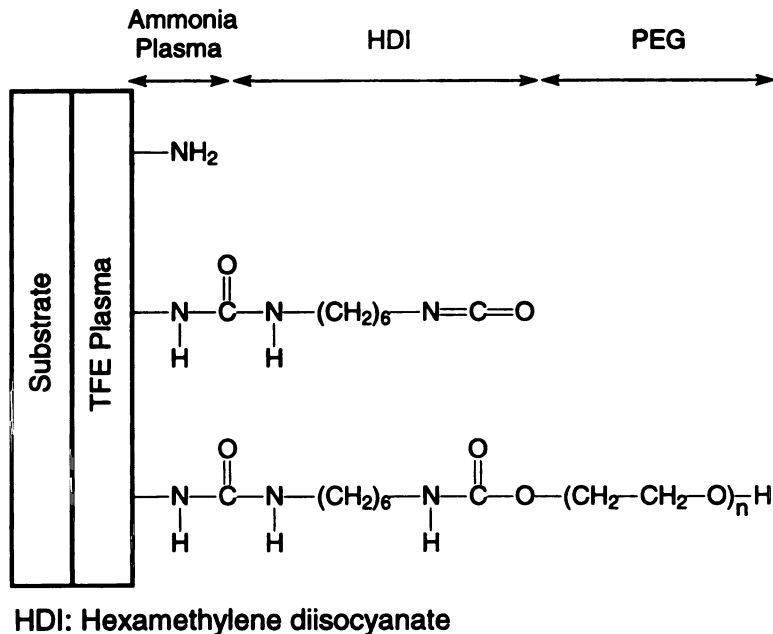
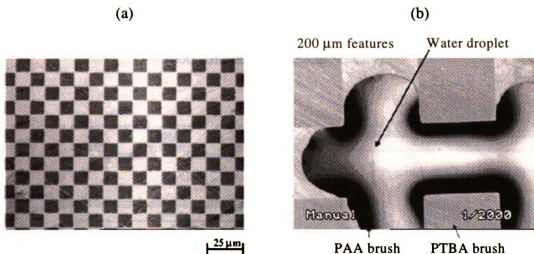


Figure 1.6. Sequential surface derivatization of PET films.

## II-8. Applications of Surface-initiated Polymerization

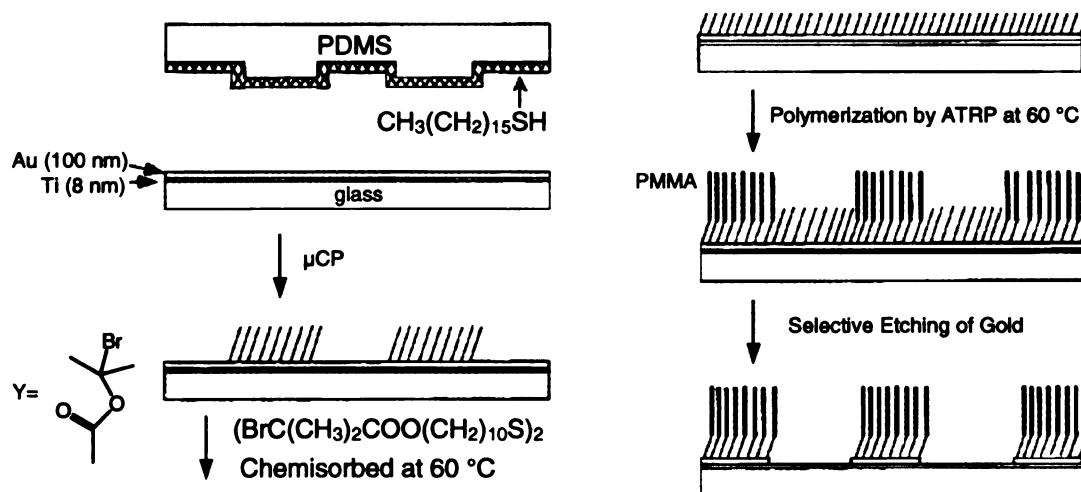
One of the most common applications of surface-initiated polymerizations is the formation of nano-patterned surfaces by soft lithography techniques that combine microcontact printing ( $\mu$ CP) and graft polymerization. Hawker *et al.* combined photolithography with nitroxide-mediated “living” free radical polymerization to yield patterned polymer brushes with well-defined hydrophobic and hydrophilic domains (Figure 1.7).<sup>90</sup> They extended this concept to surface-initiated polymerization of *tert*-butyl acrylate (PTBA). Patterned polymer layers have also been prepared by aqueous ATRP.<sup>77</sup>



**Figure 1.7.** Optical micrographs of patterned surfaces: (a) 10- $\mu$ m features in a continuous polymer brush showing regions of poly(*tert*-butyl acrylate) (dark) and poly(acrylic acid) (light) and (b) interaction of a water droplet with 200- $\mu$ m features showing an unusual wetting profile and preferential interaction with poly(acrylic acid) brush domains. Reprinted with permission from *J. Am. Chem. Soc.* **2000**, *122*, 1844-1845. Copyright 2000 American Chemical Society.

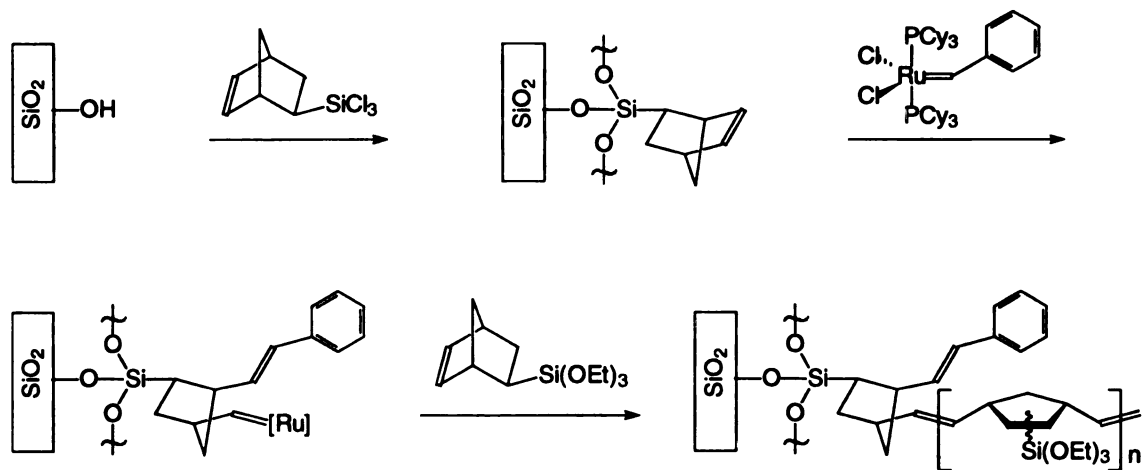
Shah *et al.* reported the use of surface-initiated ATRP to amplify patterned initiator layers on gold films. PMMA, PHEMA, PTBA, and poly(dimethylaminoethyl methacrylate) (PDMAEMA) were grown from spatially patterned initiators and then the pattern was transferred into the substrates by using the brushes as barriers to wet chemical etching of gold (Scheme 1.17).<sup>75</sup> The same group also demonstrated that patterned polymer brushes can be prepared by the surface-initiated ROP of  $\epsilon$ -caprolactone from microcontact printed gold surfaces.<sup>75</sup>

**Scheme 1.17.** Surface patterning by microcontact printing, surface-initiated ATRP, and etching (Reprinted with permission from *Macromolecules* **2000**, *33*, 597-605. Copyright 2000 American Chemical Society)



Surface-initiated ring-opening metathesis polymerization also is capable of generating patterned polymer films on silicon both in the plane and normal to the surface (**Scheme 1.18**). The combination of  $\mu$ CP and surface-initiated ROMP enables one to control polymer composition and thickness in both lateral and vertical directions at a molecular level (**Figure 1.8**), and offers new possibilities for fabricating surface features in microelectronic devices.<sup>87,91</sup> The lateral resolution of the surface features was 2  $\mu$ m, which is limited by the  $\mu$ CP technique. The thickness of the polymer films was controlled by monomer concentration and reaction time, and ranged from 5–100 nm.

**Scheme 1.18.** Surface-initiated ROMP from SiO<sub>2</sub>/Si surface



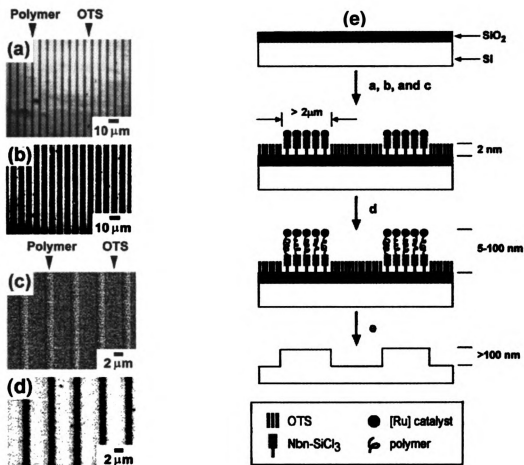


**Figure 1.8.** Surface patterning by surface-initiated ROMP: (a) optical micrograph of 2- $\mu\text{m}$ -wide lines of a patterned poly[norbornenyl-Si(OEt)<sub>3</sub>] film generated by polymerization from the surface before (thickness  $\sim 10$  nm), (b) optical micrograph of the same sample after reactive ion etching (RIE) with SF<sub>6</sub> for 3 min at 30 W in a parallel-plate etcher, (c) SEM micrograph of the sample before RIE [same sample as shown in (a)], (d) SEM micrograph of the sample after RIE, and (e) schematic representation of patterned polymer formation by  $\mu\text{CP}$ , activation, ring-opening metathesis polymerization on the surface of SiO<sub>2</sub>/Si, and RIE. Reprinted with permission from *Appl. Phys. Lett.* **1999**, 75, 4201-4203. Copyright 1999 American Institute of Physics.

Peng *et al.* synthesized poly(methacrylate) brushes with side chains of phenylbenzoate mesogens on silicon oxide surfaces and the polymer backbone and the mesogen units are connected through a flexible spacer. The thickness of these side-chain liquid crystalline polymer (LCP) brushes (up to 200 nm) could be controlled by monomer concentration and reaction time.<sup>92</sup> The optical texture of segregated polymer brushes exhibits a strong memory effect. Heating the brush or exposing it to solvent renders it isotropic, and upon cooling or removal of solvent, the identical texture reappears as it returns to the nematic state. Utilizing the LCP brushes, it was possible to induce a certain orientation of the nematic director in an adjacent bulk LC phase. This orientation could be tilted because there may be a competition between the orienting action of the stretched polymer chains and the uncovered fraction of the substrate (**Figure 1.9**).

Wirth *et al.* used surface-initiated ATRP to grow 10 nm thick films of polyacrylamide on the surface of porous silica gel (86 nm pore size, 36 m<sup>2</sup>/g surface area).<sup>78,93</sup> Size-exclusion chromatography of proteins using the modified silica as the stationary phase confirmed that the silica pores remained open after polymerization; four proteins, thyroglobulin (669 kDa), ovalbumin (44 kDa), ribonuclease A (13.7 kDa) and aprotinin (6.5 kDa) eluted in order of decreasing size, in accordance with a size-exclusion mechanism. Electrophoresis capillaries were coated with linear or cross-linked polyacrylamide by surface-initiated ATRP.<sup>94</sup> Using free radical polymerization to coat capillaries with cross-linked polyacrylamide films is impractical because of concurrent polymerization of acrylamide in solution. The modified capillaries were used to separate a mixture of three proteins, cytochrome c, lysozyme, and ribonuclease A by electrophoresis, and could be used for more than 100 runs without clogging.

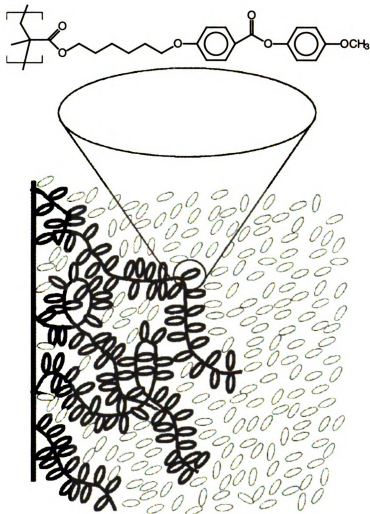


**Figure 1.9.** Schematic depiction of an LC brush swollen in a low molecular weight nematic. Competing orienting actions from the brush and the bare surface may result in a tilted alignment. The chemical structure of the mesogen used in this study is indicated in the inset. Reprinted with permission from *Macromolecules* **1999**, *32*, 6759-6766. Copyright 1999 American Chemical Society.

There are examples of similar grafting techniques applied to different substrates. For example, Tsubokawa *et al.* used a variety of surface grafting techniques to tailor the surface properties of carbon thin films using radical, cationic, and anionic graft polymerization,<sup>95</sup> and Piletsky *et al.* utilized surface photograft polymerization and molecular imprinting techniques to introduce specific binding sites into porous membranes.<sup>96</sup>

### **III. References**

- (1) Wang, J.-S.; Matyjaszewski, K. *J. Am. Chem. Soc.* **1995**, *117*, 5614-5615.
- (2) Kato, M.; Kamigaito, M.; Sawamoto, M.; Higashimura, T. *Macromolecules* **1995**, *28*, 1721-1723.
- (3) Matyjaszewski, K.; Xia, J. *Chem. Rev.* **2001**, *101*, 2921-2990.
- (4) Matyjaszewski, K.; Mueller, A. H. E. *Polym. Prepr. (Am. Chem. Soc., Div. Polym. Chem.)* **1997**, *38*, 6-9.
- (5) Curran, D. P. *Synthesis* **1988**, 489-513.
- (6) Bellus, D. *Pure Appl. Chem.* **1985**, *57*, 1827-1838.
- (7) Fischer, H. *Macromolecules* **1997**, *30*, 5666-5672.
- (8) Fischer, H. *J. Am. Chem. Soc.* **1986**, *108*, 3925-3927.
- (9) Matyjaszewski, K.; Kajiwarra, A. *Macromolecules* **1998**, *31*, 548-550.
- (10) Matyjaszewski, K.; Nakagawa, Y.; Jasieczek, C. B. *Macromolecules* **1998**, *31*, 1535-1541.

- (11) Matyjaszewski, K.; Goebelt, B.; Paik, H.-j.; Horwitz, C. P. *Macromolecules* **2001**, *34*, 430-440.
- (12) Davis, K. A.; Paik, H.-j.; Matyjaszewski, K. *Macromolecules* **1999**, *32*, 1767-1776.
- (13) Matyjaszewski, K. *Macromolecules* **1999**, *32*, 9051-9053.
- (14) Percec, V.; Barboiu, B. *Macromolecules* **1995**, *28*, 7970-7972.
- (15) Haddleton, D. M.; Jasieczek, C. B.; Hannon, M. J.; Shooter, A. J. *Macromolecules* **1997**, *30*, 2190-2193.
- (16) Ando, T.; Kato, M.; Kamigaito, M.; Sawamoto, M. *Macromolecules* **1996**, *29*, 1070-1072.
- (17) Granel, C.; Dubois, P.; Jerome, R.; Teyssie, P. *Macromolecules* **1996**, *29*, 8576-8582.
- (18) Uegaki, H.; Kotani, Y.; Kamigaito, M.; Sawamoto, M. *Macromolecules* **1997**, *30*, 2249-2253.
- (19) Ando, T.; Kamigaito, M.; Sawamoto, M. *Macromolecules* **1997**, *30*, 4507-4510.
- (20) Matyjaszewski, K.; Patten, T. E.; Xia, J. *J. Am. Chem. Soc.* **1997**, *119*, 674-680.
- (21) Moineau, G.; Granel, C.; Dubois, P.; Jerome, R.; Teyssie, P. *Macromolecules* **1998**, *31*, 542-544.
- (22) Patten, T. E.; Matyjaszewski, K. *Acc. Chem. Res.* **1999**, *32*, 895-903.
- (23) Shen, Y.; Zhu, S.; Zeng, F.; Pelton, R. H. *Macromol. Chem. Phys.* **2000**, *201*, 1169-1175.
- (24) Kerr, J. A. *Chem. Rev.* **1966**, *66*, 465-500.
- (25) Matyjaszewski, K.; Woodworth, B. E. *Macromolecules* **1998**, *31*, 4718-4723.

- (26) Kitagawa, S.; Munakata, M. *Inorg. Chem.* **1981**, *20*, 2261-2267.
- (27) Shipp, D. A.; Wang, J.-L.; Grimaud, T.; Matyjaszewski, K. *Polym. Prepr. (Am. Chem. Soc., Div. Polym. Chem.)* **1998**, *39*, 504-505.
- (28) Matyjaszewski, K.; Shipp, D. A.; Wang, J.-L.; Grimaud, T.; Patten, T. E. *Macromolecules* **1998**, *31*, 6836-6840.
- (29) Matyjaszewski, K. *ACS Symp. Ser.* **1998**, *685*, 258-283.
- (30) Healy, P. C.; Pakawatchai, C.; White, A. H. *J. Chem. Soc., Dalton Trans.* **1985**, 2531-2539.
- (31) Pallenberg, A. J.; Koenig, K. S.; Barnhart, D. M. *Inorg. Chem.* **1995**, *34*, 2833-2840.
- (32) Munakata, M.; Kitagawa, S.; Asahara, A.; Masuda, H. *Bull. Chem. Soc. Jpn.* **1987**, *60*, 1927-1929.
- (33) Pintauer, T.; Qiu, J.; Kickelbick, G.; Matyjaszewski, K. *Inorg. Chem.* **2001**, *40*, 2818-2824.
- (34) Goto, A.; Fukuda, T. *Macromol. Rapid Commun.* **1999**, *20*, 633-636.
- (35) Matyjaszewski, K.; Paik, H.-j.; Zhou, P.; Diamanti, S. J. *Macromolecules* **2001**, *34*, 5125-5131.
- (36) Xia, J.; Matyjaszewski, K. *Macromolecules* **1997**, *30*, 7697-7700.
- (37) Wang, J.-S.; Matyjaszewski, K. *Macromolecules* **1995**, *28*, 7901-7910.
- (38) Xia, J.; Gaynor, S. G.; Matyjaszewski, K. *Macromolecules* **1998**, *31*, 5958-5959.
- (39) Wang, J.-L.; Grimaud, T.; Matyjaszewski, K. *Macromolecules* **1997**, *30*, 6507-6512.

- (40) Haddleton, D. M.; Kukulj, D.; Duncalf, D. J.; Heming, A. M.; Shooter, A. J. *Macromolecules* **1998**, *31*, 5201-5205.
- (41) Haddleton, D. M.; Crossman, M. C.; Dana, B. H.; Duncalf, D. J.; Heming, A. M.; Kukulj, D.; Shooter, A. J. *Macromolecules* **1999**, *32*, 2110-2119.
- (42) Patten, T. E.; Xia, J.; Abernathy, T.; Matyjaszewski, K. *Science* **1996**, *272*, 866-868.
- (43) Patten, T. E.; Xia, J.; Abernathy, T.; Matyjaszewski, K. *Polym. Prepr. (Am. Chem. Soc., Div. Polym. Chem.)* **1996**, *37*, 575-576.
- (44) Bernhardt, P. V. *J. Am. Chem. Soc.* **1997**, *119*, 771-774.
- (45) Xia, J.; Matyjaszewski, K. *Macromolecules* **1999**, *32*, 2434-2437.
- (46) Carmichael, A. J.; Haddleton, D. M.; Bon, S. A. F.; Seddon, K. R. *Chem. Commun.* **2000**, 1237-1238.
- (47) Wang, X. S.; Armes, S. P. *Macromolecules* **2000**, *33*, 6640-6647.
- (48) Matyjaszewski, K. *Macromolecules* **1998**, *31*, 4710-4717.
- (49) Pyun, J.; Matyjaszewski, K. *Macromolecules* **2000**, *33*, 217-220.
- (50) Bielawski, C. W.; Louie, J.; Grubbs, R. H. *J. Am. Chem. Soc.* **2000**, *122*, 12872-12873.
- (51) Kickelbick, G.; Paik, H.-j.; Matyjaszewski, K. *Macromolecules* **1999**, *32*, 2941-2947.
- (52) Shen, Y.; Zhu, S.; Zeng, F.; Pelton, R. *Macromol. Chem. Phys.* **2000**, *201*, 1387-1394.
- (53) Shen, Y.; Zhu, S.; Pelton, R. *Macromol. Rapid Commun.* **2000**, *21*, 956-959.
- (54) Guan, Z.; Smart, B. *Macromolecules* **2000**, *33*, 6904-6906.

- (55) De Gennes, P. G. *Macromolecules* **1980**, *13*, 1069-1075.
- (56) Milner, S. T. *Science* **1991**, *251*, 905-914.
- (57) Dan, N.; Tirrell, M. *Macromolecules* **1993**, *26*, 6467-6473.
- (58) Bridger, K.; Vincent, B. *Eur. Polym. J.* **1980**, *16*, 1017-1021.
- (59) Hertler, W. R.; Sogah, D. Y.; Boettcher, F. P. *Macromolecules* **1990**, *23*, 1264-1268.
- (60) Niwa, M.; Date, M.; Higashi, N. *Macromolecules* **1996**, *29*, 3681-3685.
- (61) Prucker, O.; Ruhe, J. *Macromolecules* **1998**, *31*, 592-601.
- (62) Prucker, O.; Schimmel, M.; Tovar, G.; Knoll, W.; Ruhe, J. *Adv. Mater.* **1998**, *10*, 1073-1077.
- (63) Velten, U.; Tossati, S.; Shelden, R. A.; Caseri, W. R.; Suter, U. W.; Hermann, R.; Mueller, M. *Langmuir* **1999**, *15*, 6940-6945.
- (64) Prucker, O.; Ruhe, J. *Macromolecules* **1998**, *31*, 602-613.
- (65) Wittmer, J. P.; Cates, M. E.; Johner, A.; Turner, M. S. *Europhys. Lett.* **1996**, *33*, 397-402.
- (66) Minko, S.; Sidorenko, A.; Stamm, M.; Gafijchuk, G.; Senkovsky, V.; Voronov, S. *Macromolecules* **1999**, *32*, 4532-4538.
- (67) Sidorenko, A.; Minko, S.; Gafijchuk, G.; Voronov, S. *Macromolecules* **1999**, *32*, 4539-4543.
- (68) Stohr, T.; Ruhe, J. *Macromolecules* **2000**, *33*, 4501-4511.
- (69) Husseman, M.; Malmstrom, E. E.; McNamara, M.; Mate, M.; Mecerreyes, D.; Benoit, D. G.; Hedrick, J. L.; Mansky, P.; Huang, E.; Russell, T. P.; Hawker, C.

- J. Macromolecules* **1999**, *32*, 1424-1431.
- (70) de Boer, B.; Simon, H. K.; Werts, M. P. L.; van der Vegte, E. W.; Hadziioannou, G. *Macromolecules* **2000**, *33*, 349-356.
- (71) Ejaz, M.; Yamamoto, S.; Ohno, K.; Tsujii, Y.; Fukuda, T. *Macromolecules* **1998**, *31*, 5934-5936.
- (72) von Werne, T.; Patten, T. E. *J. Am. Chem. Soc.* **2001**, *123*, 7497-7505.
- (73) Zhao, B.; Brittain, W. J. *J. Am. Chem. Soc.* **1999**, *121*, 3557-3558.
- (74) Matyjaszewski, K.; Miller, P. J.; Shukla, N.; Immaraporn, B.; Gelman, A.; Luokala, B. B.; Siclovan, T. M.; Kickelbick, G.; Vallant, T.; Hoffmann, H.; Pakula, T. *Macromolecules* **1999**, *32*, 8716-8724.
- (75) Shah, R. R.; Merreceyes, D.; Husemann, M.; Rees, I.; Abbott, N. L.; Hawker, C. J.; Hedrick, J. L. *Macromolecules* **2000**, *33*, 597-605.
- (76) Huang, W.; Baker, G. L.; Bruening, M. L. *Angew. Chem., Int. Ed.* **2001**, *40*, 1510-1512.
- (77) Jones, D. M.; Huck, W. T. S. *Adv. Mater.* **2001**, *13*, 1256-1259.
- (78) Huang, X.; Doneski, L. J.; Wirth, M. J. *CHEMTECH* **1998**, *28*, 19-25.
- (79) Ejaz, M.; Tsujii, Y.; Fukuda, T. *Polymer* **2001**, *42*, 6811-6815.
- (80) Jordan, R.; Ulman, A. *J. Am. Chem. Soc.* **1998**, *120*, 243-247.
- (81) Seery, T. A. P.; Dhar, P.; Huber, D. L.; Vatansever, F. *Polym. Prepr. (Am. Chem. Soc., Div. Polym. Chem.)* **1999**, *40*, 148-149.
- (82) Huber, D. L.; Seery, T. A. P. *Polym. Prepr. (Am. Chem. Soc., Div. Polym. Chem.)* **1999**, *40*, 709-710.
- (83) Patten, T. E.; Novak, B. M. *Macromolecules* **1993**, *26*, 436-439.

- (84) Jordan, R.; Ulman, A.; Kang, J. F.; Rafailovich, M. H.; Sokolov, J. *J. Am. Chem. Soc.* **1999**, *121*, 1016-1022.
- (85) Zhou, Q.; Fan, X.; Xia, C.; Mays, J.; Advincula, R. *Chem. Mater.* **2001**, *13*, 2465-2467.
- (86) Buchmeiser, M. R.; Sinner, F.; Mupa, M.; Wurst, K. *Macromolecules* **2000**, *33*, 32-39.
- (87) Kim, N. Y.; Jeon, N. L.; Choi, I. S.; Takami, S.; Harada, Y.; Finnie, K. R.; Girolami, G. S.; Nuzzo, R. G.; Whitesides, G. M.; Laibinis, P. E. *Macromolecules* **2000**, *33*, 2793-2795
- (88) Crispin, X.; Lazzaroni, R.; Geskin, V.; Baute, N.; Dubois, P.; Jerome, R.; Bredas, J. L. *J. Am. Chem. Soc.* **1999**, *121*, 176-187.
- (89) Cohn, D.; Stern, T. *Macromolecules* **2000**, *33*, 137-142.
- (90) Husemann, M.; Morrison, M.; Benoit, D.; Frommer, J.; Mate, C. M.; Hinsberg, W. D.; Hedrick, J. L.; Hawker, C. J. *J. Am. Chem. Soc.* **2000**, *122*, 1844-1845.
- (91) Jeon, N. L.; Choi, I. S.; Whitesides, G. M.; Kim, N. Y.; Laibinis, P. E.; Harada, Y.; Finnie, K. R.; Girolami, G. S.; Nuzzo, R. G. *Appl. Phys. Lett.* **1999**, *75*, 4201-4203.
- (92) Peng, B.; Johannsmann, D.; Rhe, J. *Macromolecules* **1999**, *32*, 6759-6766.
- (93) Huang, X.; Wirth, M. J. *Macromolecules* **1999**, *32*, 1694-1696.
- (94) Huang, X.; Doneski, L. J.; Wirth, M. J. *Anal. Chem.* **1998**, *70*, 4023-4029.
- (95) Tsubokawa, N.; Ueno, H. *J. Appl. Polym. Sci.* **1995**, *58*, 1221-1227.
- (96) Piletsky, S. A.; Matuschewski, H.; Schedler, U.; Wilpert, A.; Piletska, E. V.; Thiele, T. A.; Ulbricht, M. *Macromolecules* **2000**, *33*, 3092-3098.

## Chapter 2

### Surface-Initiated ATRP on Gold at Ambient Temperature

#### I. Introduction

This chapter describes the surface-initiated ATRP of MMA on gold surfaces at room temperature. The polymerization temperature in this polymer brush synthesis is the lowest reported for surface-initiated radical polymerizations, and it is the first report of the direct measurement of the molecular weight of polymer brushes grown on a flat surface. The molecular weight of the polymer brushes suggests a high grafting density of PMMA on gold surfaces. No polymer forms in solution, and a simple solvent rinse can clean the polymer brushes on the surface.

Growth of polymer brushes is an attractive method to modify and control interface properties.<sup>1-5</sup> Strategies for attaching polymer brushes to surfaces include the "grafting to" technique,<sup>6</sup> tethering preformed polymer chains from solution onto a surface, and the "grafting from" technique,<sup>7,8</sup> polymerizing from surface-anchored initiators. The latter results in a higher density of polymer brushes on a surface because the "grafting to" technique eventually faces serious steric hindrance that prevents incoming polymer chains from diffusing through the film to surface reaction sites.

Several research groups used radical,<sup>9</sup> cationic,<sup>10</sup> anionic,<sup>11</sup> ring-opening,<sup>12</sup> ring-opening metathesis<sup>13</sup> and ATRP<sup>7,14</sup> to grow polymer chains from a surface. Of these approaches, ATRP is especially attractive because it is a living process that gives a low polydispersity index (PDI). To prepare well-organized polymer brushes, the PDI ( $M_w/M_n$ )

should be close to 1. Block copolymers can also be prepared<sup>15,16</sup> with ATRP by changing monomer solutions and re-initiating at dormant sites. Utilizing ATRP for surface polymerization is a very convenient way to avoid the occurrence of polymerization in solution. This feature reduces purification of the polymer brushes to a simple washing process. As shown in **Figure 2.1**, surface-initiated ATRP generates only surface-bound radicals, while surface-initiated free radical polymerization produces surface-bound radicals and radicals in solution. Polymerization in solution is problematic since the polymer surface is easily contaminated by physisorbed polymer from solution. This problem is magnified for cross-linkable monomers, as solution polymerization can lead to gelation.

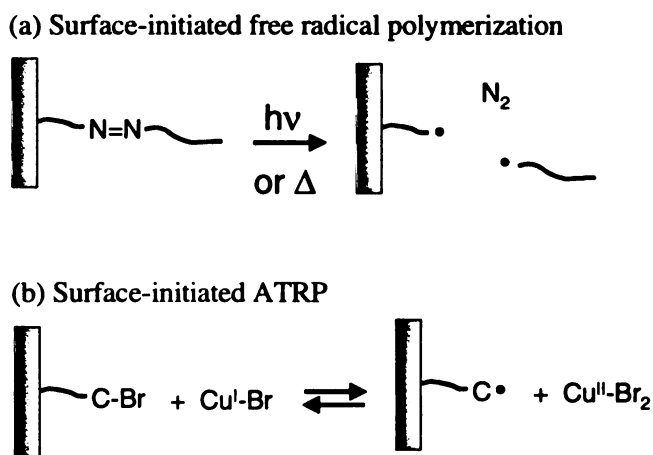


**Figure 2.1.** Differences in the radical generation mechanism for surface-initiated free radical polymerization and surface-initiated ATRP.

Building polymer layers on gold is interesting because gold surfaces are chemically homogeneous, virtually free of contamination, easy to clean, and applicable to a wide variety of analytical techniques for thin film characterization. In addition, SAMs of  $\omega$ -functionalized thiols enable easy preparation of a variety of well-ordered initiator monolayers. Research on surface-initiated polymerization has focused on silicon substrates, and studies on gold<sup>12,17</sup> are rare. Since the Au-S bond is somewhat unstable above 60 °C<sup>17-20</sup> or under UV irradiation,<sup>21</sup> growing well-ordered polymer brushes from thiols on gold is a challenge. Shah *et al.* showed that the thermal stability of the SAM affects the overall thickness of polymer brushes.<sup>17</sup> To create a more thermally stable SAM at high polymerization temperatures, they intentionally prepared the SAM at the polymerization temperature. Polymerization at room temperature (RT) will thus be beneficial for preparing grafted polymer layers from thiol monolayers on gold. Until recently, controlled radical polymerizations at RT were not possible. However, Matyjaszewski described the synthesis of polyacrylates by ATRP at RT using a copper catalyst derived from CuBr and Me<sub>6</sub>TREN.<sup>22</sup> This highly active catalyst system was adapted to the synthesis of polymer brushes at room temperature.

One challenge in surface-initiated polymerization is the characterization of polymer chains grown on surfaces.<sup>11,16</sup> Two research groups published direct measurements of the molecular weight of polymer chains detached from a curved surface.<sup>7,9</sup> To have measurable amounts of detached polymers, they grew polymer chains on silica gel with a large surface area. As Jordan *et al.* pointed out, polymer growth on a flat surface might be quite different from growing polymers on a curved surface, because these sterically different systems might have different kinetics and different polymer

brush conformations.<sup>11</sup> This chapter describes the application of RT ATRP to the growth of polymer brushes from thiol monolayers on gold, and the direct measurement of the molecular weight of polymer chains grown from a flat surface.

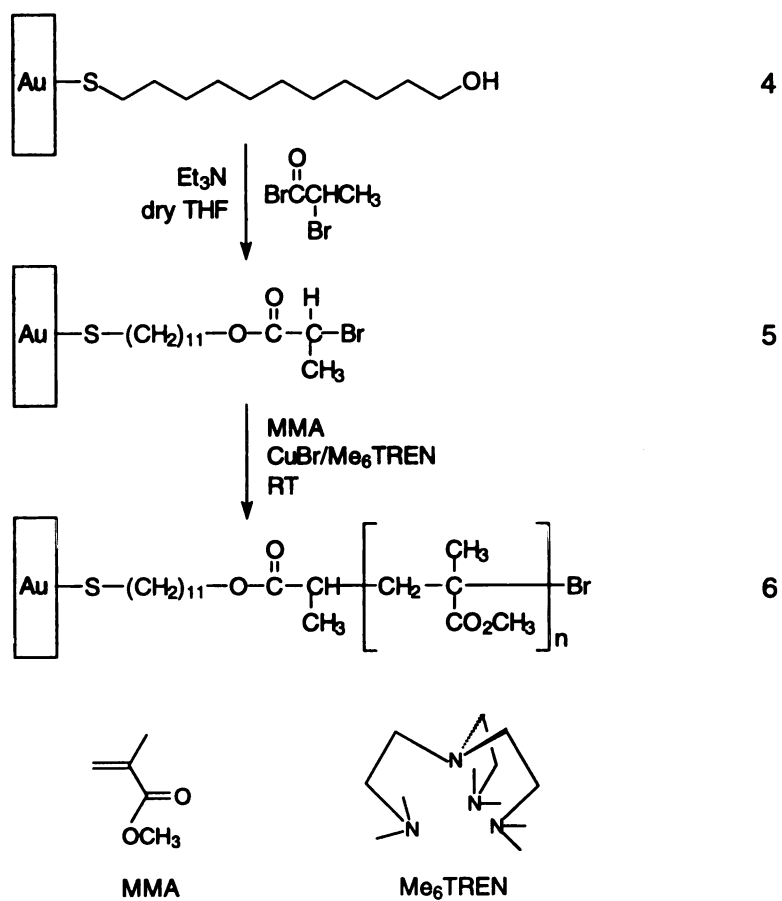
## II. Surface-initiated ATRP with Me<sub>6</sub>TREN

**Scheme 2.1** outlines the synthetic pathway for the preparation of grafted PMMA chains. **4** was prepared by immersing a gold-coated Si substrate in a 1 mM solution of 1-mercaptoundecanol (MUD) for one day. The ellipsometric thickness of the MUD layer was 12±1 Å. To produce the anchored initiator (**5**), **4** was treated with 2-bromopropionyl bromide (2-BPB) in the presence of triethylamine. A concentrated 2-BPB solution (0.1 M) was used to achieve near-quantitative initiator immobilization. Since a thiol SAM could be unstable in the presence of acid bromides, **4** was dipped in the acid bromide solution for only 2 min. This step was carried out in a dry box because acid bromides are moisture sensitive, especially in the presence of an organic base.

Initiator immobilization is apparent from the appearance of a carbonyl peak at 1743 cm<sup>-1</sup> in the reflectance FTIR spectrum (**Figure 2.2**, spectrum b). To perform ATRP, **5** was immersed in MMA containing 0.1 mol % CuBr and 0.1 mol % Me<sub>6</sub>TREN<sup>23</sup> at 25 °C for 12 hours. Since ligated Cu(I) is sensitive to O<sub>2</sub>, all polymerizations were carried out in a dry box filled with helium. After polymerization, the newly formed film was washed with dry THF. A large increase in the carbonyl peak, at 1745 cm<sup>-1</sup> in the external reflection FTIR spectrum confirmed the formation of PMMA brushes (**Figure 2.2**, spectrum c). The ellipsometric thickness of the polymer film measured at 5 different

spots on a  $75 \text{ cm}^2$  wafer was  $370 \pm 5 \text{ \AA}$  showing that the polymer film is remarkably uniform.

**Scheme 2.1.** Surface-initiated ATRP of MMA with  $\text{Me}_6\text{TREN}$  at RT



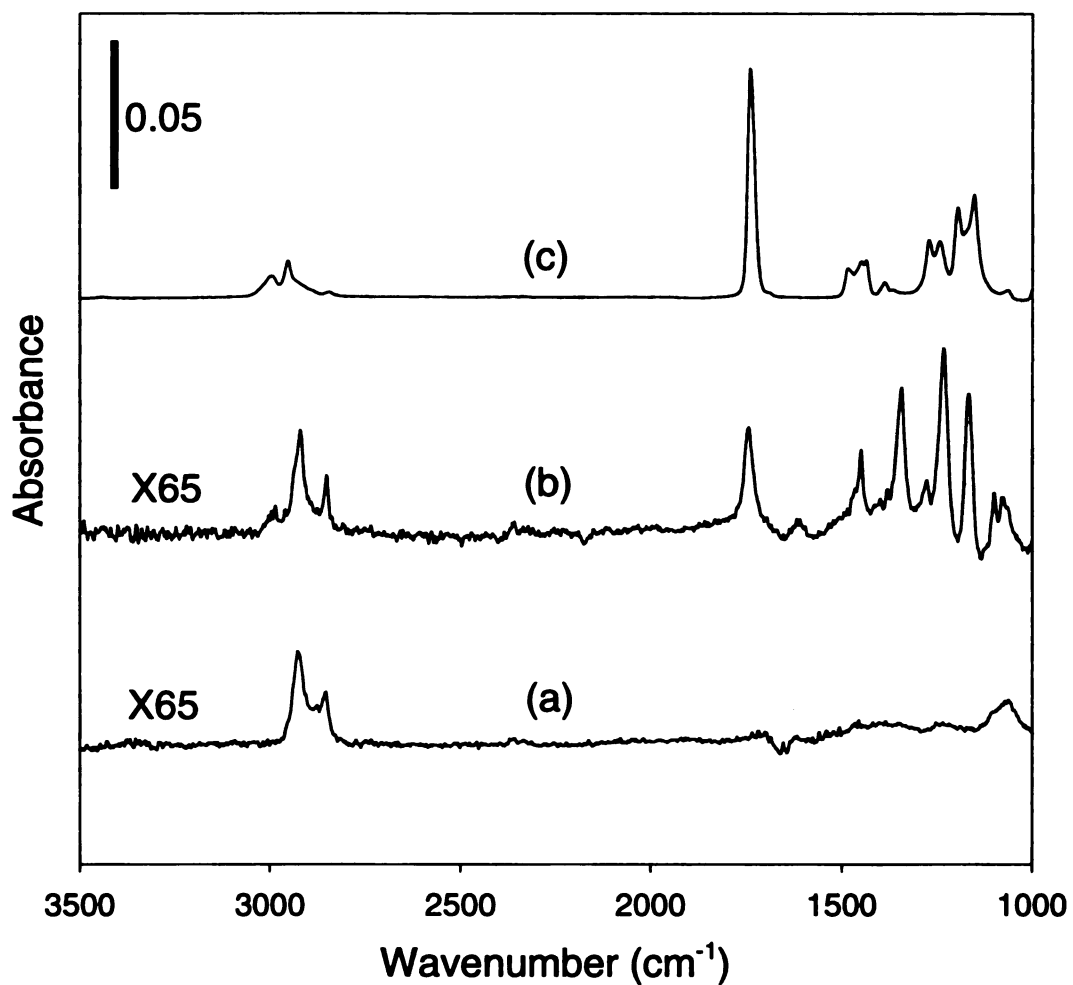
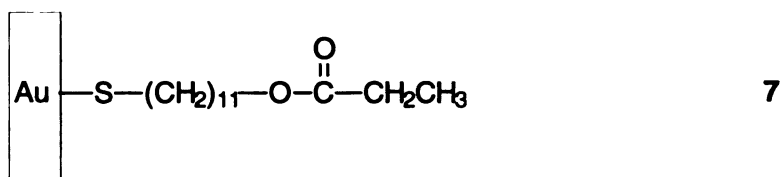


**Figure 2.2.** Reflectance FTIR spectra of (a) a SAM of MUD (4), (b) initiator immobilized on a MUD SAM (5), and (c) a grafted PMMA layer on the initiator surface (6).

### III. Control Experiment

To show that MMA polymerization only occurs on surfaces with immobilized initiators, **7** was prepared by the immersion of **4** in a solution of 0.1 M propionyl chloride and pyridine for 2 min. Thus, the only difference between the initiator-immobilized surface (**5**) and the control surface (**7**) is the existence of the  $\alpha$ -bromocarbonyl functionality that acts as a radical initiator for ATRP.



The evidence for the synthesis of **7** is again based on the appearance of an ester carbonyl peak at  $1746 \text{ cm}^{-1}$  (**Figure 2.3**, spectrum b). A control polymerization was carried out on **7** under the same polymerization conditions used with **5**. Ellipsometry and FTIR confirm that no polymerization occurs on this surface. There was no change in the thickness of the organic layer or in the IR intensity of the carbonyl peak after the polymerization (**Figure 2.3**, spectrum c).

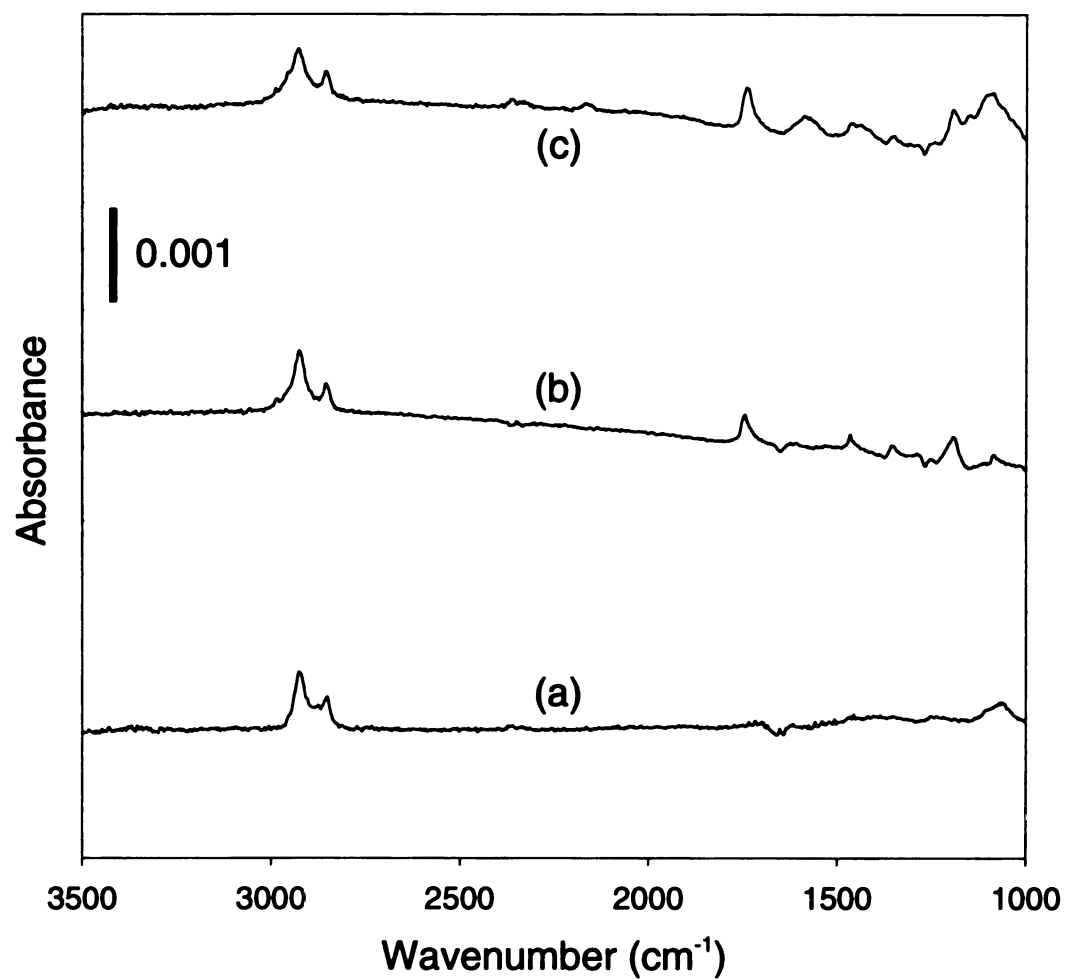


**Figure 2.3.** Reflectance FTIR spectra of (a) a SAM of MUD (4), (b) propionyl group anchored MUD SAM (7), and (c) after surface polymerization.

#### IV. Molecular Weight Determination

To determine the molecular weight and polydispersity of the grafted brushes, the PMMA chains were detached from the surface using  $I_2$ , and characterized by GPC (Figure 2.4). For the 370 Å-thick film, GPC yields an  $M_n$  of 44,500 and a PDI of 1.3. As shown in Table 1, these polymerizations are very repeatable.

**Table 2.1.** Molecular weight of PMMA brushes

PMMA film thickness (Å)	$M_n$	PDI ( $M_w/M_n$ )
331	33,100	1.3
370	44,500	1.3
402	68,900	1.5

\* The thickness of PMMA films was measured by ellipsometry, and the number average molecular weights ( $M_n$ ) of PMMA chains are relative to PMMA standard samples.

Since the detached PMMA brushes should exist as disulfides,<sup>24</sup> the S-S bonds were cleaved with  $NaBH_4$ <sup>25</sup> and the GPC measurements were repeated. The same  $M_n$  value and PDI were obtained, which implies that the disulfides ( $R_1S-SR_2$ ), if formed, are likely to be unsymmetrical disulfides formed from the PMMA chain and a MUD molecule that was buried by the growing PMMA brushes during polymerization. Thus,  $M_n$  only depends on the length of the PMMA brush since the molecular weight of the short chain thiolate is negligible compared to that of the PMMA brush. Based on the film thickness and  $M_n$ , ~10% of the surface-bound initiators actually initiate PMMA chains,

and thus each PMMA brush is surrounded by 9 short chain thiolates. Thus it is natural that a polymer brush desorbs as an unsymmetrical disulfide.

Using the  $M_n$  value from GPC analysis, the average cross-sectional area was calculated. For the calculation,  $A_x = M/\rho t N_A$  was used, where  $A_x$  is the average cross-sectional area of polymer chain,  $M$  is the molecular weight of the chain,  $\rho$  is the density of PMMA ( $1.1 \text{ g/cm}^3$ ),  $t$  is the polymer thickness, and  $N_A$  is Avogadro's number. The average cross-sectional area calculated by this method is  $\sim 180 \text{ \AA}^2$ . This result suggests a high grafting density, and is consistent with results of Shah *et al.*<sup>17</sup> Using the polymer that formed in solution as a proxy, they used  $M_n$  to calculate an average cross-sectional area of  $\sim 200 \text{ \AA}^2/\text{chain}$ . AFM and ellipsometry show that these films are both macroscopically and microscopically uniform. After grafting of PMMA, the surface roughness decreased from 1.92 nm (bare gold) to 0.54 nm (gold with grafted PMMA) as shown in **Figure 2.5**.

## V. Conclusions

There are several advantages in using room-temperature ATRP for “grafting from” surfaces. First, the process is compatible with substrates that are sensitive to high polymerization temperatures. Second, a simple washing step *without* Soxhlet extraction gives clean polymeric thin films because polymer chains grow only on the surface. There should be no polymerization in solution as long as there is no chain transfer from surface propagating sites to solution. Thus, thermal polymerization will be negligible at RT. NMR analysis showed no signs of polymerization in solution. This implies that the

monomer could be recovered from solution and reused. Perhaps the biggest advantage of this technique is the high grafting density of polymer brushes, which results in films that are uniform at the Å level.

In conclusion, ambient temperature ATRP using Me<sub>6</sub>TREN allows successful synthesis of dense chemically bound PMMA brushes on gold surfaces. The polymer films are uniform over large areas, and grow only on the surface without parallel formation of polymer in solution.

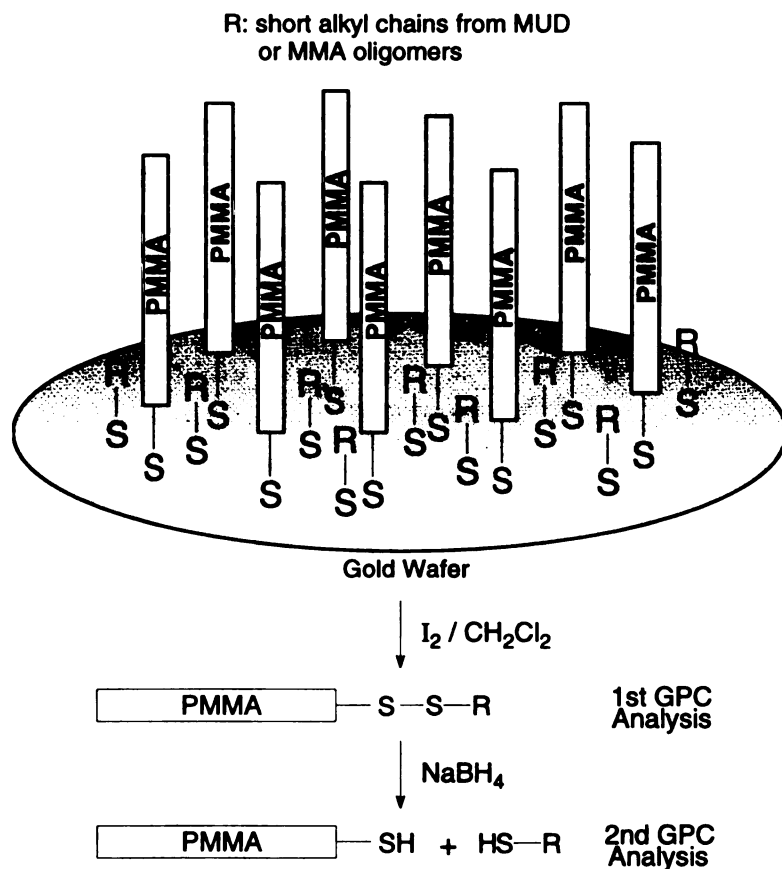


**Figure 2.4.** Detachment of polymer brushes from gold by I<sub>2</sub> treatment followed by molecular weight determination by GPC.

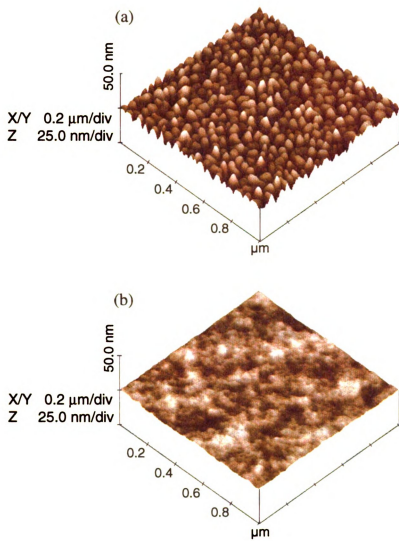


**Figure 2.5.** Tapping mode AFM images of (a) a bare gold surface and (b) PMMA brushes on gold. Images in this dissertation are presented in color.

## VI. References

- (1) Milner, S. T. *Science* **1991**, *251*, 905-914.
- (2) Huang, X.; Doneski, L. J.; Wirth, M. J. *CHEMTECH* **1998**, *28*, 19-25.
- (3) Bruening, M. L.; Zhou, Y.; Aguilar, G.; Agee, R.; Bergbreiter, D. E.; Crooks, R. M. *Langmuir* **1997**, *13*, 770-778.
- (4) Sidorenko, A.; Minko, S.; Schenk-Meuser, K.; Duschner, H.; Stamm, M. *Langmuir* **1999**, *15*, 8349-8355.
- (5) Prucker, O.; Naumann, C. A.; Rhe, J.; Knoll, W.; Frank, C. W. *J. Am. Chem. Soc.* **1999**, *121*, 8766-8770.
- (6) Bridger, K.; Vincent, B. *Eur. Polym. J.* **1980**, *16*, 1017-1021.
- (7) Husseman, M.; Malmstrm, E. E.; McNamara, M.; Mate, M.; Mecerreyes, D.; Benoit, D. G.; Hedrick, J. L.; Mansky, P.; Huang, E.; Russell, T. P.; Hawker, C. J. *Macromolecules* **1999**, *32*, 1424-1431.
- (8) Herrmann, W. A.; Stumpt, A. W.; Priermeier, T.; Bogdanovic, S.; Dufaud, V.; Basset, J.-M. *Angew. Chem., Int. Ed. Engl.* **1997**, *35*, 2803-2805.
- (9) Prucker, O.; Rhe, J. *Macromolecules* **1998**, *31*, 592-601.
- (10) Jordan, R.; Ulman, A. *J. Am. Chem. Soc.* **1998**, *120*, 243-247.
- (11) Jordan, R.; Ulman, A.; Kang, J. F.; Rafailovich, M. H.; Sokolov, J. *J. Am. Chem. Soc.* **1999**, *121*, 1016-1022.
- (12) Husemann, M.; Mecerreyes, D.; Hawker, C. J.; Hedrick, J. L.; Shah, R.; Abbott, N. L. *Angew. Chem., Int. Ed.* **1999**, *38*, 647-649.

- (13) Jeon, N. L.; Choi, I. S.; Whitesides, G. M.; Kim, N. Y.; Laibinis, P. E.; Harada, Y.; Finnie, K. R.; Girolami, G. S.; Nuzzo, R. G. *Appl. Phys. Lett.* **1999**, *75*, 4201-4203.
- (14) Ejaz, M.; Yamamoto, S.; Ohno, K.; Tsujii, Y.; Fukuda, T. *Macromolecules* **1998**, *31*, 5934-5936.
- (15) Zhao, B.; Brittain, W. J. *J. Am. Chem. Soc.* **1999**, *121*, 3557-3558.
- (16) Matyjaszewski, K.; Miller, P. J.; Shukla, N.; Immaraporn, B.; Gelman, A.; Luokala, B. B.; Siclovan, T. M.; Kickelbick, G.; Vallant, T.; Hoffmann, H.; Pakula, T. *Macromolecules* **1999**, *32*, 8716-8724.
- (17) Shah, R. R.; Merreceyes, D.; Husemann, M.; Rees, I.; Abbott, N. L.; Hawker, C. J.; Hedrick, J. L. *Macromolecules* **2000**, *33*, 597-605.
- (18) Bain, C. D.; Troughton, E. B.; Tao, Y. T.; Evall, J.; Whitesides, G. M.; Nuzzo, R. G. *J. Am. Chem. Soc.* **1989**, *111*, 321-335.
- (19) Schlenoff, J. B.; Li, M.; Ly, H. *J. Am. Chem. Soc.* **1995**, *117*, 12528-12536.
- (20) Camillone, N., III; Chidsey, C. E. D.; Liu, G. Y.; Scoles, G. *J. Chem. Phys.* **1993**, *98*, 3503-3511.
- (21) de Boer, B.; Simon, H. K.; Werts, M. P. L.; van der Vegte, E. W.; Hadziioannou, G. *Macromolecules* **2000**, *33*, 349-356.
- (22) Xia, J.; Gaynor, S. G.; Matyjaszewski, K. *Macromolecules* **1998**, *31*, 5958-5959.
- (23) Ciampolini, M.; Nardi, N. *Inorg. Chem.* **1966**, *5*, 41-44.
- (24) Templeton, A. C.; Hostetler, M. J.; Kraft, C. T.; Murray, R. W. *J. Am. Chem. Soc.* **1998**, *120*, 1906-1911.
- (25) Stahl, C. R.; Siggia, S. *Anal. Chem.* **1957**, *29*, 154-155.

## Chapter 3

# Kinetic Study of Surface-initiated Atom Transfer Radical Polymerization from Flat Surfaces

### I. Introduction

This chapter describes elucidation of the termination mechanism of surface-initiated atom transfer radical polymerization (ATRP). To demonstrate the dependence of kinetics on radical concentration, polymer brushes were synthesized at different catalyst concentrations. The surface-initiated ATRP of methyl methacrylate (MMA) with no addition of  $\text{Cu(II)Br}_2$  showed rapid initial growth followed by early termination, whereas polymerization with initial addition of  $\text{Cu(II)Br}_2$  and use of a  $\text{CuCl}$  catalyst showed less deviation from ideal, constant growth. For a given reaction time, there is a specific catalyst concentration that yields maximum film thickness. Reduction in film thickness when stirring the solution suggests that stirring increases chain mobility and enhance termination by recombination. Solution phase ATRP of MMA was also tested to study early stages of polymerization kinetics and the evolution of molecular weight.

Because Atom Transfer Radical Polymerization (ATRP) normally gives polymers with narrow molecular weight distributions, it has become one of the most popular polymerization methods for vinyl monomers such as acrylates, methacrylates, and styrene.<sup>1</sup> ATRP also offers additional advantages when used to grow polymers from surfaces.<sup>2-4</sup> The thickness of grafted polymer brushes is easily controlled by varying reaction time, and in the absence of added free initiator and chain transfer, polymer

chains grow only from the surface. This reduces the purification procedure to a simple rinsing of the polymer surface.<sup>5</sup> In some cases, surface-initiated ATRP can proceed even at ambient temperature in both organic<sup>6</sup> or aqueous media.<sup>7,8</sup> ATRP is a controlled/living process, and thus a surface-confined polymerization can be quenched and re-initiated to synthesize multi-block copolymer brushes.<sup>9</sup> Polymer thin films tethered through covalent bonds can be prepared by surface-initiated polymerizations, and the resulting thin polymer films can be used to modify and control surface properties.<sup>10</sup> Tethered polymer films have many potential applications including anticorrosion layers, chemical separations, control of surface wetting and morphology, and as a route to nanostructured surfaces.<sup>11-16</sup>

In surface-initiated radical polymerizations, there have been some reports of radical termination. The kinetics and mechanism of surface-initiated free radical polymerization were investigated by Prucker and Ruhe.<sup>18</sup> They confirmed that the immobilization of the azo initiator does not alter initiator properties significantly because the observed initial rates of polymerization are in close agreement with those in the polymerization of bulk styrene with 2,2'-azobisisobutyronitrile (AIBN). They also noted that the main differences between surface and solution polymerizations are mostly due to changes in termination reactions. The concentration of growing radicals on a surface increases with elevated temperature, resulting in an increased probability of termination of growing radicals by recombination or disproportionation because the radicals on a surface are located in close vicinity. For the same polymerization system, Minko *et al.* predicted that termination between surface free radicals can occur when initiation is

rapid.<sup>19</sup> Very soon after the start of polymerization, however, termination will decrease greatly as the concentration of surface free radicals decreases.

Matyjaszewski *et al.* simulated the kinetics of surface-initiated polymerization,<sup>5</sup> and concluded that initiator coverage ( $\theta$ ) is a major factor in defining whether the growth in layer thickness depends linearly on reaction time. High densities of surface-immobilized initiators ( $\theta > 0.5$ ) lead to a nonlinear dependence of conversion on time and a much broader distribution in chain length. They predicted that distributions might become even broader for systems with additional bimolecular activation/ deactivation equilibria (ATRP, for example) because the bimolecular processes require diffusion of catalysts and monomer to the chain ends. Niwa *et al.* also observed that surface polymerization depends on initiator coverage.<sup>20</sup> Polymerization hardly proceeded when the surface coverage of a photoactive xanthate was high ( $\theta \approx 1$ ).  $R_p$  showed the smallest value at  $\theta = 1$ , and with decreasing  $\theta$ ,  $R_p$  gradually increased and gave a maximum value at  $\theta = 0.2$ . These results are good indications that a high radical concentration on two-dimensional surfaces results in extensive termination.

Plots of polymer film thickness as a function of polymerization time are similar for surface-initiated free radical polymerization (FRP) and ATRP.<sup>21</sup> The similarity between ATRP and FRP kinetics suggests that termination of growing chain ends. Since the presence of two growing radicals next to each other or in close proximity is a matter of probability, it might be impossible to avoid termination by recombination of two radicals. Interestingly, Prucker and R  he showed that in thermally induced surface radical polymerization the film thickness decreases as polymerization temperature increases. To understand these observations, the authors noted that the film thickness

depends on both the number of polymer chains attached to surface and the molecular weight of these chains. They suggested that too high concentration of radicals on surface at high temperature can not yield maximum thickness because termination reaction becomes serious during polymerization.

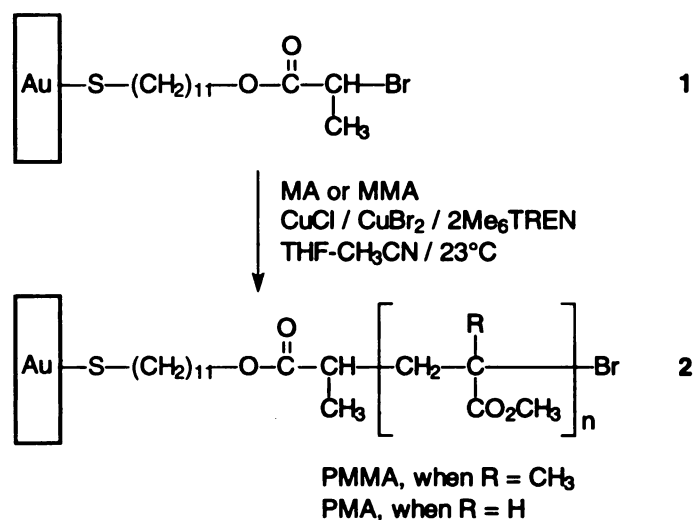
To date, most research on surface-initiated ATRP focused on the synthesis, characterization, and application of grafted polymer layers, while systematic kinetic studies are rare. Because polymerization kinetics depend on the concentrations of catalytic system, temperature, solvent polarity, and mixing/diffusion effects, polymerization from a two-dimensional surface and solution polymerizations could show quite different kinetic behavior. Even though there have been suggestions in the literature that termination reactions significantly impact on polymer brush growth, the termination mechanism of surface polymerization is not well understood. Here, we report kinetic data for surface-initiated ATRP of methyl methacrylate (MMA) and methyl acrylate (MA) to help elucidate the dominant termination mechanism in surface polymerizations.

## II. Dependence of Polymer Film Growth on Radical Concentration

**Scheme 3.1** shows the preparation of PMMA brushes grafted on gold. The self-assembled monolayer initiator, **1** was prepared using a literature procedure.<sup>6</sup> To perform ATRP, **1** was immersed in a solution of MMA or MA at 23 °C containing the copper catalyst, prepared *in situ* from the appropriate copper halides and ligands. The formation of polymer brushes is apparent from the increase in the ellipsometric thickness of the

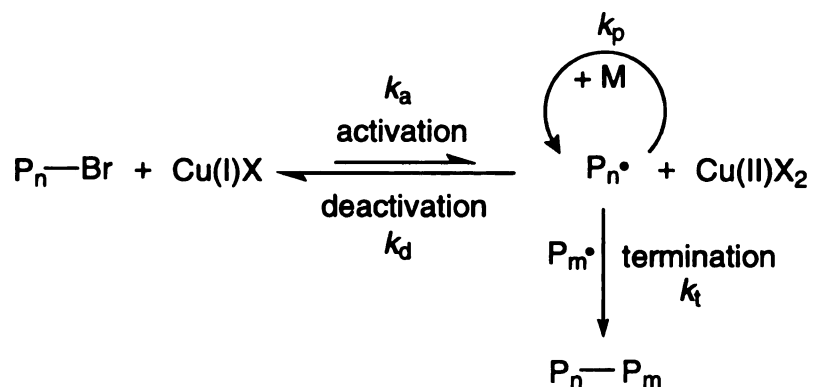
organic layer and the appearance of large carbonyl peaks at 1743–1745  $\text{cm}^{-1}$  in the reflectance FTIR spectrum.

**Scheme 3.1.** Surface-initiated ATRP of (meth)acrylates on gold



ATRP (**Scheme 3.2**) is described as a “living/controlled” radical polymerization because the irreversible termination reactions that consume radicals are suppressed. In the absence of termination, one should observe a linear growth in the thickness of polymer films during surface-initiated ATRP. Shown in **Figure 3.1a** is the evolution of thickness during the surface-initiated ATRP of MMA using CuBr/Me<sub>6</sub>TREN as the catalyst and without added CuBr<sub>2</sub>.

**Scheme 3.2.** Kinetic scheme for ATRP: pathways for radical generation and consumption



Contrary to expectation, the data show a rapid initial growth followed by a decline in the growth rate and cessation of film growth by 10 hr. Similar kinetic data were reported by Ejaz *et al.* for the surface-initiated ATRP of MMA from SAMs of immobilized *p*-toluenesulfonyl chloride,<sup>22</sup> and Jones and Huck reported that surface-initiated ATRP of acrylates and methacrylates slowed down and lost their controlled character at long reaction times.<sup>16</sup> In their study of the surface-initiated ATRP of HEMA in water, they also observed rapid growth at early stages of the polymerization and termination after about 60 min. This behavior can be explained by the loss of active catalyst, or through the loss of surface initiating sites, most likely through the recombination of two growing radicals.

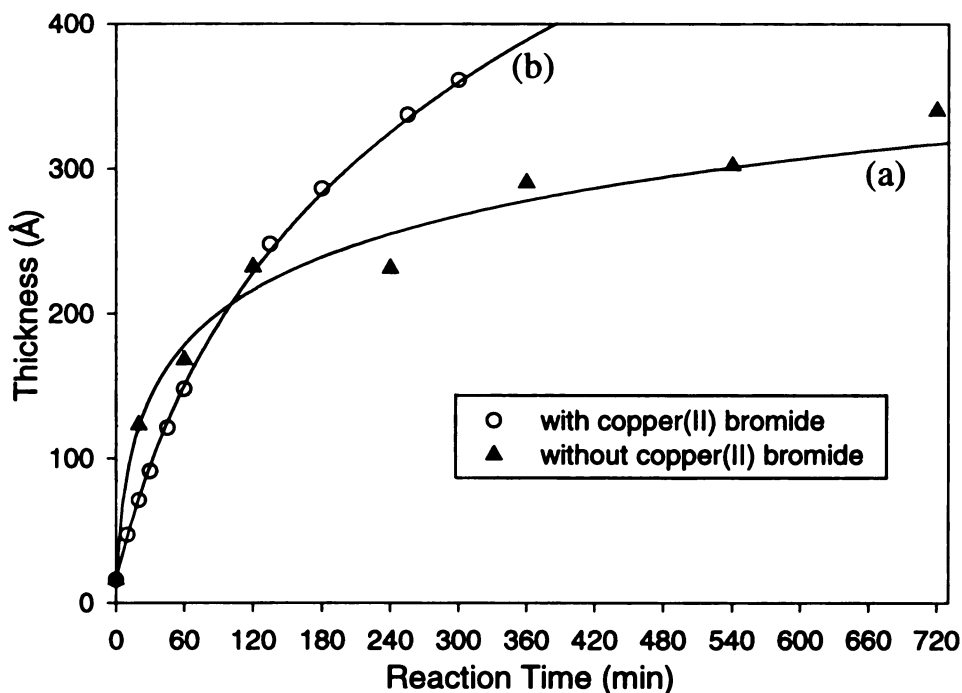


**Figure 3.1.** Dependence of PMMA film growth on the presence of  $\text{Cu(II)Br}_2$ : (a) without initial addition of  $\text{Cu(II)Br}_2$  and (b) with initial addition of  $\text{Cu(II)Br}_2$

Two publications related to surface-initiated ATRP display plots of grafted polymer thickness vs polymerization time. ATRP of a sugar-carrying methacrylate using  $\text{CuBr}/4,4'$ -di-*n*-heptyl-2,2'-bipyridine catalyst showed curvature<sup>2</sup> similar to that of **Figure 3.1**, while ATRP of methyl acrylate using  $\text{CuBr-CuBr}_2/\text{N,N,N',N'',N''}$ -pentamethyldiethylenetriamine (PMDETA) catalysts showed a linear growth of polymer thickness until  $\sim 6$  hr.<sup>5</sup> The curvature seen in the first case is consistent with some portion of surface-initiators being lost during polymerization by termination reactions, while the linear growth observed in the second example may reflect choices of monomer structure, catalytic system, and reaction media, that minimize the radical concentration and

recombination reactions. According to Wittmer's suggestion for surface-initiated polymerization, longer chains compete more effectively for access to monomers than shorter chains, resulting in a wider molecular weight distribution, compared to the same polymerization in solution.<sup>23</sup> However, the polydispersities of polymer chains detached from surfaces,<sup>3,6,9,17</sup> did not show the expected wide molecular weight distribution. Thus, termination of growing radicals seems to be the major factor that determines kinetics of surface polymerization and molecular weight distribution of final polymers.

To confirm the loss of surface initiating sites and rule out loss of catalyst activity, 5 samples were collected at various stages during a surface polymerization. The samples were rinsed with THF, dried under a stream of nitrogen, and the film thickness for each sample was measured by ellipsometry (filled triangles, **Figure 3.2**). Each sample was then immersed in a solution of monomer with fresh catalyst. For this "regrowth" process the concentration of the catalyst was reduced and  $\text{CuBr}_2$  was added to promote thicker film growth. After 4 hours, the samples were removed from the reaction vials and immediately washed with THF. As shown in **Figure 3.2a'** (hollow triangles), the thickness added (equal to the length of the arrows) during the regrowth process was largest for the 30 min sample, and decreased as the contact time with the catalyst increased. Since the change in film thickness is a proxy for the number of surface-bound initiators, the data are consistent with a continuous loss of surface-bound initiators through radical disproportionation or coupling during ATRP.

Termination by disproportionation generates a saturated chain end and a polymer chain end that contains a double bond. Disproportionation was excluded as a termination mechanism since no bands were detected by surface reflectance FTIR near 1620–1670

$\text{cm}^{-1}$  that could be attributed to C=C stretching. The loss of the double bonds via polymerization also was discounted since that process should lead to cross-linking, and only soluble products were obtained. As described in Chapter 2, we successfully used iodine to detach polymer brushes from similar surfaces, which demonstrates that there is no significant cross-linking between polymer chains. However, iodine treatment failed to detach cross-linked polymer films of poly(ethyleneglycol dimethacrylate) and PHEMA layers. Thus the data are consistent with termination by coupling.

To test whether the observed kinetic behavior is specific to surface polymerization, we carried out a comparable solution phase ATRP at room temperature as a control. As shown in the first order kinetic plot (**Figure 3.3a**) the solution polymerization using Cu(I)Br/Me<sub>6</sub>TREN as the catalyst shows qualitatively the same trends seen in the surface polymerizations, indicating that termination also is a problem in solution polymerization. This kinetic plot resembles simulations of solution ATRP that include termination,<sup>27</sup> but the experimental plot shows less curvature.

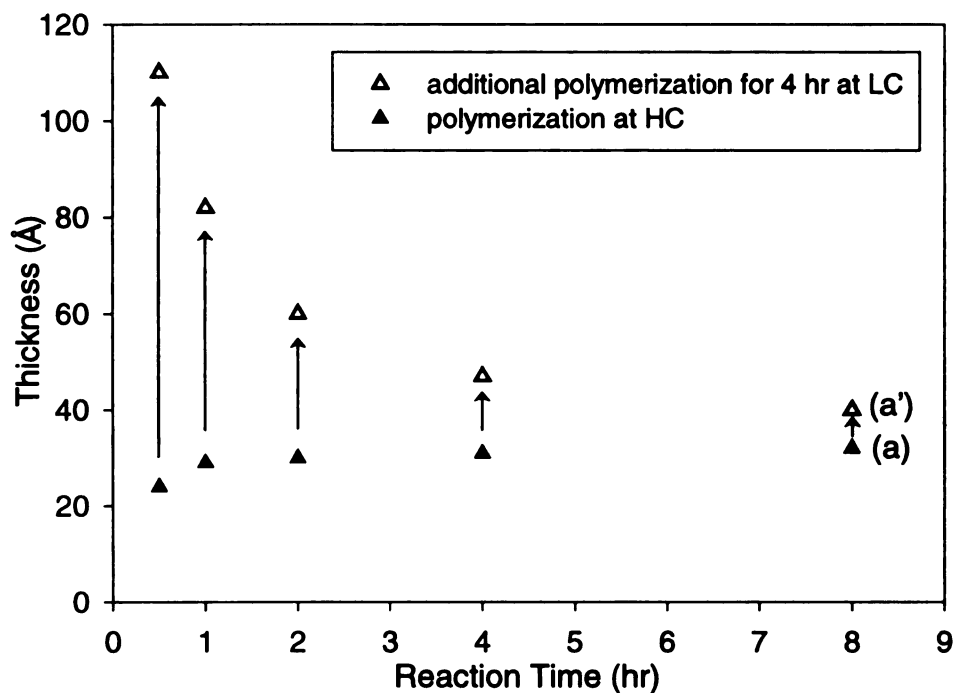


**Figure 3.2.** Dependence of additional PMA film growth on the amounts of remaining surface-initiating sites: (a) represents the same polymerization shown in Figure 3.4 and (a') the reused samples after polymerization for 4 hr at [MA] 2 M, [CuCl/Me<sub>6</sub>TREN] 40 mM, [CuBr<sub>2</sub>/Me<sub>6</sub>TREN] 12 mM. The thickness of the PMA film was measured by ellipsometry at two different spots on a sample and averaged. The thickness deviations for the samples are within  $\pm 2$  Å

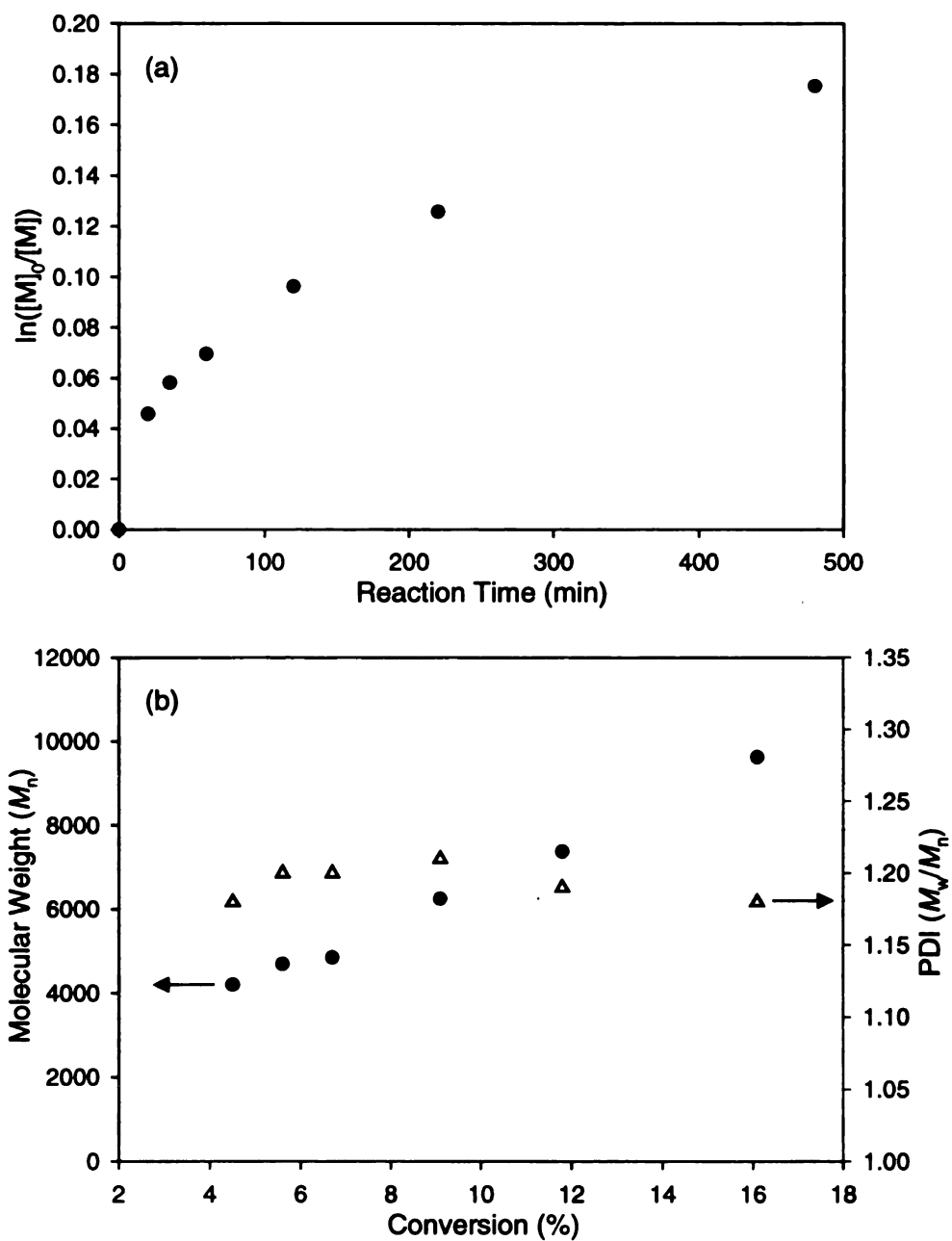


**Figure 3.3.** Solution phase ATRP results: (a) first order kinetic plot of MMA polymerization and (b) molecular weight and distribution of polymers.

The data in **Figure 3.3b** show a near-linear increase in molecular weight and a PDI of  $\sim 1.20$ . This suggestion of control must be tempered with the non-zero y-intercept for the  $M_n$  data, which is consistent with poor control in the 0–6 % conversion range. The higher than expected molecular weight must reflect an inefficient deactivation step, and substantial termination. The high activity of the Cu(I)Br/Me<sub>6</sub>TREN system<sup>24</sup> enables room temperature ATRP, but complete control over the polymerization has not yet been achieved. Since avoiding termination might not be possible, minimizing termination could be a more realistic goal.

In ATRP, control over the polymer architecture depends on the fast reversible generation of radicals. Thus, a suitable concentration of a soluble Cu(II)Br<sub>2</sub> deactivator is essential. Most homogeneous ATRPs do not require the addition of Cu(II)Br<sub>2</sub> to the polymerization since the concentration of the deactivator automatically builds up at early stages in the polymerization. In surface-initiated ATRP, however, the absolute amount of initiator on the surface is small, and thus the concentration of Cu(II)Br<sub>2</sub> formed in solution will be negligible. Once radicals are generated on the surface, they cannot easily revert to their dormant state and eventually they will terminate by coupling. Exacerbating coupling is the confinement of the surface initiators to a layer, which ensures that radicals on the surface will be in close proximity. Thus addition of Cu(II)Br<sub>2</sub> at the beginning of the reaction is indispensable for reversible radical generation, and suppression of radical termination reactions.

To try to achieve a more linear growth rate, Cu(I)Br was replaced by Cu(I)Cl and Cu(II)Br<sub>2</sub> was added at the beginning of the polymerization. Mixed halide systems (R-Br/CuCl) effectively slow the polymerization rate and reduce termination<sup>25</sup> by

maintaining a lower concentration of growing radicals. The resulting polymerization kinetics showed less deviation from linear growth (**Figure 3.1b**), but the curvature indicated that termination was still significant.

In principal, a sufficiently high  $k_{deact}$  should reduce the steady state concentration of radicals to the point where bimolecular termination processes are unlikely. At the same time, however, the rate of polymerization may be reduced to impractical levels. Thus, for a given polymerization time, there should be an optimum set of reaction conditions that lead to the thickest polymer brush. Shown in **Figures 3.4** and **3.5** are the results from a series of surface initiated ATRPs of MA run at different catalyst concentrations. In each polymerization, the ratio of the Cu(I) catalyst and the Cu(II)Cl<sub>2</sub> deactivator was held constant. At the highest catalyst concentration (plot a in **Figure 3.4**), there was almost no growth of PMA, but the thickness of the polymer film increased with decreases in catalyst concentration. At even lower catalyst concentrations, (plots d and e), the rate of film growth slowed considerably but showed relatively linear growth over an 8 hour period. These data are consistent with chain termination via coupling playing an important role in defining the film growth profile. Given the two-dimensional nature of surface-bound initiators, one can envision that high concentrations of catalyst lead to a spatially dense concentration of surface-tethered radicals that recombine easily. Thus,  $[R\bullet]$  is generally not constant and polymer film growth fails to follow first order kinetics.

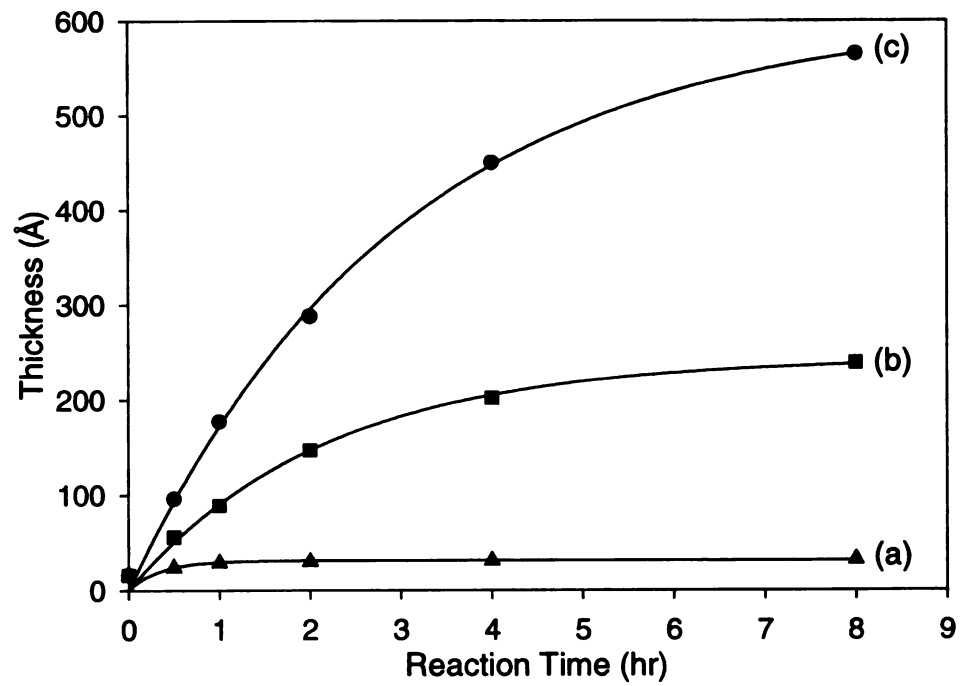
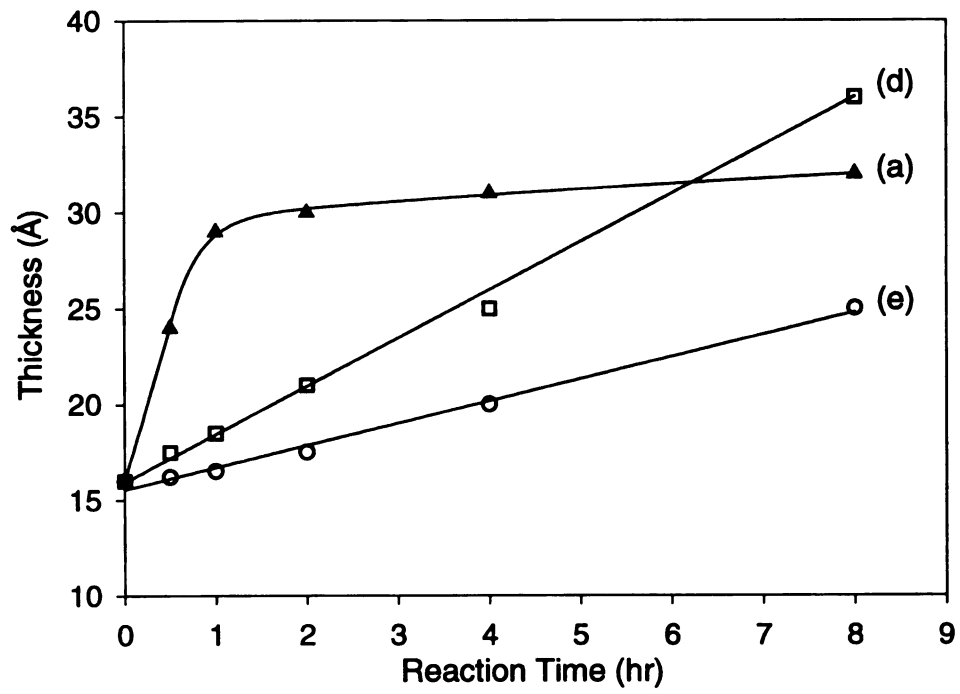


**Figure 3.4.** Growth of PMA layer thickness vs polymerization time: (a) [MA] 2 M, [CuCl/Me<sub>6</sub>TREN] 40 mM, [CuBr<sub>2</sub>/Me<sub>6</sub>TREN] 12 mM; (b) [MA] 2 M, [CuCl/Me<sub>6</sub>TREN] 2 mM, [CuBr<sub>2</sub>/Me<sub>6</sub>TREN] 0.6 mM; (c) [MA] 2 M, [CuCl/Me<sub>6</sub>TREN] 0.1 mM, [CuBr<sub>2</sub>/Me<sub>6</sub>TREN] 0.03 mM; (d) [MA] 2 M, [CuCl/Me<sub>6</sub>TREN]  $5 \times 10^{-3}$  mM, [CuBr<sub>2</sub>/Me<sub>6</sub>TREN]  $1.5 \times 10^{-3}$  mM; (e) [MA] 2 M, [CuCl/Me<sub>6</sub>TREN]  $2.5 \times 10^{-4}$  mM, [CuBr<sub>2</sub>/Me<sub>6</sub>TREN]  $7.5 \times 10^{-5}$  mM. Surface-initiated ATRP was done without stirring in a (1:1) mixture of CH<sub>3</sub>CN-THF at 23 °C, and in drybox. The thickness of the PMA film was measured by ellipsometry at two different spots on a sample and averaged. The thickness deviations for the samples are within  $\pm 2$  Å.

To validate the idea that polymerizations from surface-immobilized initiators can be optimized to yield maximum growth of polymer film for a specific reaction time, we plot in **Figure 3.5** data from polymerizations run for 4 hours at various catalyst concentrations. The observance of an optimum catalyst concentration is reminiscent of data for the UV-initiated polymerization of styrene from surface-bound azo initiators.<sup>21</sup> In that case, the optimum light intensity represents a balance between propagation rate and the irreversible termination of radicals.

A computer simulation was designed to model the temporal variation in the surface radical concentration and the observed polymer brush growth rate. A suitable model would enable accurate prediction of the Cu (I) and Cu (II) concentrations needed to attain the desired rate of polymerization and the final polymer brush thickness. The growth process was divided into short time intervals and the concentration of active chain ends, [R•] was calculated for that interval. We assumed that the cumulative concentration

of active chain ends,  $[R\bullet]$  is proportional to the final thickness of the polymer brushes, i.e. the monomer concentration is constant.

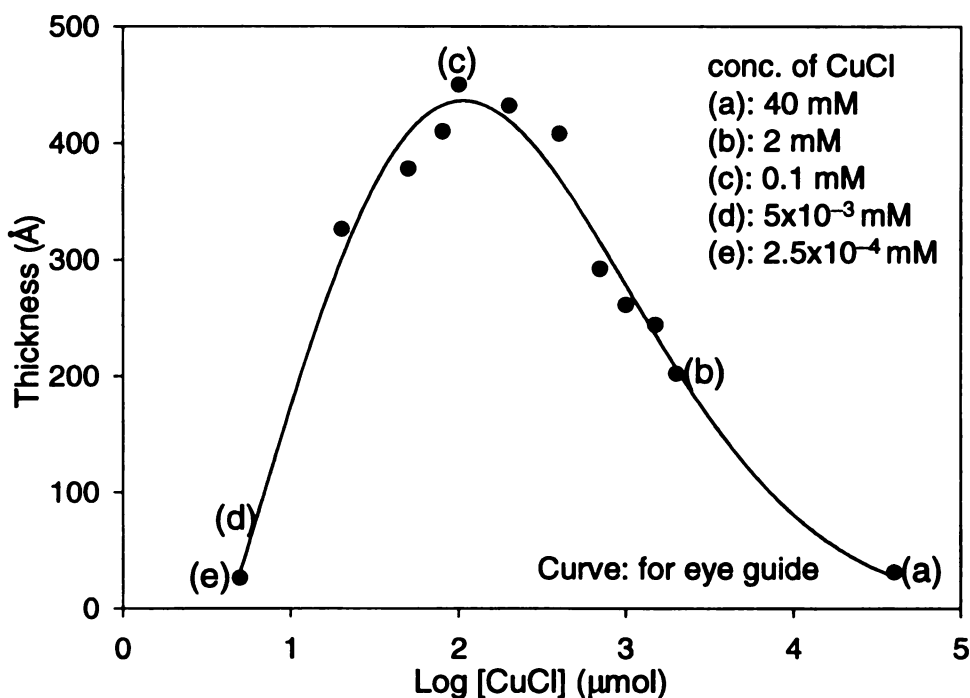


**Figure 3.5.** Optimum catalyst concentration that yields the thickest PMA film after 4 hr of polymerization. (a)–(e) 30 mol% of  $\text{CuBr}_2$  relative to CuCl was used for each polymerization.

Based on the ATRP kinetic scheme depicted in **Scheme 3.2**, the change in the radical concentration with time,  $d[R\bullet]/dt$  (equation 3) can be described by three terms, the rate of radical generation via the reaction of Cu(I) with initiator, and the loss of radicals through deactivation and bimolecular termination.

$$\frac{d[\text{R}\bullet]}{dt} = k_a[\text{RBr}][\text{CuX}] - k_d[\text{R}\bullet][\text{CuX}_2] - k_t[\text{R}\bullet]^2 \quad (3)$$

Different values of  $k_a$ ,  $k_d$ , and  $k_t$ <sup>26</sup> were tested in the simulation, with  $k_a = 0.8$  L/mol·sec,  $k_d = 1 \times 10^5$  L/mol·sec, and  $k_t = 1 \times 10^9$  L/mol·sec giving the best fit to the experimental data. The Cu(I)/Cu(II) concentrations used in the simulation match those used in the experiments (runs a-e of **Figure 3.4**). The simulation results are plotted in **Figure 3.6**.

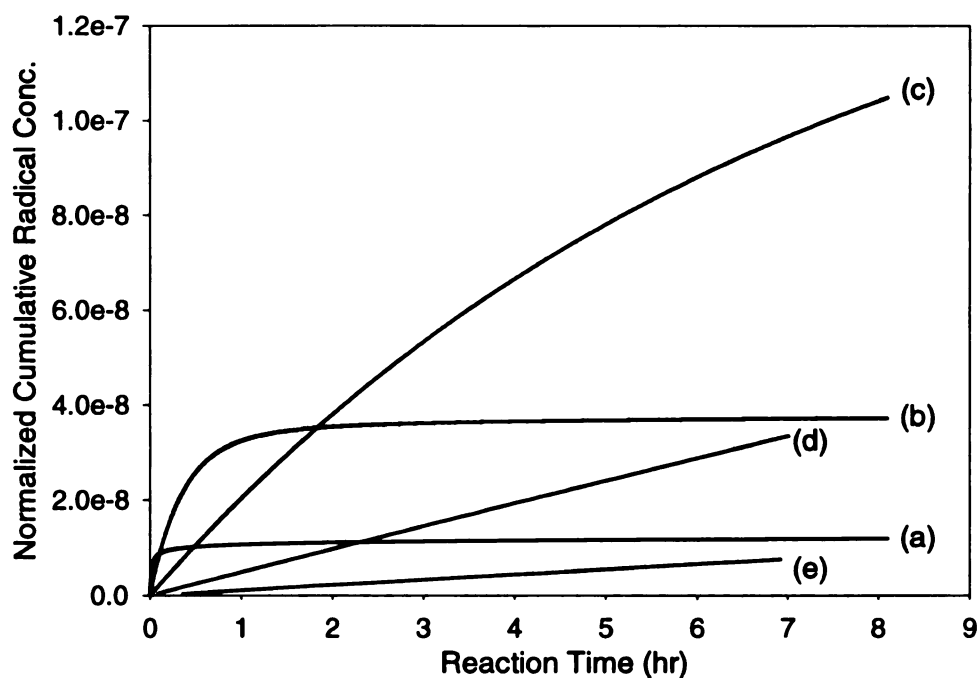


**Figure 3.6.** Simulation of surface-tethered radical concentrations as a function of catalyst concentration: the same values of copper concentrations as in **Figure 3.4** were used for (a), (b), (c), (d) and (e).

The simulations capture the general trends seen in the experimental data, although they show some deviation from the experimental data. For example, runs a, b, and c all have the same initial growth rate, while the simulation of run c yields a lower initial slope. Also, run d crosses run a earlier in the simulation than is seen in the experimental data. The most likely explanation is that the simulation fails to capture all of the details of the surface polymerization. In particular, the model does not address the 2-dimensional nature of the surface-bound initiator layer at the beginning of polymer growth, and its evolution toward 3-dimensionality during polymerization. As shown in **Figure 3.7**, the chain ends are in close proximity in surface polymerizations, enhancing the likelihood of termination. In addition, the rate constants for radicals tethered to surfaces may deviate from those measured in solution. The simulations also show that the linear growth seen for runs d and e does not correspond to a controlled polymerization. These polymerizations are better described as steady state systems where  $[R\bullet]$  is constant.

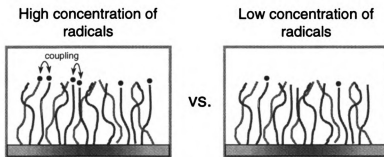


**Figure 3.7.** Influence of radical concentrations on the probability of recombination.

### III. Dependence of Polymer Film Growth on Stirring

In solution ATRP, a homogeneous solution of the deactivating complex is critical for control over the polymerization, and the use of a polar co-solvent to dissolve Cu(II) complexes and/or stirring is commonly used to ensure homogeneity during the polymerization. In contrast, polymerizations from surfaces are inherently heterogeneous since polymer growth is limited to a thin layer near the surface. It is plausible that access to monomer, catalyst, or deactivating agent may be diffusion-limited and the kinetics of surface-initiated polymerizations may be different from homogeneous reactions in solution. **Figure 3.8** shows two polymerizations designed to test for such effects. The evolution of the thickness of PMMA films with time are shown for polymerizations run without (plot a) and with stirring (plot b). The polymerization run with stirring reached a limiting thickness of  $\sim 200$  Å before 400 min, but a parallel reaction run in the absence of stirring (**Figure 3.8b**) grew to nearly twice the thickness in the same time. For the stirring experiments, we used a glass reactor shown in **Figure 3.9**.

The simulation results would suggest that the limiting thickness for the stirred reaction reflects more termination by coupling than the non-stirred reaction. One could argue that stirring increases the mobility of chain ends and improves the probability that two radicals to be located near each other, which results in early termination by recombination. An alternative mechanism is the formation of a Cu concentration gradient. If the Cu(II) formed by the activation process remains localized near the radical, then the rate of the deactivation process would be enhanced and the probability for termination by coupling would decrease.

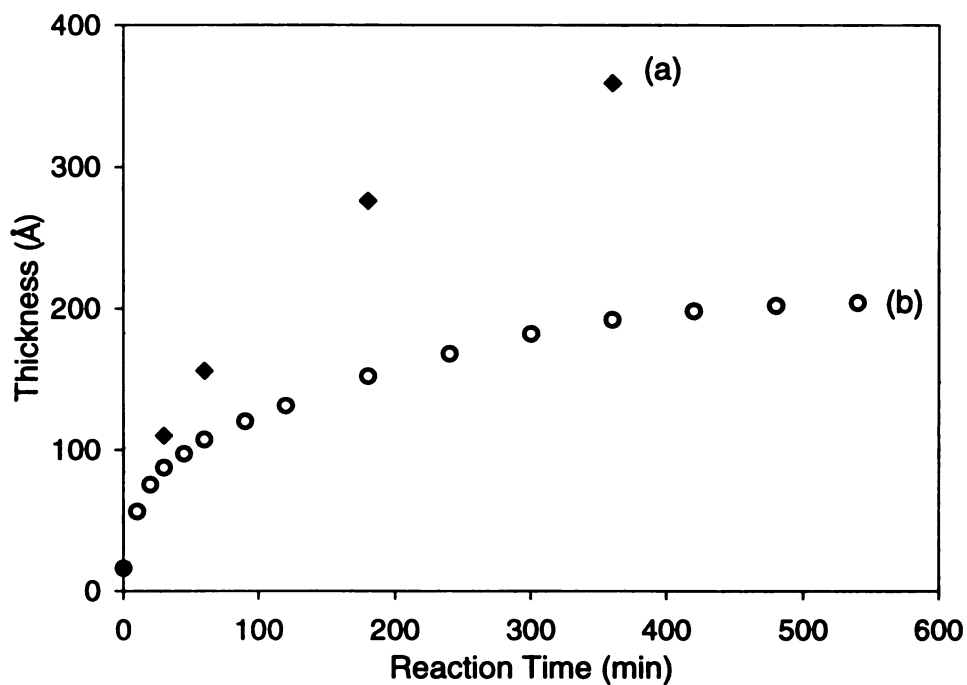


**Figure 3.8.** Growth of PMMA layer thickness vs polymerization time: (a) polymerization without stirring; (b) polymerization with stirring. Polymerization conditions for surface-initiated ATRP: [MMA] 2 M, [CuBr/Me<sub>6</sub>TREN] 2 mM, [CuBr<sub>2</sub>/2dnNbpy] 0.6 mM, in solvent mixture of CH<sub>3</sub>CN-THF (1:1), at 23 °C, and in drybox. The thickness of the PMMA film was measured by ellipsometry at three different spots on a sample and averaged. The thickness deviations for the samples without stirring and with stirring are  $\pm 4$  Å and  $\pm 9$  Å respectively.

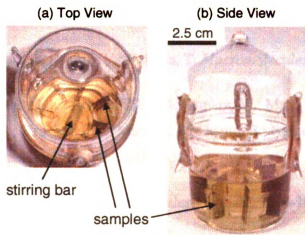


**Figure 3.9.** Digital images of the glass reactor used for polymerization with stirring. Images in this dissertation are presented in color.

#### IV. Conclusions

MMA polymerizations with stirring terminated after 6 hr, while the polymerizations without stirring showed faster growth during the same time period. The results might imply that stirring increases the mobility of chain ends and increases the chance that two radicals near each other meet and recombine, leading to termination. Polymerizations using high catalyst concentration (40 mM) showed almost no growth of PMA, while the polymerization using low catalyst concentration (0.1 mM) resulted in a thick PMA film. The results from polymerizations at different catalyst concentration indicate that the longer the samples are kept at high concentration of catalyst, the more initiators on surface are lost. Finally, it can be concluded that the major termination mechanism of surface-initiated ATRP is recombination.

## V. References

- (1) Matyjaszewski, K.; Xia, J. *Chem. Rev.* **2001**, *101*, 2921-2990.
- (2) Ejaz, M.; Ohno, K.; Tsujii, Y.; Fukuda, T. *Macromolecules* **2000**, *33*, 2870-2874.
- (3) Husseman, M.; Malmstroem, E. E.; McNamara, M.; Mate, M.; Mecerreyes, D.; Benoit, D. G.; Hedrick, J. L.; Mansky, P.; Huang, E.; Russell, T. P.; Hawker, C. *J. Macromolecules* **1999**, *32*, 1424-1431.
- (4) Huang, X.; Wirth, M. J. *Macromolecules* **1999**, *32*, 1694-1696.
- (5) Matyjaszewski, K.; Miller, P. J.; Shukla, N.; Immaraporn, B.; Gelman, A.; Luokala, B. B.; Siclovan, T. M.; Kickelbick, G.; Vallant, T.; Hoffmann, H.; Pakula, T. *Macromolecules* **1999**, *32*, 8716-8724.
- (6) Kim, J.-B.; Bruening, M. L.; Baker, G. L. *J. Am. Chem. Soc.* **2000**, *122*, 7616-7617.
- (7) Huang, W. X.; Baker, G. L.; Bruening, M. L. *Angew. Chem., Int. Ed.* **2001**, *40*, 1510-1512.
- (8) Huang, W.; Kim, J.-B.; Bruening, M. L.; Baker, G. L. *Macromolecules* **2002**, *35*, 1175-1179.
- (9) Kim, J.-B.; Huang, W.; Bruening, M. L.; Baker, G. L. *Macromolecules* Submitted.
- (10) Zhao, B.; Brittain, W. J. *Prog. Polym. Sci.* **2000**, *25*, 677-710.
- (11) Huang, X.; Doneski, L. J.; Wirth, M. J. *CHEMTECH* **1998**, *28*, 19-25.
- (12) Sedjo, R. A.; Mirous, B. K.; Brittain, W. J. *Macromolecules* **2000**, *33*, 1492-1493.

- (13) Zhao, B.; Brittain, W. J.; Zhou, W.; Cheng, S. Z. D. *Macromolecules* **2000**, *33*, 8821-8827.
- (14) Husemann, M.; Mecerreyes, D.; Hawker, C. J.; Hedrick, J. L.; Shah, R.; Abbott, N. L. *Angew. Chem., Int. Ed.* **1999**, *38*, 647-649.
- (15) Shah, R. R.; Mecerreyes, D.; Husemann, M.; Rees, I.; Abbott, N. L.; Hawker, C. J.; Hedrick, J. L. *Macromolecules* **2000**, *33*, 597-605.
- (16) Jones, D. M.; Huck, W. T. S. *Adv. Mater.* **2001**, *13*, 1256-1259.
- (17) Prucker, O.; Ruehe, J. *Macromolecules* **1998**, *31*, 592-601.
- (18) Prucker, O.; Ruehe, J. *Macromolecules* **1998**, *31*, 602-613.
- (19) Minko, S.; Sidorenko, A.; Stamm, M.; Gafijchuk, G.; Senkovsky, V.; Voronov, S. *Macromolecules* **1999**, *32*, 4532-4538.
- (20) Niwa, M.; Date, M.; Higashi, N. *Macromolecules* **1996**, *29*, 3681-3685.
- (21) Prucker, O.; Schimmel, M.; Tovar, G.; Knoll, W.; Ruehe, J. *Adv. Mater.* **1998**, *10*, 1073-1077.
- (22) Ejaz, M.; Yamamoto, S.; Ohno, K.; Tsujii, Y.; Fukuda, T. *Macromolecules* **1998**, *31*, 5934-5936.
- (23) Wittmer, J. P.; Cates, M. E.; Johner, A.; Turner, M. S. *Europhys. Lett.* **1996**, *33*, 397-402.
- (24) Queffelec, J.; Gaynor, S. G.; Matyjaszewski, K. *Macromolecules* **2000**, *33*, 8629-8639.
- (25) Xia, J.; Matyjaszewski, K. *Macromolecules* **1999**, *32*, 2434-2437.
- (26) Matyjaszewski, K.; Paik, H.-j.; Zhou, P.; Diamanti, S. J. *Macromolecules* **2001**, *34*, 5125-5131.

## Chapter 4

# Synthesis of Triblock Copolymer Brushes by Surface-Initiated Atom Transfer Radical Polymerization

### I. Introduction

This chapter describes the synthesis and characterization of triblock copolymer brushes. Surface-tethered triblock copolymers composed of poly(methyl acrylate), poly(methyl methacrylate), and poly(2-hydroxyethyl methacrylate) were grown from gold surfaces by a series of atom transfer radical polymerizations at ambient temperature. GPC determination of the molecular weights of model triblock polymer brushes demonstrate that this method can yield relatively homogeneous polymer brushes. After the synthesis of each block, films were either exposed to a large excess of Cu(II)Br<sub>2</sub> to quench polymerization prior to washing and reinitiation, or were simply rinsed with solvent. Comparison of the thicknesses of multiblock homopolymer films with those prepared using a single initiation step shows that in the Cu(II) quenching approach, >95% of the active chains support growth of an additional block. However, when simple solvent rinsing was used after each block, only 85-90% of active chains were preserved during the quenching step.

Block copolymers are especially attractive materials because of their ability to phase separate and self assemble into spherical, rod-like, and lamellar geometries. When deposited on surfaces, thin films of block copolymers can phase-segregate by the selective adsorption of one block of the copolymer<sup>1,2</sup> or orient upon application of

external fields.<sup>3</sup> Each of these techniques leads to formation of a pattern that can be used as a template for further materials deposition. Recent examples of materials patterned in this way include vertically oriented nanowires,<sup>4</sup> SiO<sub>2</sub> posts on surfaces,<sup>5</sup> and surface-induced nanopatterns of diblock copolymer films on mica.<sup>6</sup>

Tethering multiblock copolymers to surfaces is particularly interesting because it provides responsive, controllable interfaces<sup>7</sup> with nanoscale features.<sup>8</sup> Brittain *et al.* showed that copolymer brushes reversibly self-organize on exposure to different solvents.<sup>9-11</sup> The topology of multiblock copolymer brushes also suggests their use in forming multilayered materials where the layers can be arranged in a predetermined order. Growth of such films from tethered initiators complements other approaches to the formation of layered interfaces, such as deposition of Langmuir-Blodgett films,<sup>12</sup> zirconium phosphonates,<sup>13-15</sup> and layered polyelectrolytes.<sup>16</sup>

The most common approaches for surface-tethered block copolymer synthesis are (1) the preparation of polymeric macroinitiators that can be isolated and used later to initiate the polymerization of a second block, and (2) the sequential addition of two or more monomers to a polymerization. The first approach often employs different polymerization mechanisms to form each block, while the second approach is restricted to monomers that can be polymerized sequentially. Examples of the macroinitiator approach include the synthesis of surface-tethered polystyrene-*b*-poly(methyl methacrylate) (PS-*b*-PMMA), polystyrene-*b*-poly(methyl acrylate) (PS-*b*-PMA) and PS-*b*-poly(N,N-dimethylaminoethyl methacrylate) by sequential carbocationic polymerization and atom transfer radical polymerization (ATRP).<sup>9,17,18</sup> PS-*b*-PMMA was also prepared from surface-immobilized azo initiators by successive reverse-ATRP and

ATRP.<sup>11</sup> Using the second approach, surface-tethered PS-*b*-PMA and PS-*b*-poly(*tert*-butyl acrylate) were synthesized by sequential ATRP,<sup>19</sup> and surface-immobilized alkoxyamines were used for the preparation of PS-*b*-poly(styrene-*co*-methyl methacrylate) brushes.<sup>20</sup>

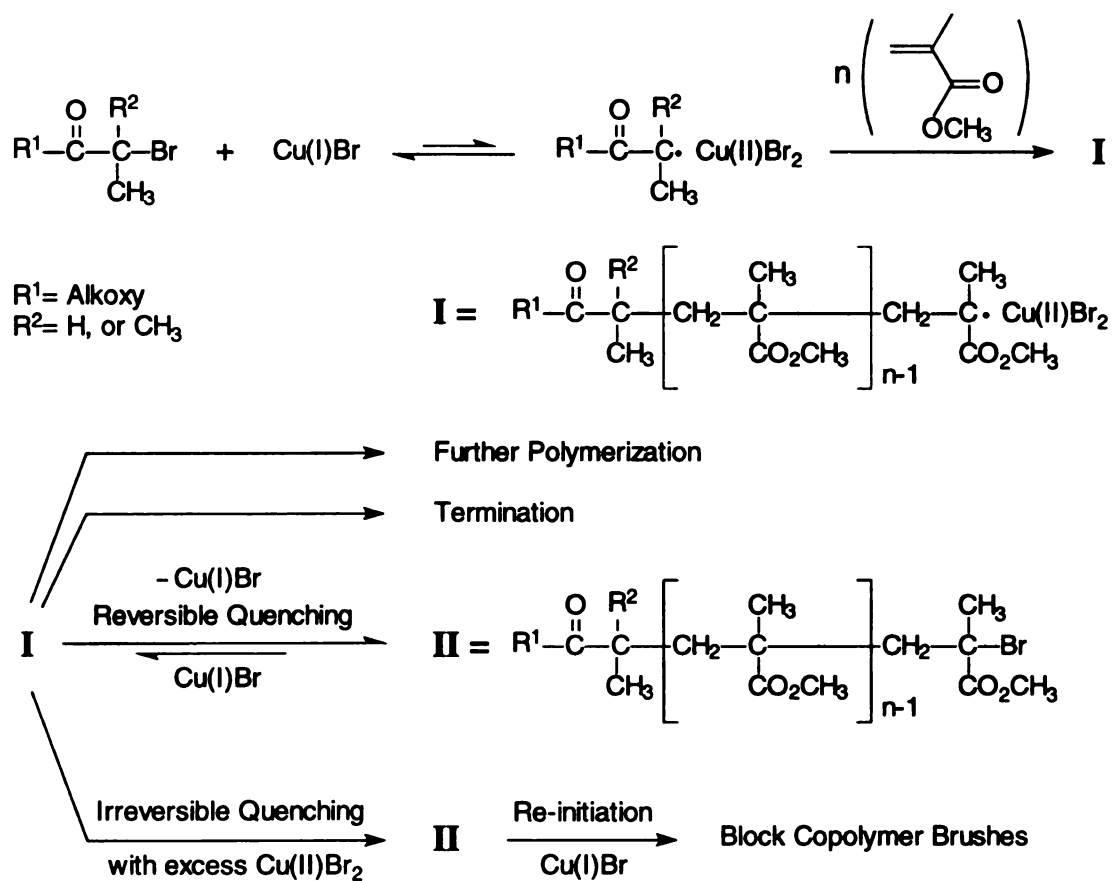
This study extends the surface-initiated synthesis of block copolymers from diblock to triblock systems using low-temperature ATRP. The major focus of this work is determining the efficiency with which additional blocks can be added to chains growing from a surface. When working with polymers composed of many blocks, this efficiency becomes especially important as shown by significant thickness differences between heptablock films prepared using two different strategies for radical quenching between the deposition of blocks.

ATRP is very attractive for formation of block copolymers because radical generation is “reversible” due to an equilibrium between the active (radical/Cu(II)Br<sub>2</sub>/ligand) and dormant (initiator/Cu(I)Br/ligand) states. **Scheme 4.1** shows the reversible generation and quenching of a radical in the ATRP of methyl methacrylate (MMA). Ignoring chain transfer reactions, polymer radical **I** can either undergo further polymerization by adding more monomer, convert to the dormant macroinitiator **II**, or terminate through bimolecular coupling or disproportionation reactions. Since the radical concentration in ATRP is very low,<sup>21</sup> termination is usually the least common scenario. One can intentionally favor the formation of the dormant macroinitiator by adding a high concentration of Cu(II)Br<sub>2</sub> to capture the radicals and shift the equilibrium to the dormant state.<sup>11</sup> This quenching should effectively stop

polymerization and keep growing chain ends alive for polymerization of subsequent blocks.

This quenching and re-initiation (Q & R) approach is particularly powerful for the preparation of surface-tethered block copolymers because the polymeric radical is confined to the substrate, and the quenching step simply involves transferring substrates to a concentrated  $\text{Cu(II)Br}_2$  solution that does not contain  $\text{Cu(I)Br}$ . Thus the length of the polymer chain is controlled by the elapsed polymerization time before exposure to the  $\text{Cu(II)Br}_2$  solution. After rinsing to remove residual  $\text{Cu(II)Br}_2$ , the polymerization can be re-initiated to extend the chains, or multiblock copolymers can be synthesized by simply switching to a different monomer after each cycle. The main advantages of this approach are the facile synthetic procedure, easy control over the thickness of each polymeric layer, restriction of polymerization to surface-bound chains, and a low polymerization temperature that is compatible with temperature-sensitive substrates.

**Scheme 4.1.** Possible reaction pathways for a polymeric radical in ATRP of MMA

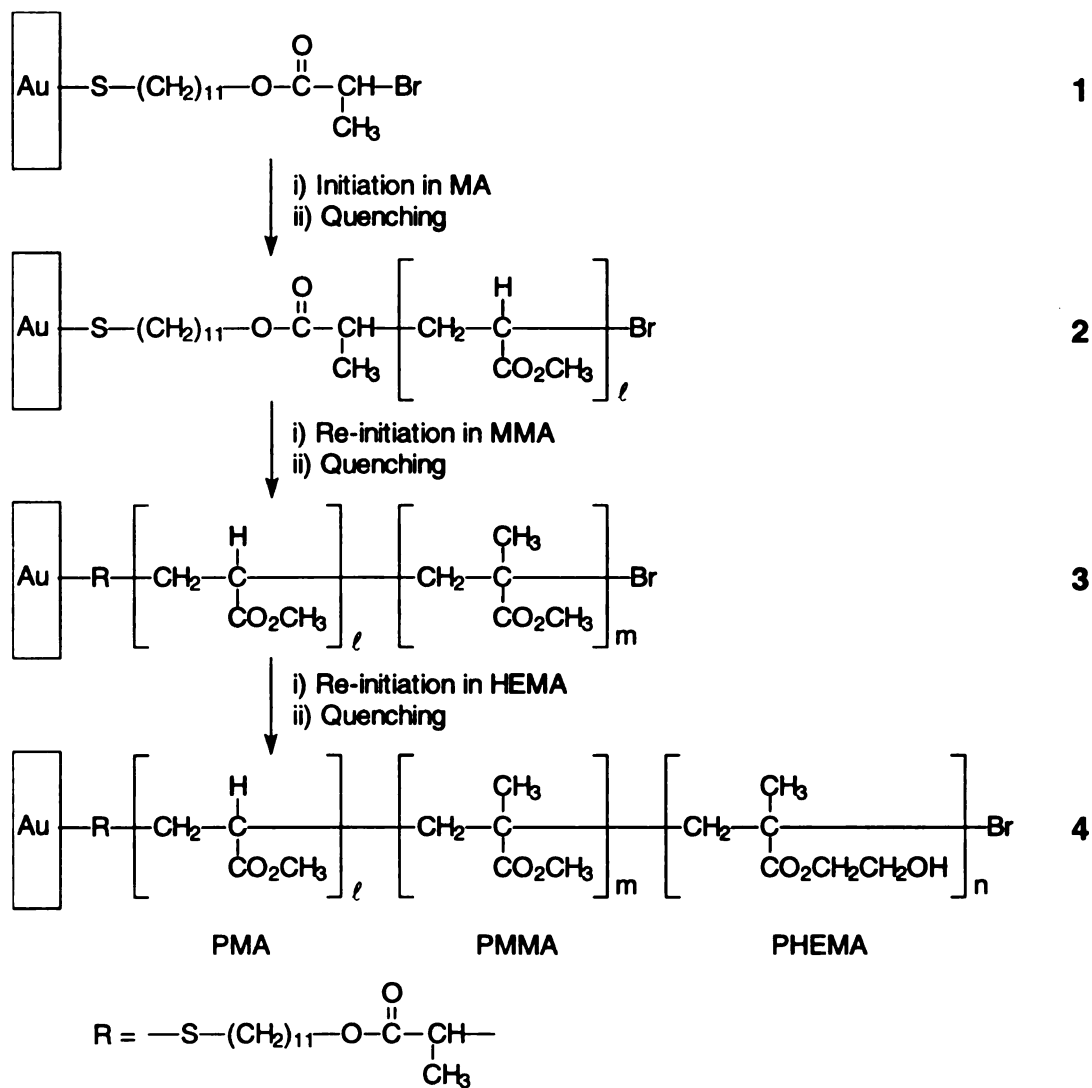


## II. Synthesis of Tethered PMA-*b*-PMMA-*b*-PHEMA Brushes on Gold

The synthetic route to tethered PMA-*b*-PMMA-*b*-PHEMA brushes is shown in **Scheme 4.2** and synthetic details appear in the Experimental section. To perform ATRP, a self-assembled monolayer of initiator, **1**, was immersed in a MA solution containing Cu(I)Br/Me<sub>6</sub>TREN and Cu(II)Br<sub>2</sub>/2(dnNbpy) at 25 °C. Although Cu(I)Br/Me<sub>6</sub>TREN complexes are active and allow ATRP to proceed at room temperature, the presence of Cu(II)Br<sub>2</sub> is indispensable for controlling polymerization. Because of the poor solubility<sup>22</sup> of the Cu(II)Br<sub>2</sub> complex in neat monomer, a mixture of CH<sub>3</sub>CN and THF (1:1 v:v) was used as a polar medium to obtain a homogeneous reaction system. These polar solvent mixtures should not affect the polymerization because ATRP is very tolerant toward functional groups such as ethers and nitriles.<sup>23</sup> After 20 min, the MA polymerization was quenched by transferring the substrate to a solution of Cu(II)Br<sub>2</sub>/2(dnNbpy) in CH<sub>3</sub>CN-THF (1:1). Matyjaszewski *et al.* reported that the Cu(II)Br<sub>2</sub> complex with dnNbpy successfully controls surface-initiated ATRP, acting as a deactivator and removing the necessity for sacrificial initiators.<sup>19</sup>

The formation of PMA on the surface is apparent from the appearance of a carbonyl peak at 1743 cm<sup>-1</sup> in the reflectance FTIR spectrum of these films (**Figure 4.1**, spectrum a). After polymerization of the initial block and quenching, **2** was washed with CH<sub>3</sub>CN-THF, and polymerization was re-initiated at 25 °C by transferring the substrate to a MMA solution containing fresh copper catalyst. Following the MMA polymerization and quenching, the reflectance FTIR spectrum of the film contained a more intense methyl peak at 2953 cm<sup>-1</sup> and an increased carbonyl peak, confirming the formation of the PMMA block (**Figure 4.1**, spectrum b).

**Scheme 4.2.** Synthesis of PMA-*b*-PMMA-*b*-PHEMA triblock copolymer brushes



Polymerization from **3** was then initiated in a HEMA solution at 40 °C. After the HEMA polymerization, the substrate was simply rinsed with a series of solvents including CH<sub>3</sub>CN-THF, DMF, EtOAc, EtOH, and deionized water. Since little, if any, polymer formed in solution,<sup>24</sup> a simple solvent rinse was sufficient to clean the copolymer brushes on the surface. Evidence for the formation of the third block, PHEMA, is the appearance of a broad hydroxy (OH) peak at 3200–3600 cm<sup>-1</sup> and a further increase in the intensity of the carbonyl peak (**Figure 4.1**, spectrum c). The ellipsometric thicknesses of the film after addition of each layer were: **2**: 65±1 Å, **3**: 133±1 Å, and **4**: 271±3 Å. The thicknesses were measured at three different spots on the same sample. Each succeeding polymer layer was purposely doubled in thickness by controlling the polymerization time to provide clear changes in the IR spectrum after each polymerization cycle. Formation of the last block required longer polymerization times because fewer initiators were left on the surface (*vide infra*). Ellipsometry and FTIR spectroscopy showed that no polymerization occurred from a propionylated MUD SAM (no α-bromocarbonyl functionality) under the same polymerization and washing conditions used for the synthesis of each block of the triblock copolymer brushes. This result demonstrates that polymer grows only from surfaces with immobilized initiators.

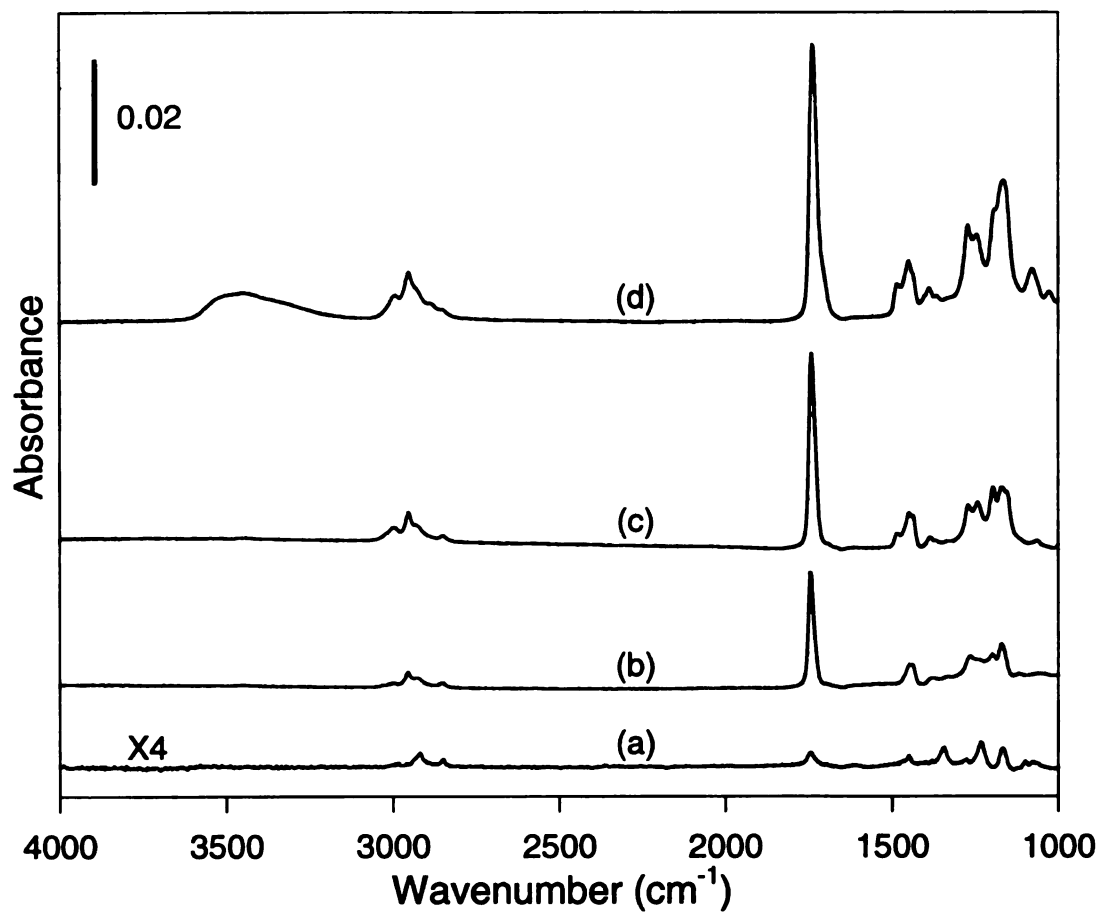


**Figure 4.1.** Reflectance FTIR spectra of (a) a layer of initiator immobilized on gold (1), (b) a grafted PMA layer on the initiator surface (2), (c) a grafted PMA-*b*-PMMA diblock copolymer (3), and (d) a grafted PMA-*b*-PMMA-*b*-PHEMA triblock copolymer (4).

As mentioned earlier, one of the most interesting properties of multiblock copolymers is their ability to form patterned structures. AFM images of surface-tethered PMA-*b*-PMMA-*b*-PHEMA films suggest formation of nanodomains whose properties depend on their environment. Upon exposure to a nonpolar solvent, hexanes, these nanodomains form separate islands (**Figure 4.2a**). Presumably, chains in the hydrophilic PHEMA block strongly self-assemble in a nonpolar medium to minimize surface energy, while the relatively hydrophobic PMMA block moves to the subsurface (valley) region to form discrete islands. Treatment with deionized water leads to relatively smooth surfaces with pseudo spherical domains in contact with each other (**Figure 4.2b**). This probably occurs because water is a better solvent for PHEMA than for PMMA.

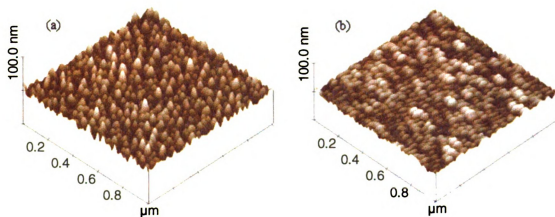


**Figure 4.2.** Tapping mode AFM images of PMA(58Å)-*b*-PMMA(111Å)-*b*-PHEMA(75Å) (a) after immersing in hexanes at ~60 °C for 30 min, and (b) after immersing in deionized water at ~70 °C for 30 min. Images in this dissertation are presented in color.

### III. Molecular Weights of Triblock Homopolymer Brushes

To determine the molecular weight of polymer brushes, one must detach the polymer chains from the substrate. **Figure 2.4** shows the detachment of PMMA brushes from a gold surface. As previously shown for gold colloids,  $I_2$  is capable of breaking Au–S bonds.<sup>25</sup> After the iodine treatment, detachment of the polymer chains was confirmed by reflectance FTIR and NMR. The FTIR spectrum of the  $I_2$ -treated surface did not show any significant polymer peaks and the NMR of the collected polymer chains from solution was identified as PMMA. Since detached polymer brushes should exist as disulfides,<sup>25</sup> we treated detached PMMA homopolymer brushes with  $NaBH_4$  to cleave the S–S bonds.<sup>26</sup> GPC determination of the  $M_n$  and PDI values for the PMMA homopolymer brushes were the same before and after reduction with  $NaBH_4$ ,<sup>24</sup> suggesting that the disulfides are asymmetric (PMMA–S–S–R) and that the molecular weights of R groups (MUD initiator fragments or oligomers) are negligible compared to those of the PMMA chains.

Due to the insolubility of PHEMA,<sup>27,28</sup> PMMA-*b*-PMMA-*b*-PMMA (triblock PMMA, which is in fact a homopolymer) was synthesized by the Q & R strategy to confirm the formation of reasonably well-defined triblock chains. Comparison of the  $M_n$  and molecular weight distribution of PMMA-*b*-PMMA-*b*-PMMA with those for a PMMA brush of comparable thickness grown using a single initiation step provides information about the efficiency of the Q & R cycles. If a significant fraction of initiating sites were lost during each Q & R step, the molecular weight distribution of the triblock brush would be broadened, resulting in a larger polydispersity index ( $PDI = M_w/M_n$ ). The average thickness of the three separate PMMA-*b*-PMMA-*b*-PMMA films was  $381 \pm 3 \text{ \AA}$ ,

including 16 Å for the initiator monolayer, and the thickness of each layer was about 120 Å. After detaching the PMMA brushes from the surface using iodine,<sup>24,25</sup> the molecular weight distribution was determined by GPC. The results ( $M_n = 37,400$ , PDI = 1.48) agree reasonably well with the values for PMMA homopolymers grown by a single initiation step without Q & R. The reported  $M_n$  and PDI values for a 370 Å thick PMMA film grown by a single initiation step are 44,500 and 1.30, respectively.<sup>24</sup> The slightly lower  $M_n$  and higher PDI of PMMA-*b*-PMMA-*b*-PMMA may suggest, however, that some termination reactions occur during Q & R cycles. A second triblock polymer brush, PMA-*b*-PMA-*b*-PMA, synthesized by the Q & R strategy and characterized in the same way yielded  $M_n = 41,600$  and PDI = 1.32 for  $389 \pm 2$  Å thick films. The  $M_n$  and low PDI values from these experiments provide further confirmation that Q & R steps are capable of forming triblock copolymers.

**Table 4.1** shows  $M_n$  and PDI values as well as portions of the GPC chromatograms for brushes detached from gold substrates. The table also includes two control experiments using commercial PMMA standards: runs a and b confirm that exposure of polymer chains to iodine should not affect  $M_n$  and PDI, while run c shows that the detection limit for PMMA in the GPC system (RI detector, THF as solvent) is <0.2 mg/mL. When the detached polymer brushes are dissolved in 150 µL THF, their calculated concentration would be about 0.2 mg/mL, assuming that there is no loss during the work-up procedure. The fact that the signal to noise ratio is a little higher for the control sample than for detached brushes indicates that some portion of the polymer brushes was probably lost during the µg-scale work-up and GPC sample injection. At these low concentrations of polymer, lower molecular weight species may be difficult to

detect due to their minimal weight fraction, which might exclude some low molecular weight polymer chains. Additionally, the baseline at longer retention times is difficult to determine. Thus, we note that PDI values for the polymer brushes are probably artificially low. Approximate baselines used for the GPC determinations are shown as dotted lines in **Table 4.1**. Triblock PMMA (run d) shows same baseline drift, while triblock PMA (run e) has a relatively stable baseline. The use of polymerization conditions that minimize termination (see below) may reduce the polydispersity of polymer brushes.

#### **IV. Quantification of the Efficiency of Q & R**

To quantify the efficiency of the Q & R process, the thicknesses of PMMA films prepared using several quenching ( $\text{Cu(II)Br}_2$ ) and re-initiation cycles were compared with values for films prepared with a single initiation step. The hollow circles in **Figure 4.3** show the evolution of PMMA film thickness as a function of polymerization time when using a single initiation step. Films prepared with 1-3 Q & R cycles (triangles and diamond) have nearly the same thickness/time relationship, suggesting that most of the active polymerization sites were preserved during the quenching process.

Quantification of the quenching process requires a model of film growth because the rate of termination of growing chains is significant compared to the rate of polymerization from the surface. Loss of active chain ends during surface polymerization is implied by the nonlinear relationship between film thickness and time shown in **Figure 4.3**. This is consistent with solution ATRP using  $\text{Me}_6\text{TREN}$ , which also shows termination of growing chains.<sup>22</sup>

**Table 4.1.** GPC data for PMMA standards and polymers grown from surfaces using ATRP

polymer sample	GPC peak	measured $M_n$ & PDI
PMMA standard sample, (a)–(c)		
(a) before iodine treatment	(a)	(a) $M_n = 59,200$ PDI = 1.07
(b) after iodine treatment	(b)	(b) $M_n = 59,000$ PDI = 1.07
(c) at low conc. 0.2 mg/mL	(c)	(c) $M_n = 62,700$ PDI = 1.05
(d) Triblock PMMA (381 Å thick film)		(d) $M_n = 37,400$ PDI = 1.48
(e) Triblock PMA (389 Å thick film)		(e) $M_n = 41,600$ PDI = 1.32
(f) PMMA by single initiation step (370 Å thick film)		(f) $M_n = 44,500$ PDI = 1.30

### \*Footnotes for Table 4.1

(a)–(c) The manufacturer-specified  $M_n$  and PDI values of the PMMA standard sample were 60,200 and 1.10, respectively. The standard was purchased from Polysciences, Inc.

(b) The PMMA standard sample was dissolved in  $I_2/CH_2Cl_2$  solution and kept at room temperature for 15 hr. After removal of  $CH_2Cl_2$  and  $I_2$ , the resulting PMMA was injected into the GPC instrument.

(d),(e) Triblock polymer brushes are, in fact, homopolymers synthesized by three cycles of quenching and re-initiation. For GPC analysis, these were collected from three  $2.7\text{ cm}^2$  substrates (total area:  $\sim 8\text{ cm}^2$ ).

(c)–(e) The low signal to noise ratio is due to the low concentration of polymer. These peaks are magnified relative to a and b.

(f) The elution time is faster than other runs because two PLgel  $10\mu$  mixed-B columns were used without an additional PLgel  $3\mu$  mixed-E column in series. The polymer brushes were collected from  $\sim 75\text{ cm}^2$  surface area, yielding a relatively large amounts of polymer chains and a higher signal to noise ratio than analysis of the other polymer brushes.

Several other publications related to surface-initiated ATRP display plots of grafted polymer thickness versus polymerization time. A similar plot for the ATRP of a sugar-carrying methacrylate using a  $CuBr/4,4'$ -di-*n*-heptyl-2,2'-bipyridine catalyst showed curvature<sup>29</sup> similar to that in **Figure 4.3**, while ATRP of methyl acrylate using  $CuBr/N,N,N',N'',N''$ -pentamethyldiethylenetriamine (PMDETA) and  $CuBr_2/PMDETA$  showed a linear growth of polymer thickness with time.<sup>19</sup> The linear growth observed in the second example may reflect an optimization of monomer structure, catalytic system, and reaction medium that minimizes termination by recombination. ATRP of ethylene glycol dimethacrylate in aqueous media also showed a reasonably linear growth in polymer thickness with time.<sup>30</sup>

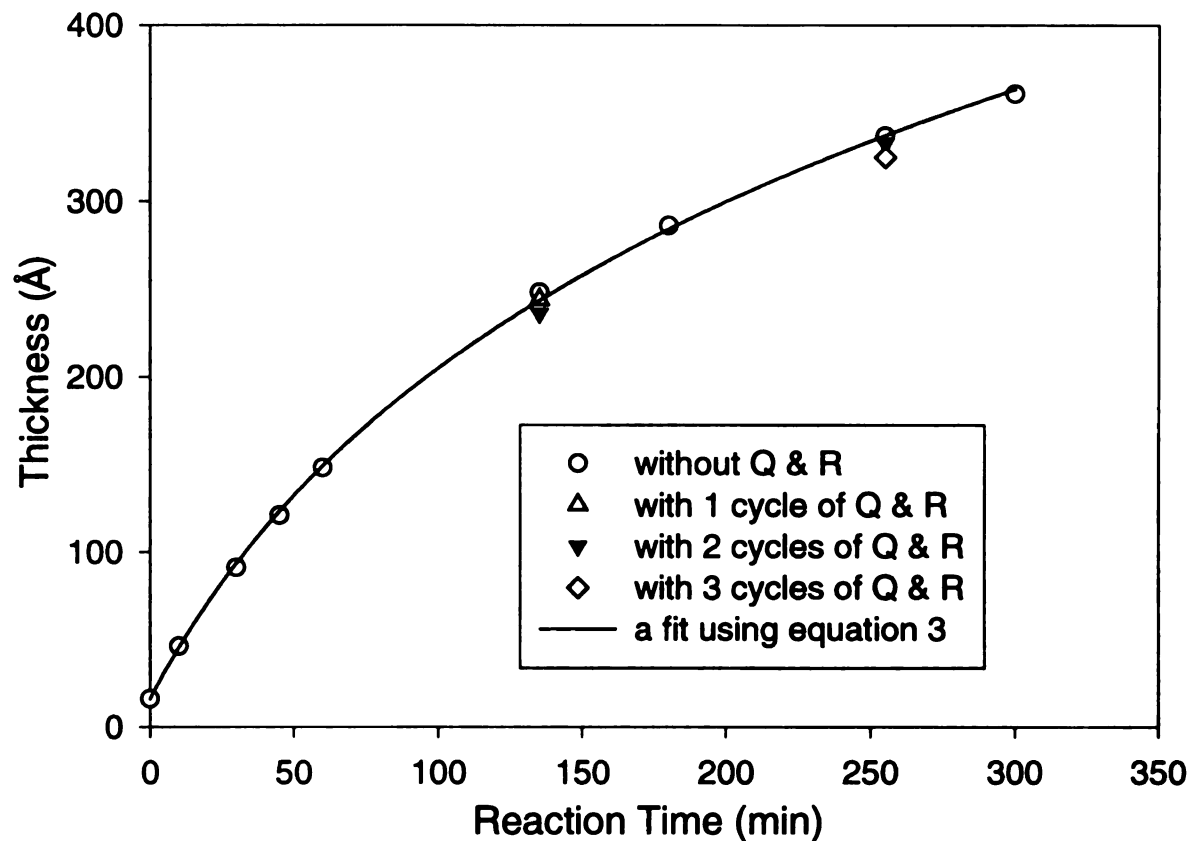


**Figure 4.3.** Ellipsometric thickness of PMMA films vs polymerization time. Thicknesses obtained at three different spots on a sample were averaged, and the standard deviation of these measurements was  $\pm 2$  Å. Polymerizations were initially quenched at 15 min or 15 min and 75 min in the case of Cu(II) quenching. The line represents a fit to the thickness of films prepared in a single reaction step (open circles) using the function, thickness =  $16 + A \ln(1+Bt)$  derived from equation 3.

To account for the loss of growing chains during polymerization from a surface, a simple kinetic model for film growth was utilized. The loss of active chains,  $A$ , is assumed to be second order with respect to surface concentration as represented by equation 1. Note that  $A$  includes chain ends in both the dormant and radical states. The increase in film thickness with time,  $dl/dt$ , should be first order with respect to the number of active chains as shown in equation 2. Integration of equation 1 yields an expression for the surface concentration of active chains at any given time, and insertion of this expression into equation 2 followed by integration yields an expression for film thickness as a function of time (equation 3), where  $[A^o]$  is the initial concentration of active initiator functionalities. To fit the data, 16 was added to the right side of equation 3 because the polymerization was initiated from a 16 Å-thick surface-immobilized initiator monolayer. The fit of the data in **Figure 4.3** and **4.4** (open circles) to this equation is excellent, showing that the model is reasonable.

$$\frac{d[A]}{dt} = -k_1[A]^2 \quad (1)$$

$$\frac{dl}{dt} = k_2[A] \quad (2)$$

$$l = \frac{k_2}{k_1} \ln(1 + k_1[A^o]t) \quad (3)$$

To account for the loss of chain ends during a quenching and re-initiation step, a quenching efficiency,  $Q$ , the ratio of active chain ends after and before quenching is introduced. Thus if the first quenching step occurs at time  $t_1$ , the number of active sites after the quenching step will be given by equation 4. For multiple quenching steps, the concentration of active sites after quenching step  $n$  (which occurs at time  $t_n$ ) is given by equation 5, where  $n$  is the number of quenching steps and the  $t_n$  values represent the times at which each of the quenching steps occurred. The growth in film thickness,  $\Delta l$  between the  $(n-1)$ th and  $n$ th quenching steps for  $n \geq 2$  will thus be given by equation 6. This equation is obtained by substituting values of  $[A(t_{n-1})]$  for  $[A^o]$  and values of  $(t_n - t_{n-1})$  for  $t$  in equation 3. Equation 3 is still valid for film growth prior to the first quenching step. The total film thickness is simply the sum of the  $\Delta l_n$  values.

$$[A] = \frac{[A^o]Q}{1 + k_1[A^o]t_1} \quad (4)$$

$$[A(t_n)] = \frac{[A^o]Q^n}{1 + k_1[A^o]t_1 + Qk_1[A^o](t_2 - t_1) + Q^2k_1[A^o](t_3 - t_2) + \dots + Q^{n-1}k_1[A^o](t_n - t_{n-1})} \quad (5)$$

$$\Delta l_n = \frac{k_2}{k_1} \ln \left( 1 + \frac{k_1[A^o]Q^{n-1}(t_n - t_{n-1})}{1 + k_1[A^o]t_1 + Qk_1[A^o](t_2 - t_1) + Q^2k_1[A^o](t_3 - t_2) + \dots + Q^{n-2}k_1[A^o](t_{n-1} - t_{n-2})} \right) \quad (6)$$

The efficiency of quenching,  $Q$  can be estimated from equation 6 and the data in **Figure 4.3**. These calculations show that  $Q > 0.95$  as would be expected from the similar thicknesses of films prepared in a single step and films prepared with quenching and reinitiation. Equation 6 also shows that the effect of quenching will be more pronounced as termination of active chains is reduced (lower  $k_1$  values) or as the number of quenching steps increases. In the next section we compare thicknesses of films prepared using up to six quenching steps and two different quenching procedures.

## V. Comparison of Cu(II)Br<sub>2</sub> Quenching with Simple Solvent Washing

Considering the short lifetime of radicals in ATRP,<sup>31</sup> their concentration at any given time should be very low. The combination of this low radical concentration and the inertness of the dormant chain ends might allow replacement of the Cu(II)Br<sub>2</sub> quenching with simple solvent washing to remove unreacted monomer after each block is formed. Matyjaszewski<sup>21</sup> and Dadmun<sup>32</sup> reported recently that multiblock copolymers could be prepared by ATRP in solution without a quenching step. However, in some cases, polydispersity slightly increased with the number of blocks, implying that some termination of polymer chains possibly happens during separation and re-initiation procedures.<sup>32</sup> This trend led us to use the Cu(II) quenching strategy to shift the equilibrium to inert dormant chains during separation and re-initiation procedures. Cu(II) quenching might be especially important for the preparation of copolymer brushes, because chain ends growing from surfaces are in close proximity and may recombine more readily than similar chains in solution.

To see whether the Cu(II) quenching step is necessary, polymerizations were either quenched with a Cu(II)Br<sub>2</sub> solution or simply washed with solvent after formation of each block. FTIR spectroscopy and ellipsometry show that both approaches lead to the successful formation of multiblock polymer brushes. However, the films prepared using the solvent washing protocol repeatedly showed 2-4 % less increase (per cycle) in the subsequent block thickness than those prepared by the Q&R strategy. To determine whether this difference was significant, heptablock PMMA brush ([PMMA-*b*-]<sub>6</sub>PMMA) was prepared with and without Cu(II)Br<sub>2</sub> quenching steps. Polymer films were either quenched or solvent-washed after 15, 25, 40, 60, 90, and 150 min of reaction time and re-initiated to prepare the next block. **Figure 4.4** shows that as the number of Q & R cycles increased, the difference in the thicknesses of films synthesized by the two methods also increased. The results for heptablock PMA films ([PMA-*b*-]<sub>6</sub>PMA) prepared using both Cu(II)Br<sub>2</sub> quenching and solvent washing are shown in **Figure 4.5**. Again, the higher efficiency of the Cu(II)Br<sub>2</sub> quenching strategy becomes evident as the number of quenching steps increases. The termination of growing chain ends by recombination may be unavoidable, but Cu(II)Br<sub>2</sub> quenching can preserve more surface initiating species and lead to thicker polymer layers. After heptablock formation, the accumulated difference in the thicknesses of the samples prepared by the two methods were ~21 % and ~13 % for [PMMA-*b*-]<sub>6</sub>PMMA and [PMA-*b*-]<sub>6</sub>PMA, respectively.

Assuming that the Cu(II)Br<sub>2</sub> quenching step had an efficiency of 100%, equation 3 was used to fit the data for PMMA film growth (open circles, **Figure 4.4**). This allowed us to obtain values for  $k_2/k_1$  and  $k_1[A^0]$ . Using these values and equation 6, Q for solvent washing is estimated to be around 87%. Thus the Cu(II) quenching method is

considerably more efficient than solvent washing. In the case of PMA, the fit of the thickness data for Cu(II) quenching to equation 3 was not sufficiently good to estimate the quenching efficiency for the solvent washing procedure. However, the data clearly show the lower efficiency of solvent washing compared to Cu(II) quenching.

## VI. Conclusions

Surface-initiated ATRP was successfully quenched by a Cu(II)Br<sub>2</sub>/2(dnNbpy) solution, and dormant initiating sites were preserved for re-initiation of multiblock synthesis. Direct GPC measurement of the molecular weights of polymer brushes detached from the surface demonstrates that this Q & R method is capable of producing relatively homogeneous brushes. Reflectance FTIR spectroscopy, ellipsometry, and molecular weight data confirm the formation of triblock copolymer brushes on gold surfaces. After heptablock formation, the accumulated difference in the thicknesses of the samples prepared by Cu(II)Br<sub>2</sub> quenching and solvent washing became significant: ~21 % and ~13 % for [PMMA-*b*-]<sub>6</sub>PMMA and [PMA-*b*-]<sub>6</sub>PMA, respectively. The efficiency of a Cu(II)Br<sub>2</sub> Q & R cycle determined from the growth rate of PMMA films was >95 %, while the same efficiency for solvent washing was 85-90%. The Cu(II)Br<sub>2</sub> Q & R approach allows preparation of multiblock copolymers with control over the thickness of each block at ambient temperature.

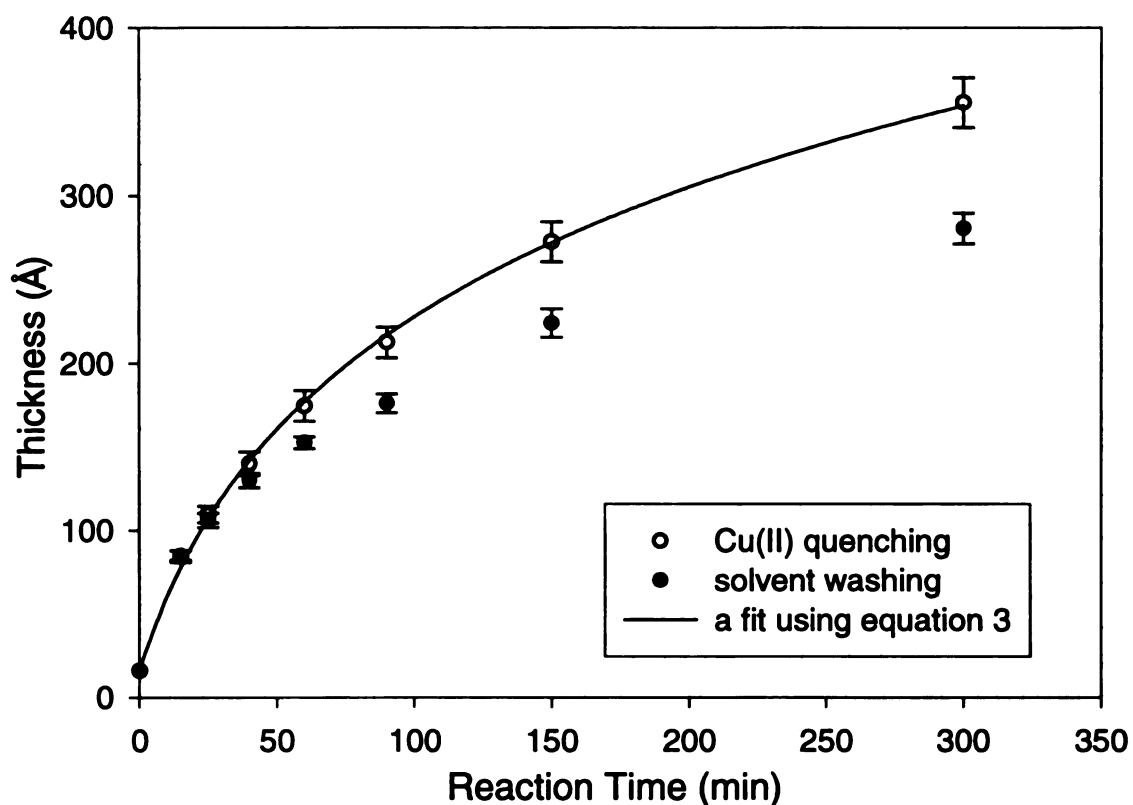


**Figure 4.4.** Thickness of multiblock PMMA films vs polymerization time. Each subsequent point represents one more cycle of polymerization followed by Cu(II) quenching or solvent washing, e.g., 300 min data were obtained after 7 polymerization steps with quenching or washing between each step. Error bars represent the standard deviations of thickness determinations on at least three different spots on two different samples. The line represents a fit to the thickness of films prepared with Cu(II)Br<sub>2</sub> quenching (open circles) using the function, thickness = 16 + A ln(1+Bt) derived from equation 3.

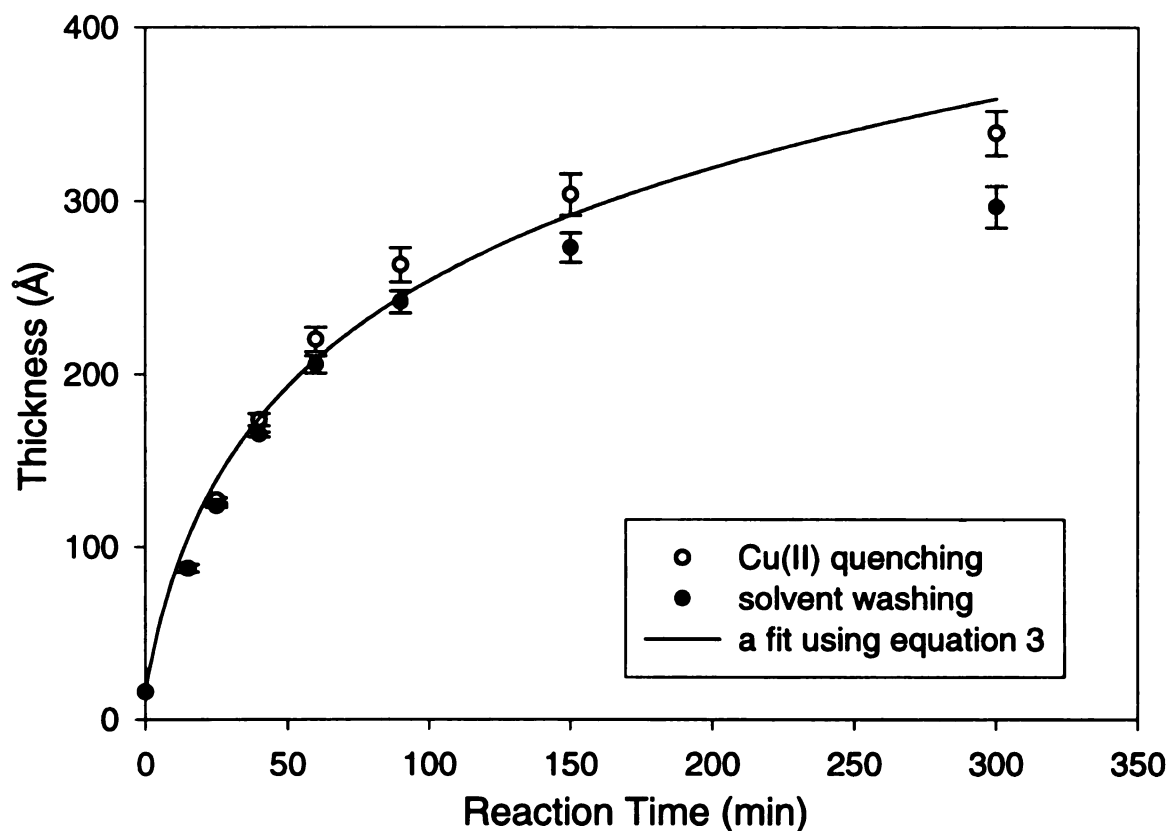


**Figure 4.5.** Thickness of multiblock PMA films vs polymerization time. Each subsequent point represents one more cycle of polymerization followed by Cu(II) quenching or solvent washing. Error bars represent the standard deviations of thickness determinations on at least three different spots on two different samples. The line represents a fit to the thickness of films prepared with Cu(II)Br<sub>2</sub> quenching (open circles) using the function, thickness = 16 + A ln(1+Bt) derived from equation 3.

## VII. References

- (1) Dan, N.; Tirrell, M. *Macromolecules* **1993**, *26*, 4310-4315.
- (2) Hadziioannou, G.; Patel, S.; Granick, S.; Tirrell, M. *J. Am. Chem. Soc.* **1986**, *108*, 2869-2876.
- (3) Morkved, T. L.; Lu, M.; Urbas, A. M.; Ehrichs, E. E.; Jaeger, H. M.; Mansky, P.; Russell, T. P. *Science* **1996**, *273*, 931-933.
- (4) Thurn-Albrecht, T.; Schotter, J.; Kastle, G. A.; Emley, N.; Shibauchi, T.; Krusin-Elbaum, L.; Guarini, K.; Black, C. T.; Tuominen, M. T.; Russell, T. P. *Science* **2000**, *290*, 2126-2129.
- (5) Kim, H.-C.; Jia, X.; Stafford, C. M.; Kim, D. H.; McCarthy, T. J.; Tuominen, M.; Hawker, C. J.; Russell, T. P. *Adv. Mater.* **2001**, *13*, 795-797.
- (6) Spatz, J. P.; Eibeck, P.; Moessmer, S.; Moeller, M.; Kramarenko, E. Y.; Khalatur, P. G.; Potemkin, I. I.; Khokhlov, A. R.; Winkler, R. G.; Reineker, P. *Macromolecules* **2000**, *33*, 150-157.
- (7) Mansky, P.; Liu, Y.; Huang, E.; Russell, T. P.; Hawker, C. *Science* **1997**, *275*, 1458-1460.
- (8) Zhao, B.; Brittain, W. J. *Prog. Polym. Sci.* **2000**, *25*, 677-710.
- (9) Zhao, B.; Brittain, W. J. *J. Am. Chem. Soc.* **1999**, *121*, 3557-3558.
- (10) Zhao, B.; Brittain, W. J.; Zhou, W.; Cheng, S. Z. D. *Macromolecules* **2000**, *33*, 8821-8827.
- (11) Sedjo, R. A.; Mirous, B. K.; Brittain, W. J. *Macromolecules* **2000**, *33*, 1492-1493.
- (12) Corkery, R. W. *Langmuir* **1997**, *13*, 3591-3594.

- (13) Alberti, G.; Casciola, M.; Costantino, U.; Vivani, R. *Adv. Mater.* **1996**, *8*, 291-303.
- (14) Katz, H. E. *Chem. Mater.* **1994**, *6*, 2227-32.
- (15) Kaschak, D. M.; Mallouk, T. E. *J. Am. Chem. Soc.* **1996**, *118*, 4222-4223.
- (16) Decher, G. *Science* **1997**, *277*, 1232-1237.
- (17) Zhao, B.; Brittain, W. J. *Macromolecules* **2000**, *33*, 8813-8820.
- (18) Huang, X.; Wirth, M. J. *Macromolecules* **1999**, *32*, 1694-1696.
- (19) Matyjaszewski, K.; Miller, P. J.; Shukla, N.; Immaraporn, B.; Gelman, A.; Luokala, B. B.; Siclovan, T. M.; Kickelbick, G.; Vallant, T.; Hoffmann, H.; Pakula, T. *Macromolecules* **1999**, *32*, 8716-8724.
- (20) Husseman, M.; Malmström, E. E.; McNamara, M.; Mate, M.; Mecerreyes, D.; Benoit, D. G.; Hedrick, J. L.; Mansky, P.; Huang, E.; Russell, T. P.; Hawker, C. J. *Macromolecules* **1999**, *32*, 1424-1431.
- (21) Davis, K. A.; Matyjaszewski, K. *Macromolecules* **2001**, *34*, 2101-2107.
- (22) Queffelec, J.; Gaynor, S. G.; Matyjaszewski, K. *Macromolecules* **2000**, *33*, 8629-8639.
- (23) Matyjaszewski, K.; Patten, T. E.; Xia, J. *J. Am. Chem. Soc.* **1997**, *119*, 674-680.
- (24) Kim, J.-B.; Bruening, M. L.; Baker, G. L. *J. Am. Chem. Soc.* **2000**, *122*, 7616-7617.
- (25) Templeton, A. C.; Hostetler, M. J.; Kraft, C. T.; Murray, R. W. *J. Am. Chem. Soc.* **1998**, *120*, 1906-1911.
- (26) Stahl, C. R.; Siggia, S. *Anal. Chem.* **1957**, *29*, 154-155.

- (27) Robinson, K. L.; Khan, M. A.; de Banez, M. V.; Wang, X. S.; Armes, S. P. *Macromolecules* **2001**, *34*, 3155-3158.
- (28) Huang, W.; Kim, J.-B.; Bruening, M. L.; Baker, G. L. *Macromolecules* **2002**, *35*, 1175-1179.
- (29) Ejaz, M.; Ohno, K.; Tsujii, Y.; Fukuda, T. *Macromolecules* **2000**, *33*, 2870-2874.
- (30) Huang, W.; Baker, G. L.; Bruening, M. L. *Angew. Chem., Int. Ed.* **2001**, *40*, 1510-1512.
- (31) Matyjaszewski, K. *Macromolecules* **1999**, *32*, 9051-9053.
- (32) Eastwood, E. A.; Dadmun, M. D. *Macromolecules* **2001**, *34*, 740-747.

## Chapter 5

### Controlled Growth and Degradation of Biodegradable Nanometer-Thick Films of PLA from PHEMA Surfaces

#### I. Introduction

This chapter describes the surface-initiated ring-opening polymerization (ROP) of lactide on poly(2-hydroxyethyl methacrylate) (PHEMA) surfaces as a route to the controlled growth of biodegradable thin films of polylactide (PLA). Using a combination of atom transfer radical polymerization (ATRP) and ROP, we successfully synthesized PHEMA-*g*-PLA on gold and used the polymerization time to control the growth of PLA. The growth of PLA on PHEMA followed 1st order kinetics with a linear increase in PLA thickness versus polymerization time, indicating a polymerization with living character.

Polymers based on renewable resources are increasingly attractive alternatives to those derived from petroleum. Poly(lactic acid) or poly(lactide) is environmentally degradable and the monomer, lactic acid, is available from renewable resources such as corn. PLA's biodegradability and biocompatibility have led to applications as surgical sutures, tissue scaffolds, and drug delivery systems, and now PLA is being introduced as a commodity polymer for fibers and packaging. A number of block copolymers have been synthesized to gain better control over PLA's physical properties.<sup>1-6</sup>

In addition to bulk forms of PLA, thin films of PLA are especially important for applications in drug delivery systems<sup>7</sup> and as drug-eluting coatings on medical devices.<sup>8,9</sup> The thickness of a coating and its degradation profile are important factors that must be

considered in designing materials for controlled drug release. Therefore, precise control over the thickness of the PLA layer is indispensable. Various techniques have been developed to prepare thin-film coatings on solid substrates. Physically adsorbed layers are often thermally unstable due to weak interactions between the polymer and solid substrate and lack resistance to solvents and friction. Covalently attached films should offer improved thermal stability and mechanical properties.

Surface-initiated ROP of lactide provides a unique method for the synthesis of PLA layers covalently linked to hydroxy-terminated surfaces. While surface-initiated polymerization has attracted much attention, there are a limited number of reports devoted to surface-initiated ring opening polymerization. Husemann *et al.* used surface-initiated ring opening polymerization to graft poly( $\epsilon$ -caprolactone) from hydroxy-terminated self-assembled monolayers (SAMs) as a step in a soft lithography patterning scheme.<sup>10</sup> Two recent examples of the surface-initiated ROP of lactides were reported by Choi<sup>11</sup> and Möller.<sup>12</sup> In both cases, PLA was initiated from  $-OH$  or  $-NH_2$  groups at the termini of long chain alkyl thiolates on gold or silicate surfaces. However, neither study reports a kinetic study of PLA growth, which is necessary for control over the thickness of biodegradable films. Here we describe the synthesis and the kinetics of lactide polymerization from PHEMA grafted on gold surfaces.

If we think of PHEMA as functioning in the same way as a SAM, one should expect a relatively low grafting density. A comparison of the contact angles for water on PHEMA,<sup>24</sup> 63°, and on an  $\omega$ -hydroxyalkyl thiolate SAM,<sup>25</sup> 34°, suggests that the surface density of PHEMA  $-OH$  groups is less than full surface coverage. However, participation of subsurface  $-OH$  groups would increase the grafting efficiency and

produce a comb-like structure. To prepare the surface anchored PLA film, a layer of PHEMA on gold was synthesized by ATRP, and then ROP was used to grow PLA from the PHEMA layer. Since both polymerizations are living processes, the thickness of each layer is easily controlled by the polymerization time. The thickness of the PLA film could be controlled from several nm up to 450 nm.

The PHEMA-*g*-PLA system on gold has several important features. Polymer layers on gold are chemically homogeneous and are compatible with a wide variety of thin film characterization techniques. In addition, gold is biocompatible with potential applications in drug delivery devices.<sup>13</sup> Compared to thiolate on gold SAMs, PHEMA provides the thermal stability needed to support lactide polymerization. The Au-S bond is unstable above ~60 °C<sup>14-16</sup> and organic monolayers often detach from surfaces. Finally, the PHEMA-*g*-PLA system is a biocompatible hydrogel<sup>17</sup> that can be used as a drug delivery system.<sup>18-21</sup>

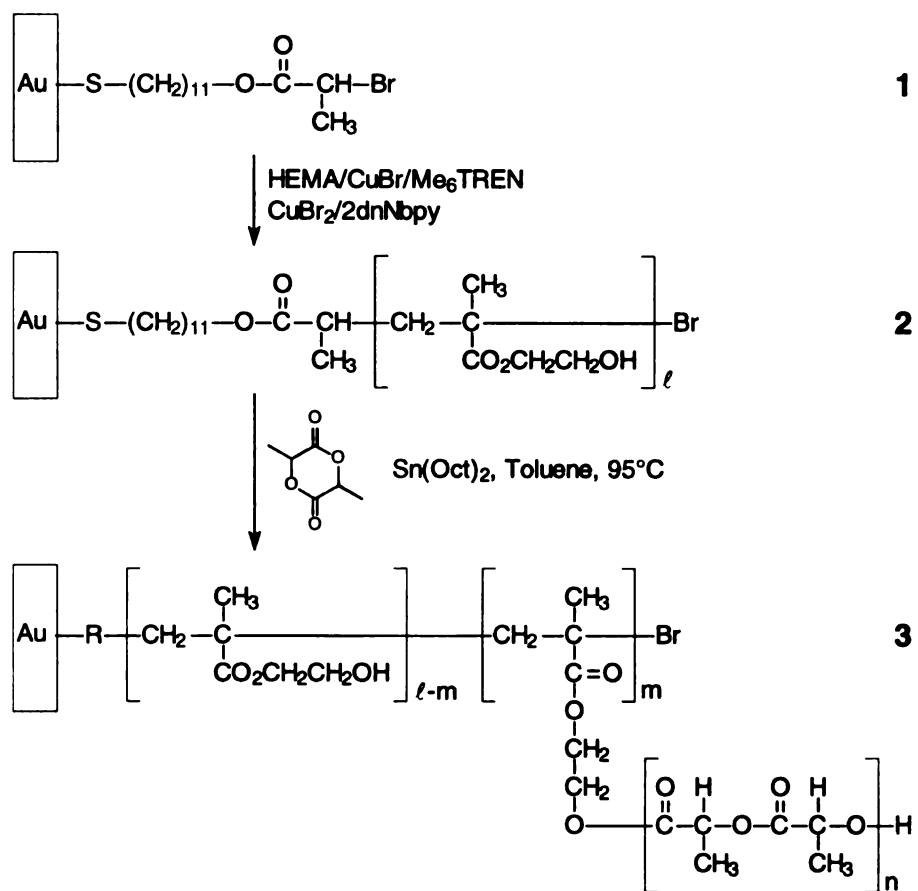
## II. Synthesis of PHEMA-*g*-PLA

**Scheme 5.1** outlines the synthesis of PHEMA-*g*-PLA tethered to a gold surface. The detailed procedure for the preparation of a SAM of initiator **1** is described in the Experimental section. ATRP of HEMA (2-hydroxyethyl methacrylate) was initiated from the surface-bound initiator layer. The catalyst system was a mixture of Cu(I)Br/tris[2-(dimethylamino)ethyl]amine (Me<sub>6</sub>TREN) (0.1 mol % based on monomer) and Cu(II)Br<sub>2</sub>/2 equivalents of 4,4'-di-*n*-nonyl-2,2'-bipyridine (dnNbpy). The Cu(II) complex (30 mol %, relative to Cu(I)), ensures the deactivation of active radicals and provides some control over the polymerization. The dormant  $\alpha$ -bromocarbonyl initiator was

activated by immersing substrate **1** in a 1:1 (v/v) CH<sub>3</sub>CN-THF solution of HEMA and the copper catalyst. Polymerizations of HEMA were run at room temperature with the thickness of the PHEMA film controlled by the reaction time. Detailed conditions for the ATRP of HEMA can be found in Experimental section. After HEMA polymerization, the substrate was washed sequentially with DMF, EtOH, EtOAc, EtOH and deionized water, and was then dried under a stream of nitrogen. The formation of PHEMA was apparent from the appearance of a carbonyl peak at 1733 cm<sup>-1</sup> and a broad hydroxy peak at 3200–3600 cm<sup>-1</sup> in the reflectance FTIR spectrum (**Figure 5.1**, spectrum a). A number of PHEMA substrates were prepared to support kinetic experiments of the ROP of lactide from PHEMA. The PHEMA films on these substrates all had similar ellipsometric thicknesses, 174±2 nm.

Using the hydroxy groups of PHEMA side chains as initiators, *rac*-lactide was polymerized in toluene at 95 °C with Sn(II) octanoate, (Sn(Oct)<sub>2</sub>) as the catalyst. The polymerizations were run in a drybox to avoid contamination from water, which can act as a competing initiator. At regular intervals, samples were removed for IR and film thickness measurements. The IR spectra in **Figure 5.1** show the growth of PLA on PHEMA. The initial spectrum (a) showed a single carbonyl peak at 1733 cm<sup>-1</sup> from PHEMA, but after 90 min of lactide polymerization, the carbonyl peak broadened (**Figure 5.1**, spectrum b) and shifted to higher wavenumbers. Eventually, the PLA carbonyl peak dominated the spectrum and only a single peak at 1767 cm<sup>-1</sup> was observed (**Figure 5.1**, spectrum e). Parallel growth in the methyl stretching peak at 2993 cm<sup>-1</sup> and a decline of the hydroxy peak at 3200–3600 cm<sup>-1</sup> also confirm PLA formation.

**Scheme 5.1.** Synthetic pathway for PHEMA-*g*-PLA



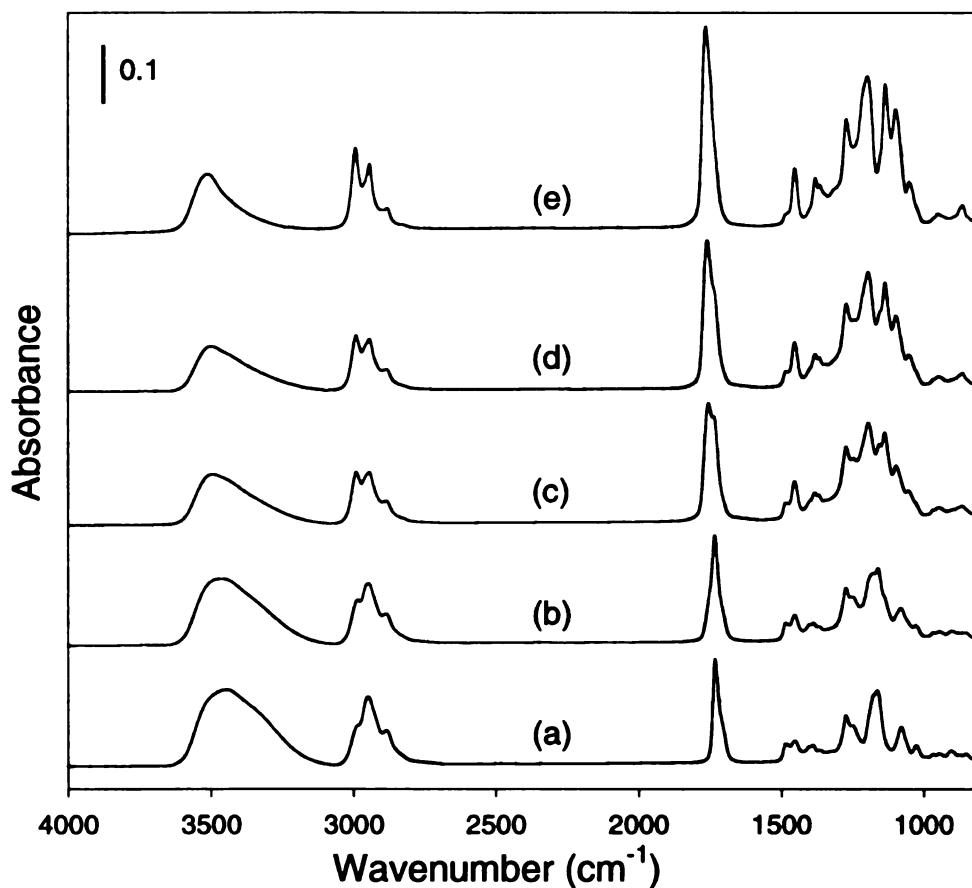


**Figure 5.1.** Reflectance FTIR spectra of (a) **2**: a grafted PHEMA layer (174 nm) on gold, (b) **3**: a grafted PHEMA(170 nm)-g-PLA(29 nm) layer after 90 min of lactide polymerization, (c) **3**: a grafted PHEMA(173 nm)-g-PLA(127 nm) layer after 180 min of lactide polymerization, (d) **3**: a grafted PHEMA(178 nm)-g-PLA(179 nm) layer after 240 min of lactide polymerization, and (e) **3**: a grafted PHEMA(178 nm)-g-PLA(409 nm) layer after 480 min of lactide polymerization. For clarity, the 2700–3700  $\text{cm}^{-1}$  region in each spectrum is magnified 5 times relative to the remainder of the spectrum.

### III. Kinetics of Lactide Polymerization from PHEMA Surface

The growth of the PLA film was followed by monitoring the change in the film thickness with time. Each sample was characterized by surface reflectance FTIR, and ellipsometric data were collected at three different spots on the sample. Plotted in **Figure 5.2a** is the net increase in the thickness of the PLA layer, calculated by subtracting the thickness of the PHEMA film from the total film thickness. The homogeneous ROP of lactide follows a “coordination-insertion” mechanism,<sup>22</sup> and the data of **Figure 5.2a** show the expected linear increase in film thickness with polymerization time, confirming that the polymerization of lactide from PHEMA is a living process and follows 1st order kinetics. The data also show a short induction time before the onset of PLA polymerization. Similar induction times were observed for solution polymerizations of lactide,<sup>23</sup> which may be related to the time needed to form the alkoxy-Sn complex from Sn(Oct)<sub>2</sub> and the hydroxy group of PHEMA.

### IV. Control Experiments without surface –OH groups

Two control experiments show that the PLA film only grows from the –OH group of PHEMA side chain. In the first experiment, the hydroxy groups of PHEMA were blocked by acetylation with acetyl chloride. Substrates with PHEMA and acetylated PHEMA films were placed in the same vial with *rac*-lactide and Sn(Oct)<sub>2</sub> at 95 °C for 12 hr. As shown in **Figure 5.3**, the IR spectra of the PHEMA substrate (spectrum b) shows the expected changes after ROP of lactide, an increase in the carbonyl peak intensity, its shift from 1733 cm<sup>-1</sup> to 1767 cm<sup>-1</sup> and a decrease in hydroxy peak at 3200-3600 cm<sup>-1</sup>.

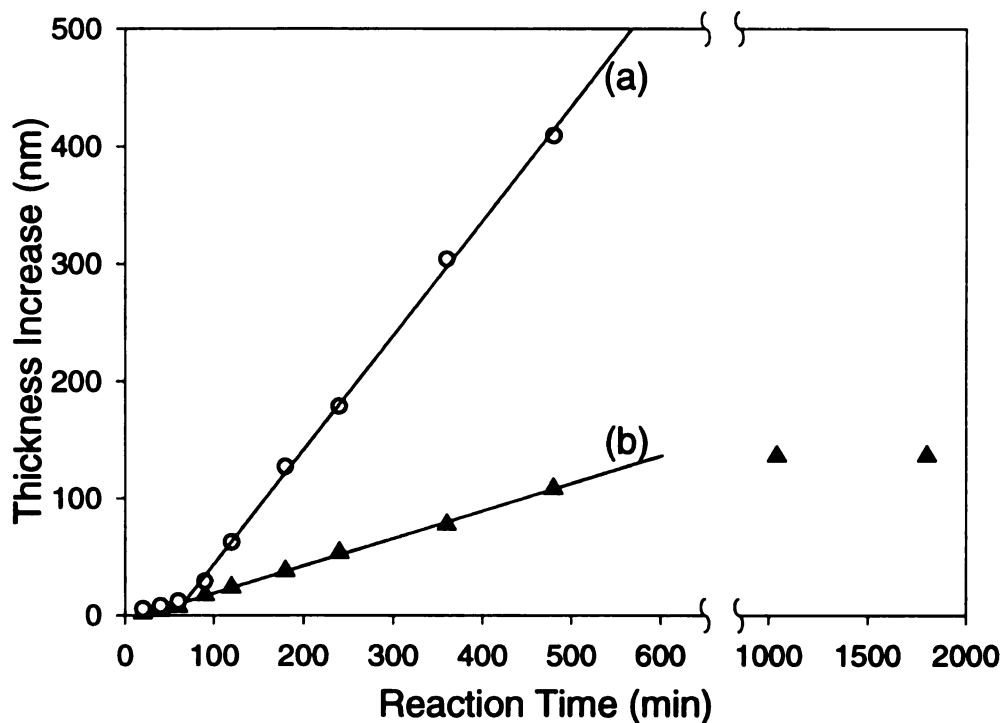


**Figure 5.2.** Plot of PLA thickness increase vs polymerization time: (a) using  $174\pm 2$  nm thick PHEMA substrates and (b) using  $49\pm 1$  nm thick PHEMA substrates. Ellipsometric thicknesses were measured at three different spots on a sample and the error bars are smaller than symbols.

However, the IR spectrum of the substrate with acetylated PHEMA shows no sign of PLA growth (spectrum d). Similarly, the behavior of substrates with PHEMA and PMMA<sup>14</sup> films were compared using the same conditions as before. As seen in **Figure 5.4**, the polylactide grew from the PHEMA layer, while the PMMA control showed no PLA growth. Instead of growing PLA, a decrease in IR intensity suggests that some of PMMA chains desorbed from surface under the polymerization conditions.

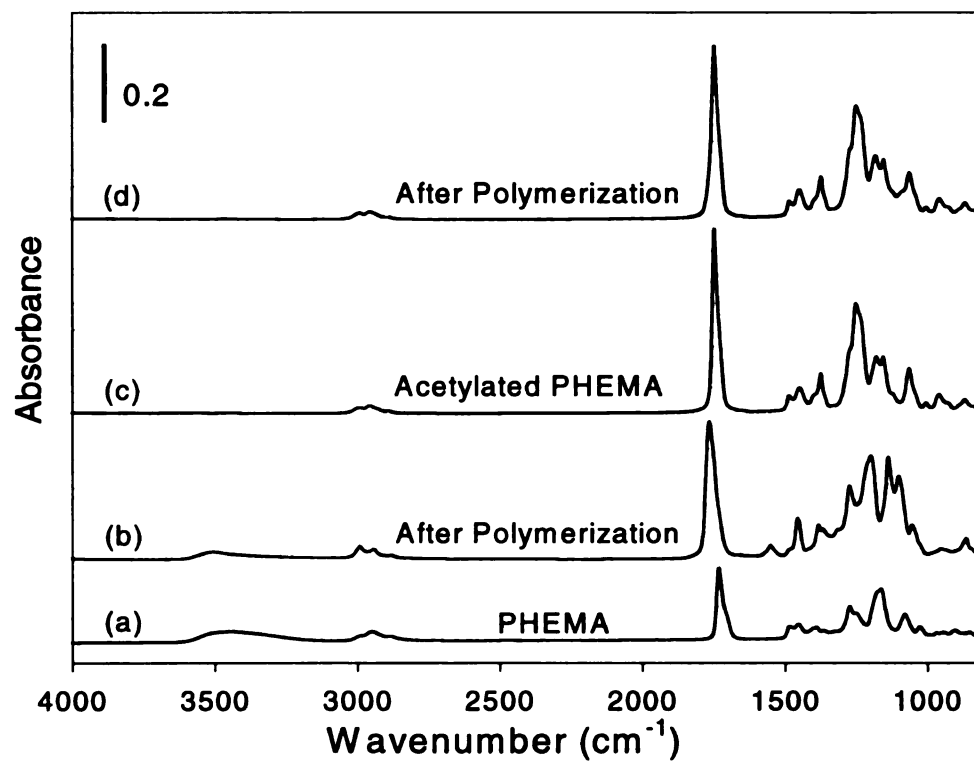


**Figure 5.3.** Reflectance FTIR spectra of (a) a surface grafted PHEMA layer on gold, (b) after lactide polymerization from PHEMA, (c) a surface grafted acetylated-PHEMA layer, and (d) after attempted lactide polymerization from acetylated-PHEMA.

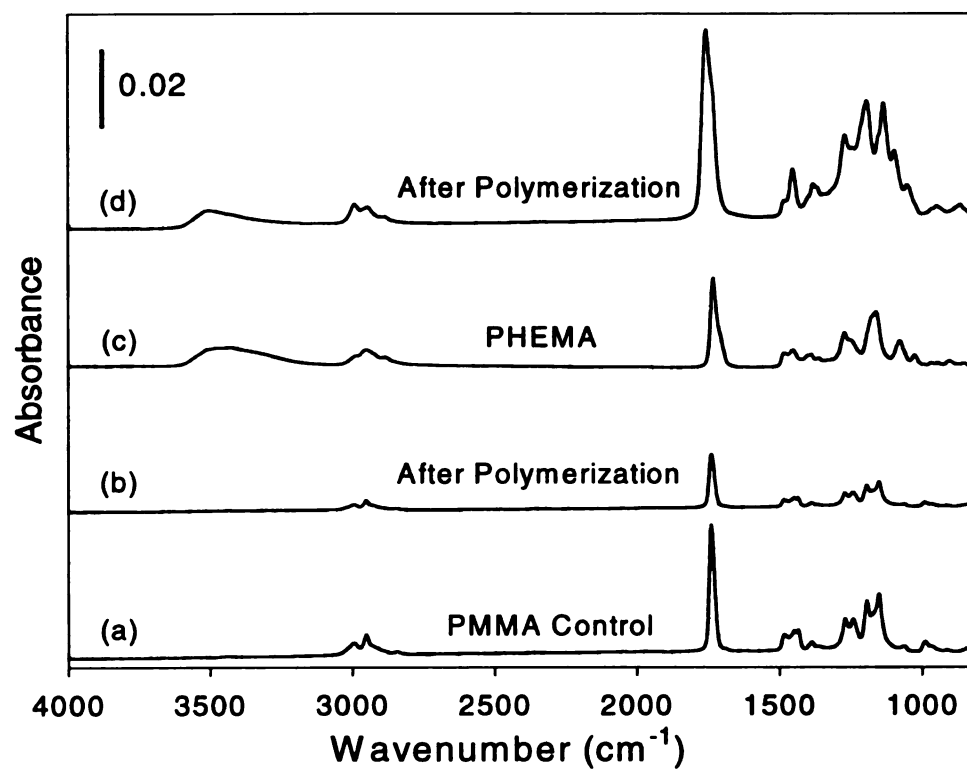


**Figure 5.4.** Reflectance FTIR spectra of (a) a surface grafted PMMA layer on gold, (b) after attempted lactide polymerization from PMMA, (c) a surface grafted PHEMA layer, and (d) after lactide polymerization initiated from PHEMA.

PLA was grown from PHEMA layers of different thicknesses. As shown in **Figure 5.2**, the growth rate was extracted from the linear portion of thickness vs. time curves. The 174 nm PHEMA film grew at 9.8 Å/min and while the growth rate of a 49 nm PHEMA film was 2.4 Å/min. The ratio of the rates, 4.1, is similar to the ratio of the film thicknesses, 3.6. This suggests that the hydroxy groups of PHEMA are accessible, and ROP of lactide can be initiated from most hydroxy groups. If initiation was restricted to a thin surface layer of hydroxy groups, then the rate of film growth should be independent of the thickness. Acetylation studies also are consistent with the view that the -OH group of PHEMA is accessible to reagents. As shown in **Figure 5.3c**, the absence of a significant -OH peak in the FTIR spectrum of PHEMA films after reacting with acetyl chloride indicates nearly complete acylation of PHEMA. In addition, the decrease in the hydroxy peak at 3200–3600 cm<sup>-1</sup> in the FTIR spectrum of PHEMA-*g*-PLA (**Figure 5.1**) is too large to be explained by initiation from a thin surface layer. Thus, the structure of PHEMA-*g*-PLA should be viewed as a graft copolymer, with at least some comb-like character.

Using 49±1 nm thick PHEMA substrates, we extended the polymerization time to test for linearity in growth at long times. As seen in **Figure 5.2b**, PLA film growth eventually ceased at ~10 hr. Examination of the polymerization solution by <sup>1</sup>H NMR revealed a 79:21 mixture of soluble PLA homopolymer and monomer. The formation of the polymer likely resulted from initiation of ROP by adventitious H<sub>2</sub>O in the solvent or on the surface of the glassware, despite efforts to exclude H<sub>2</sub>O by working in a drybox, using dry solvents, and silanizing reaction vials. The termination of growth seen in **Figure 5.2b** is consistent with equilibrium polymerization, where the propagation and

depropagation rates are identical.<sup>26-28</sup> The equilibrium concentration of monomer calculated from the NMR data,  $[M]_{eq}$ , is  $\sim 0.03$  M in good agreement with literature values. For polymerization of L-lactide in 1,4-dioxane,  $[M]_{eq} \sim 0.15$  M at 406 K and 0.06 M at 353 K.<sup>26</sup> To prove equilibrium control, we isolated a sample that had grown to a limiting PLA film thickness (131 nm), and after washing with solvent, we transferred the sample to a vial containing fresh monomer solution with catalyst. As expected, PLA growth resumed, and an additional 53 nm of PLA was added in 5 hr.

The ROP of lactide from PHEMA can be stopped the polymerization at a given thickness, and then reinitiated at a later time to increases the thickness of the PLA layer. For example, when the samples used to generate the data of **Figure 5.2a** were re-immersed in a solution of monomer and catalyst, each sample grew an additional  $\sim 470$  nm of PLA film in 12 hr. In principle, PLA films can be grown to arbitrary thicknesses as long as accessible initiating sites remain in the PHEMA layer or at the end of PLA chains.

## **V. Degradation of PLA film**

The hydrolytic degradation behavior of PHEMA-*g*-PLA on gold was investigated in phosphate buffer (pH 7.40) at 55 °C. Substrates with surface-grafted PHEMA-*g*-PLA were immersed in the buffer solution and were removed at intervals to measure their ellipsometric thickness and surface reflectance FTIR spectrum. The sample surfaces quickly became rough, and reliable ellipsometric thicknesses could not be measured after 1 day of degradation. The increase in surface roughness indicates that the degradation mechanism is not simple surface erosion. Reflectance FTIR, however, could be used to

characterize the degradation profile of the film. **Figure 5.5** shows the evolution of the FTIR spectra for a single sample during degradation. Shown in **Figure 5.5(a)** is spectrum of the 174 nm thick PHEMA film before lactide growth, while **5.5(b)** is the spectrum of the PHEMA-g-PLA film after deposition of 464 nm of PLA. As hydrolytic degradation proceeded, the methyl stretching peak at  $2993\text{ cm}^{-1}$  and the carbonyl peak at  $1767\text{ cm}^{-1}$  decreased, while the hydroxy peak at  $3200\text{--}3600\text{ cm}^{-1}$  increased. After 50 days of degradation, the IR spectrum of the sample **5.5(l)** was almost identical to the initial PHEMA spectrum **5.5(a)**, and it showed no further changes for times  $>50$  days. These results are consistent with selective hydrolysis of the PLA film.

The degradation experiments shown in **Figure 5.5** were run using the same phosphate buffer solution throughout the run. The pH of the buffer solution used in the first set of experiments decreased from 7.40 to 7.36 in 50 days. We anticipated seeing an autocatalytic effect<sup>29</sup> since degradation of PLA generates lactic acid oligomers that accelerate the acid-catalyzed cleavage of PLA chains. In a second set of degradation experiments, we changed the buffer solution every 2 days to ensure a constant pH. The PLA degradation rates for these two experiments were calculated from the FTIR spectra of the samples by subtracting the PHEMA carbonyl peak area in spectrum **5.5(a)** from the total area associated with the PLA and PHEMA carbonyls. As noted earlier, PHEMA shows no evidence of degradation over 50 days. The results, plotted in **Figure 5.6**, show a faster degradation rate for samples that were degraded in the same buffer solution, consistent with a small autocatalytic effect.

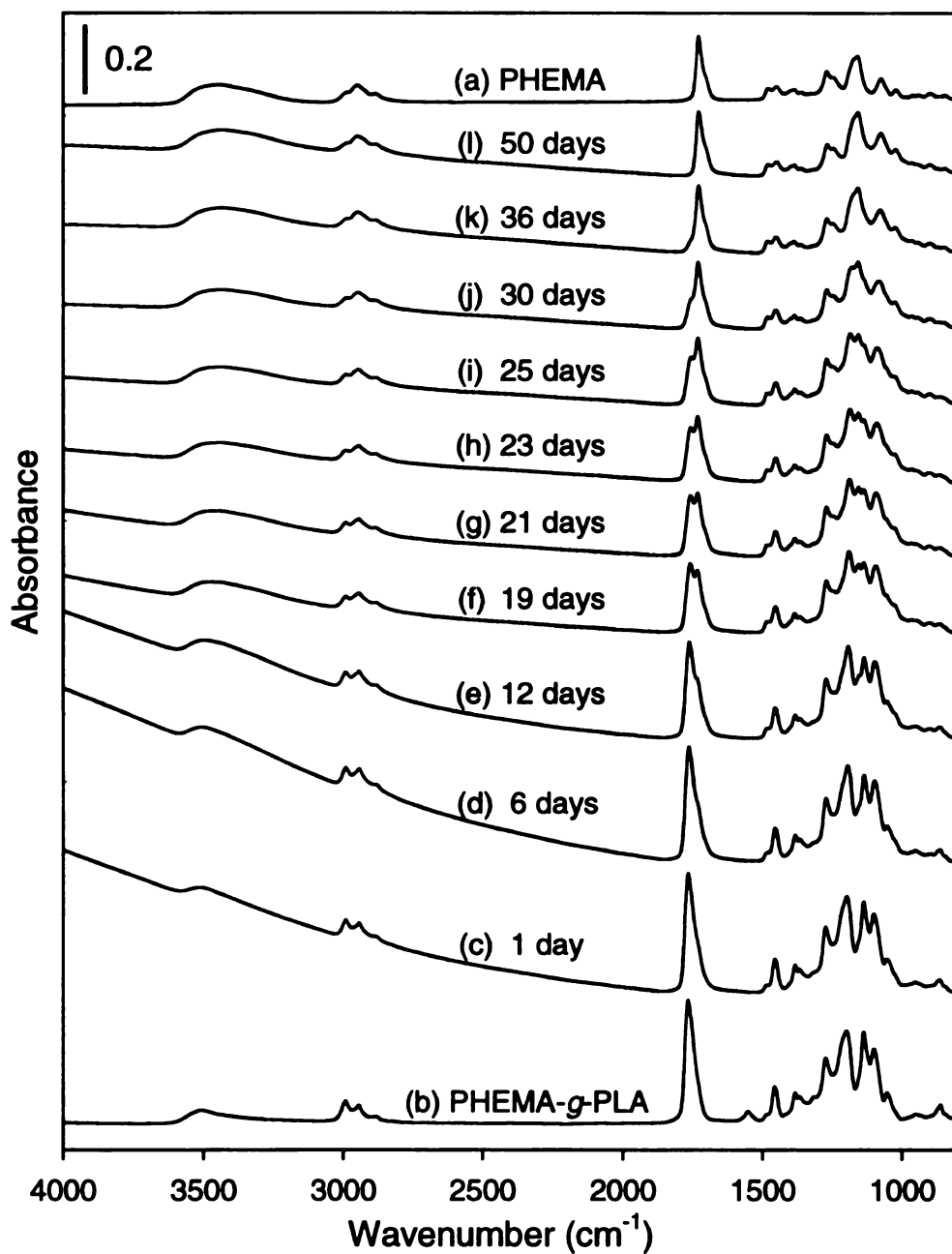


**Figure 5.5.** Reflectance FTIR spectra of (a) PHEMA (174 nm) before PLA growth, (b) PHEMA (174 nm)-*g*-PLA(464 nm) before degradation, and (c)–(l) PHEMA-*g*-PLA films at various times during hydrolytic degradation. For clarity, the 2700–3700  $\text{cm}^{-1}$  region of each spectrum was magnified 2 times relative to the remainder of the spectrum.

During the first 4 days, the PLA carbonyl peak area increased, and then decreased linearly. Although the cause of the initial increase in peak area is unclear, it may be related to the macroscopic surface roughness that appears within hours of the start of the degradation. It is well known that IR peak intensities are dependent on the orientation of functional groups relative to surface normal,<sup>30</sup> and the increased surface roughness may reflect some change in carbonyl group orientation.

The 9-30 day data are linear and are plotted in the inset in **Figure 5.6**. The calculated slopes are  $-3.06$  and  $-2.52$  for the **Figure 5.6(a)** and **5.6(b)** data respectively. For the first set of data, the initial PLA film thickness was 464 nm, which corresponds to a degradation rate of  $\sim 14.5$  nm/day. The second set of data was obtained with a 488 nm thick PLA film, which degraded at  $\sim 12.0$  nm/day. Thus the apparent autocatalytic effect increased the degradation rate by  $\sim 20\%$ .

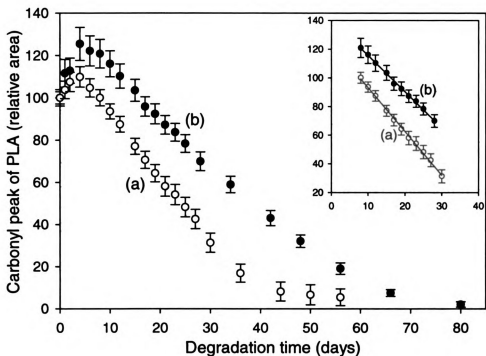


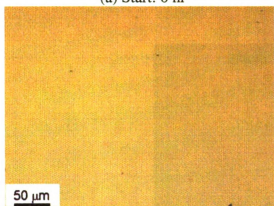
**Figure 5.6.** Plot of PLA carbonyl peak area vs degradation time: (a) a PHEMA (174 nm)-g-PLA (464 nm) film degraded in the same phosphate buffer solution throughout the experiment (hollow circles:  $\circ$ ) and (b) PHEMA (174 nm)-g-PLA (488 nm) degraded in buffer that was replaced every 2 days (filled circles:  $\bullet$ ). The error bars represent the standard deviations in determining the carbonyl peak areas in FTIR spectra, which result from two different choices for the baseline in the FTIR spectra.

## VI. Surface Morphology Study of PLA film during Degradation

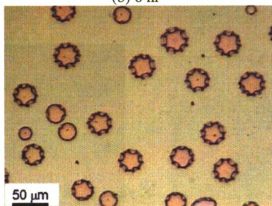
An unexpected aspect of the degradation of PHEMA-*g*-PLA films was the development of unusual surface domains. These domains form several hours after the start of the degradation experiment, and then evolve over several days. As shown in **Figure 5.7(a)**, PHEMA-*g*-PLA films are smooth when observed using an optical microscope. However, after 6 hr of degradation, the dried surface was covered with numerous gear-shaped domains—**5.7(b)**. If the surface is swelled with water and dried several times, the gear-like structures evolve into star-like domains—**5.7(c)** and **5.7(d)**, with most being five and six-pointed stars. The stars were surprisingly symmetrical with a circle in the center of each star. With further degradation, the domains evolved into pentagonal and hexagonal domains—**5.7(e)** and **5.7(f)**, and eventually dendrimer-like structures—**5.7(g)** and **5.7(h)**. At long times, the domains developed into flower-like patterns separated by mottled areas—**5.7(i)**. **Figure 5.8** shows the typical stages seen in the evolution of the surface features.

The domains depicted in **Figure 5.7(b)-5.7(d)** are not flat, as can be concluded from the inability to have the entire image in focus for any one setting of the focus. This is illustrated in **Figure 5.9(a)**, where the circular features are clearly in the same focal plane as the substrate, while in **Figure 5.9(b)**, the curved features that give rise to the geometrical pattern of the domains are above the focal plane of the substrate. The features and the topography of the sample suggest that the dark lines may correspond to overlapping PLA layers or folds that reflect light differently than the bulk sample.

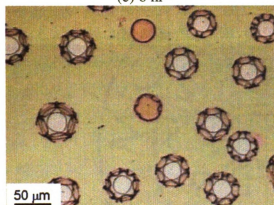
(a) Start: 0 hr



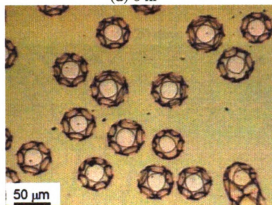
(b) 6 hr



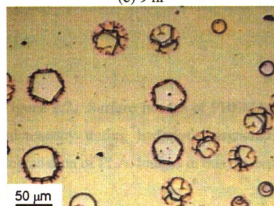
(c) 6 hr



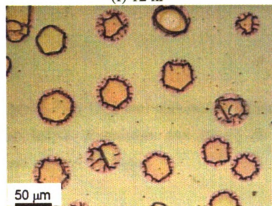
(d) 6 hr



(e) 9 hr



(f) 12 hr



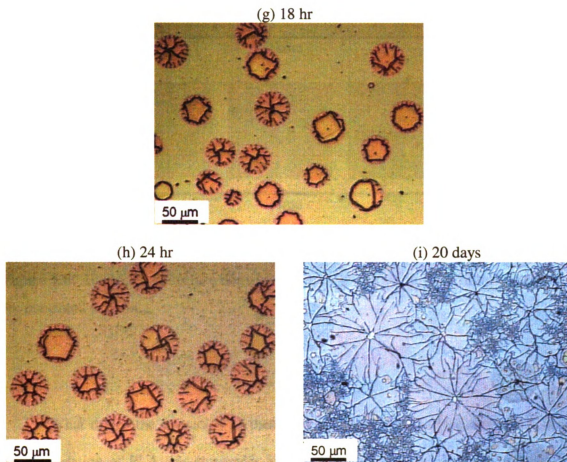


**Figure 5.7.** Surface images of PHEMA (177 nm)-g-PLA (353 nm) obtained by optical microscopy during hydrolytic degradation: (a) before degradation and (b)–(i) after degradation of PLA. Images in this dissertation are presented in color.

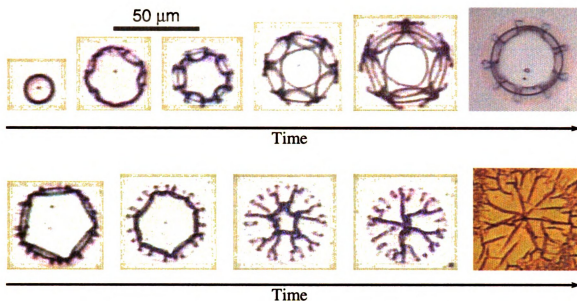


**Figure 5.8.** Evolution of surface domains during degradation. Images in this dissertation are presented in color.

What drives the formation of these regularly patterned surface domains? Since the degradation of PLA was run under hydrolytic conditions and the bottom layer is a hydrophilic PHEMA layer, direct observation of wet surfaces should provide critical evidence for explaining the formation and nature of the domains. The wet surface of a sample that had been degraded for 6 hr was observed by optical microscopy (**Figure 5.10**). Initially, the surface was decorated with blister-like domains that collapsed as the surface dried. With further drying, the domains evolved into symmetrical structures. This process was completely reversible and could be repeated several times before the domains suffered irreversible damage.

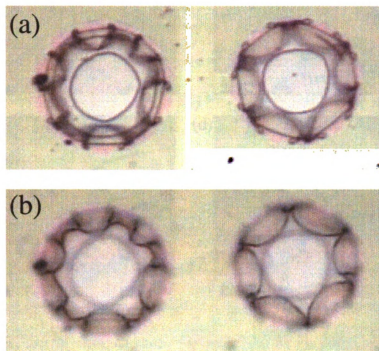


**Figure 5.9.** Differences in the optical microscopic images of domains as a function of changes in focal length: (a) image obtained by setting the focus in the plane of the substrate and (b) image obtained by focusing on the curved features of the domains. Images in this dissertation are presented in color.

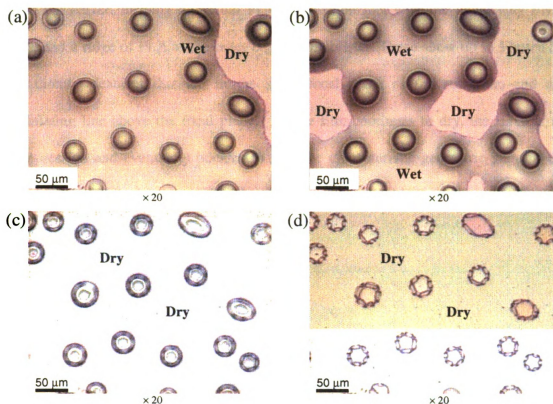


**Figure 5.10.** Evolution in surface morphology during the drying of water-swollen films: (a)–(d) show successive optical microscopic images taken during the drying process. Images in this dissertation are presented in color.

Based on these observations, we propose that surface domain formation is driven by rapid diffusion of water through pinholes in the PLA layer, leading to swelling of the PHEMA layer. Pinholes were not observed by optical microscopy in films before degradation, but may develop as water dissolves catalyst residues that contaminate the film. Swelling of the PHEMA layer causes localized blistering of the polymer film,

irreversibly stretching the PLA layer. With removal of the water, the blisters collapse from the center, forming a circular PLA layer in contact with the underlying PHEMA film, and a ridge of PLA at the outer edge of the blister. These show up in **Figure 5.9** as the circular features that are in the same focal plane as the substrate, and as the undulating line above the focal plane. As the film continues to dry, the ridge is under compression and eventually buckles to give the characteristic geometric patterns of the dried films. While this scenario is plausible, the details of this process are not known and require further study.

## **VII. Conclusions**

In conclusion, biodegradable nanometer thick films of polylactide were synthesized from PHEMA surfaces by surface-initiated ROP. The growth rate of the PLA layer was linear, and the film thickness was controlled by the polymerization time. PLA grew from the pendent hydroxy group of PHEMA films, but acetylated PHEMA and PMMA surfaces failed to initiate polymerization. There was an induction time for lactide polymerization presumably due to the slow formation of the alkoxy-Sn initiator from  $\text{Sn}(\text{Oct})_2$  and the hydroxy group of PHEMA. Once growth began, the ROP followed 1st order kinetics, which is consistent with a living polymerization. The loss of PLA from the film surface during hydrolytic degradation was linear with time and showed a small autocatalytic effect. These results support a surface erosion mechanism. Blistering in the early stages of the degradation process led to the formation of highly symmetrical structures and fracturing of the PLA layer.

### VIII. References

- (1) Otsuka, H.; Nagasaki, Y.; Kataoka, K. *Biomacromolecules* **2000**, *1*, 39-48.
- (2) Metters, A. T.; Anseth, K. S.; Bowman, C. N. *Polymer* **2000**, *41*, 3993-4004.
- (3) Ouchi, T.; Nozaki, T.; Ishikawa, A.; Fujimoto, I.; Ohya, Y. *J. Polym. Sci., Part A: Polym. Chem.* **1997**, *35*, 377-383.
- (4) Kricheldorf, H. R.; Kreiser, I. *Makromol. Chem.* **1987**, *188*, 1861-73.
- (5) Song, C.; Chen, H.; Feng, X. *Gaofenzi Tongxun* **1983**, 177-83.
- (6) Wallach, J. A.; Huang, S. J. *Biomacromolecules* **2000**, *1*, 174-179.
- (7) Jain, R. A. *Biomaterials* **2000**, *21*, 2475-2490.
- (8) Schmidmaier, G.; Wildemann, B.; Stemberger, A.; Haas, N. P.; Raschke, M. *Journal of Biomedical Materials Research* **2001**, *58*, 449-455.
- (9) Middleton, J. C.; Tipton, A. J. *Biomaterials* **2000**, *21*, 2335-2346.
- (10) Husemann, M.; Mecerreyes, D.; Hawker, C. J.; Hedrick, J. L.; Shah, R.; Abbott, N. L. *Angew. Chem., Int. Ed.* **1999**, *38*, 647-649.
- (11) Choi, I. S.; Langer, R. *Macromolecules* **2001**, *34*, 5361-5363.
- (12) Moller, M.; Nederberg, F.; Lim, L. S.; Kange, R.; Hawker, C. J.; Hedrick, J. L.; Gu, Y.; Shah, R.; Abbott, N. L. *Journal of Polymer Science, Part A: Polymer Chemistry* **2001**, *39*, 3529-3538.
- (13) Santini, J. T., Jr.; Cima, M. J.; Langer, R. *Nature (London)* **1999**, *397*, 335-338.
- (14) Kim, J.-B.; Bruening, M. L.; Baker, G. L. *J. Am. Chem. Soc.* **2000**, *122*, 7616-7617.

- (15) Bain, C. D.; Troughton, E. B.; Tao, Y. T.; Evall, J.; Whitesides, G. M.; Nuzzo, R. *G. J. Am. Chem. Soc.* **1989**, *111*, 321-35.
- (16) Schlenoff, J. B.; Li, M.; Ly, H. *J. Am. Chem. Soc.* **1995**, *117*, 12528-36.
- (17) Lim, D. W.; Choi, S. H.; Park, T. G. *Macromol. Rapid Commun.* **2000**, *21*, 464-471.
- (18) Barakat, I.; Dubois, P.; Grandfils, C.; Jerome, R. *J. Polym. Sci., Part A: Polym. Chem.* **1999**, *37*, 2401-2411.
- (19) Iijima, M.; Nagasaki, Y.; Okada, T.; Kato, M.; Kataoka, K. *Macromolecules* **1999**, *32*, 1140-1146.
- (20) Riley, T.; Stolnik, S.; Heald, C. R.; Xiong, C. D.; Garnett, M. C.; Illum, L.; Davis, S. S.; Purkiss, S. C.; Barlow, R. J.; Gellert, P. R. *Langmuir* **2001**, *17*, 3168-3174.
- (21) Barakat, I.; Dubois, P.; Jerome, R.; Teyssie, P.; Goethals, E. *J. Polym. Sci., Part A: Polym. Chem.* **1994**, *32*, 2099-110.
- (22) Stridsberg, K.; Ryner, M.; Albertsson, A.-C. *Macromolecules* **2000**, *33*, 2862-2869.
- (23) Yin, M.; Baker, G. L. *Macromolecules* **1999**, *32*, 7711-7718.
- (24) Lim, H.; Lee, Y.; Han, S.; Cho, J.; Kim, K.-J. *J. Vac. Sci. Technol., A* **2001**, *19*, 1490-1496.
- (25) Frutos, A. G.; Brockman, J. M.; Corn, R. M. *Langmuir* **2000**, *16*, 2192-2197.
- (26) Duda, A.; Penczek, S. *Macromolecules* **1990**, *23*, 1636-9.
- (27) Majerska, K.; Duda, A.; Penczek, S. *Macromol. Rapid Commun.* **2000**, *21*, 1327-1332.

- (28) Nishida, H.; Yamashita, M.; Endo, T.; Tokiwa, Y. *Macromolecules* **2000**, *33*, 6982-6986.
- (29) Siparsky, G. L.; Voorhees, K. J.; Miao, F. *J. Environ. Polym. Degrad.* **1998**, *6*, 31-41.
- (30) Porter, M. D.; Bright, T. B.; Allara, D. L.; Chidsey, C. E. D. *J. Am. Chem. Soc.* **1987**, *109*, 3559-68.

## Chapter 6. Experimental

### I. General Details

#### I-1. Materials

THF (Aldrich, 99%) was distilled from calcium hydride followed by a second distillation from sodium/benzophenone ketyl. Acetonitrile (Merck, HPLC grade) was passed through an activated basic alumina column, and fractionally distilled over calcium hydride. Triethylamine (Aldrich, 99.5%) was distilled from calcium hydride under an argon atmosphere at reduced pressure. Methyl acrylate (MA) (Aldrich, 99%) and methyl methacrylate (MMA) (Aldrich, 99%) were distilled from powdered KOH under ambient pressure. 2-Hydroxyethyl methacrylate (HEMA) (Aldrich, 97%) was passed through basic alumina columns twice to remove inhibitor. After purification, all solvents and monomers were transferred to Schlenk flasks, de-gassed using three freeze-pump-thaw cycles and then transferred into a drybox. Tris[2-(dimethylamino)ethyl]amine<sup>1</sup> (Me<sub>6</sub>TREN) and 4,4'-di-*n*-nonyl-2,2'-bipyridine<sup>2</sup> (dnNbp) were prepared by literature procedures with some modification. 11-Mercapto-1-undecanol (MUD) (Aldrich, 97%), 2-bromopropionyl bromide (Aldrich, 97%), Cu(I)Br (Aldrich, 99.999%), Cu(I)Cl (Aldrich, 99.999%), and Cu(II)Br<sub>2</sub> (Aldrich, 99.999%) were used as received.

#### I-2. Synthesis of Me<sub>6</sub>TREN

A solution of formaldehyde (43.37 g of a 37% solution in water, 0.534 mol of formaldehyde) was placed in a 250 mL round-bottomed flask with an attached water

condenser. The solution was cooled in an ice-water bath, and tris(2-aminoethyl)amine (Aldrich, 96%, 9.77 g, 0.067 mol) was added drop-wise to the formaldehyde solution. Some solid material formed during the addition. Following the drop-wise addition of formic acid (88 %) (69.88 g, 1.37 mol), the solution was heated with a heating mantle and refluxed for 12 hrs. The evolution of CO<sub>2</sub> gas was good evidence for the formation of the imine intermediate. The reaction mixture was cooled to room temperature and HCl (26.7 mL) was added to form the HCl salt of Me<sub>6</sub>TREN. Removal of the solvent under vacuum gave 47.4 g of a yellow solid. The solids were dissolved in de-ionized water and the pH of the solution was adjusted to ~12 with aqueous KOH. The top layer was extracted with diethyl ether (2×100 mL) and the combined organic layers were dried over Na<sub>2</sub>SO<sub>4</sub> and KOH pellets. Removal of the ether gave an oily product (14.56 g), which was purified by vacuum distillation (68–69 °C; 60 mmHg) to give 13.2 g (86 %) of Me<sub>6</sub>TREN. <sup>1</sup>H NMR (300 MHz, CDCl<sub>3</sub>) δ 2.53-2.60 (m, 6H), 2.30-2.37 (m, 6H), 1.80 (s, 18H). <sup>13</sup>C NMR δ 57.4, 53.1, 46.0. GC-MS m/z = 172, 72, 58.

### I-3. Synthesis of dnNbpy

Dry THF (85 mL) and dry diisopropylamine (9.20 mL, 65.1 mmol) were placed in a 500 mL round-bottomed flask under a flow of Ar. The mixture was cooled to -78 °C in a dry ice-acetone bath, and *n*-BuLi (24.8 mL of a 2.5 M solution in hexanes, 62.0 mmol) was added drop-wise. After 15 min, the bath was removed and the solution was allowed to warm to 0 °C. The reaction mixture again was cooled to -78 °C, and then a solution of 4,4'-dimethyl-2,2'-dipyridyl (5.00 g, 27.1 mmol) in THF (120 mL) was slowly added via a cannula. After stirring the mixture overnight, 1-bromooctane (15.8 g, 81.9 mmol) was

added and the reaction mixture was allowed to warm to room temperature. The solution was then poured into cold brine (250 mL), extracted with EtOAc (2×100 mL), and the combined organic layers were dried over Na<sub>2</sub>SO<sub>4</sub>. Removal of the solvent gave 15.8 g of crude product, which was purified by recrystallization from CH<sub>3</sub>CN/EtOH (1:1) to give 10.2 g of dnNbpy (92 % yield). <sup>1</sup>H NMR (300 MHz, CDCl<sub>3</sub>) δ 8.55 (d, 1H), 8.11 (s, 1H), 7.12 (m, 1H), 2.65 (t, 2H), 1.64 (quintet, 2H), 1.24 (m, 12H), 0.92 (t, 3H). <sup>13</sup>C NMR δ 148.9, 124.1, 121.6, 35.6, 32.2, 30.8, 29.5, 29.4, 29.30, 29.27, 22.8, 14.2.

#### **I-4. Analytical Methods**

Reflectance FTIR spectroscopy was performed using a Nicolet Magna-IR 560 spectrometer containing a PIKE grazing angle (80°) attachment. Ellipsometric measurements on polymer films were obtained with a rotating analyzer spectroscopic ellipsometer (model M-44; J.A. Woollam) at a 75° angle of incidence. Polymer molecular weights were measured using two PLgel 10μ mixed-B columns and a PLgel 3μ mixed-E column in series, and a Waters R410 differential refractometer detector. THF was used as the eluent at a flow rate of 1 mL/min at 35 °C, and monodisperse poly(methyl methacrylate) standards (Polysciences, Inc.) were used to calibrate the molecular weights. The molecular weights of PMMA standards were 350,000, 127,000, 30,000, and 6,000 g/mol.

## **II. Kinetic Studies of ATRP**

### **II-1. General Procedures for Surface-initiated Polymerization**

The preparation of monomer solutions, polymerization reactions, and the initial washing steps for surface polymerizations were done in a drybox filled with helium. To increase the solubility of the Cu(II)Br<sub>2</sub>/ligand complex, monomer (methyl acrylate (MA) and methyl methacrylate) solutions were prepared in 1:1 (v/v) CH<sub>3</sub>CN/THF. Polymerizations designed to investigate the dependence of polymer growth on the concentration of Cu(II)Br<sub>2</sub> were run with different catalytic systems over a wide range of catalyst concentrations. For polymerizations with no added Cu(II)Br<sub>2</sub>, Cu(I)Br/Me<sub>6</sub>TREN (0.1 mM) was used as the catalyst. The catalytic system for polymerizations with added Cu(II)Br<sub>2</sub> was a mixture of Cu(I)Cl/Me<sub>6</sub>TREN (0.1 mM) and Cu(II)Br<sub>2</sub>/Me<sub>6</sub>TREN (0.03 mM). The surface-initiated polymerization of MA was run at Cu(I)Cl/Me<sub>6</sub>TREN = 40 mM, 2 mM, 0.1 mM, 5×10<sup>-3</sup> mM, 2.5×10<sup>-4</sup> mM, and so on. The monomer concentration (2M) and the ratio of Cu(II)Br<sub>2</sub> to Cu(I)Cl (0.3) were the same for all polymerizations, and all polymerizations were run at ambient temperature (~23 °C) inside a drybox. After polymerization, the surfaces of the samples were washed with a fresh mixture of solvent and THF, and then the ellipsometric thickness of the polymer film was measured at two different spots on the sample and averaged.

### **II-2. Preparation of Monomer/Catalyst Solution**

A 40 mM catalyst solution was prepared by dissolving CuCl (0.0396 g, 0.4 mmol) and CuBr<sub>2</sub> (0.0268 g, 0.12 mmol) in 5 mL of a 1:1 mixture of CH<sub>3</sub>CN/THF. Other

catalyst solutions were prepared by dilution. MMA (2.0 g, 0.02 mol) was added to each catalyst solution (5 mL) and then mixed solvent was added to make the total volume 10 mL. 2M MA solutions were prepared by adding MA (1.72 g, 0.02 mol) to the catalyst solution and diluting to 10 mL. After the addition of each reactant, the reaction vials were swirled vigorously to give homogeneous solutions.

### II-3. Polymerization for Kinetic Study

MA and MMA were polymerized from initiator-immobilized surfaces using five different concentrations of Cu(I)Cl/Me<sub>6</sub>TREN. In each reaction, the ratio of Cu(II) to Cu(I) was 0.3. For polymerizations run at a catalyst concentration of 40 mM, 5 samples were immersed into the same reaction vial and samples were taken out at 30 min, 1 hr, 2hr, 4 hr, and 8 hr. To avoid scratching the surface of the films, samples were stacked in the vial as shown in **Figure 6.1** to prevent the gold face of the samples from touching. After removing the sample from the reaction vial, the surface was washed sequentially in 6 vials of fresh solvent. The first 3 vials contained 1:1 mixtures of CH<sub>3</sub>CN/THF and the last 3 vials contained THF. The samples were transferred from vial to vial quickly to avoid drying of the surface. After the last washing step, the surface was allowed to dry. The samples were removed from the dry box and the sample surfaces were rinsed with copious amounts of EtOAc, EtOH, and de-ionized water, and then were dried under a flow of N<sub>2</sub>. Using the same procedure, polymerizations were run at Cu(I)Cl/Me<sub>6</sub>TREN concentrations of 2 mM, 0.1 mM, 5×10<sup>-3</sup> mM, and 2.5×10<sup>-4</sup> mM.



**Figure 6.1.** Digital images of five stacked initiator-immobilized samples in a reaction vial. Images in this dissertation are presented in color.

#### **II-4. Solution Polymerization Procedures**

Three solutions were prepared for solution phase ATRP of MMA: a 4.6 M solution of MMA, a 4.8 mM solution of Cu(I)Br/Me<sub>6</sub>TREN, and a 1.6 mM solution of Cu(II)Br<sub>2</sub>/2 equivalents of dnNbpy in 1:1 (v/v) CH<sub>3</sub>CN:THF. The starting time for polymerizations was defined as the time when ethyl 2-bromoisobutyrate, the initiator, was transferred via cannula into a Schlenk flask containing the monomer and catalyst. After mixing, the concentration of the initiator was 23 mM. The polymerization reaction was stirred vigorously at 25 °C, and small samples (~2 mL) were removed using a syringe to measure the conversion from monomer to polymer. The samples were weighed and filtered through a basic alumina column to removing the copper catalyst and ligand, thus quenching the polymerization reaction. The column was rinsed 5 times with THF,

and then the combined solutions were evaporated to dryness under reduced pressure. After drying under vacuum, the mass of the recovered polymer was used to calculate the conversion, and the molecular weight and polydispersity were measured by GPC.

## **II-5. Polymerization With or Without Stirring**

To carry out ATRP from surface initiators with stirring, a glass reactor with 8 slots was designed to hold gold-coated silicon wafers. **Figure 3.9** shows the reaction vessel loaded with 8 samples and a magnetic stirring bar at the center. To avoid contact between the magnetic stirring bar and the samples, a glass O-ring was inserted between the stirring bar and the sample holder. The O-ring ensures smooth stirring and prevents damage to the gold surfaces. The reaction solvent was 1:1 (v/v) CH<sub>3</sub>CN/THF containing MMA (2M), Cu(I)Br/Me<sub>6</sub>TREN (2 mM), and Cu(II)Br<sub>2</sub>/2dnNbpy (0.6 mM). Polymerizations were run at 23 °C in a drybox. For kinetic studies, samples were regularly taken out, washed with the co-solvent mixture and THF, and then the ellipsometric thicknesses of polymer films were measured. A duplicate set of surface-initiated ATRP was run under the same reaction conditions as described above, but this time with no stirring. The samples were treated and measured in the same way.

## **II-6. Simulation of Polymer Brush Growth at Different Catalyst Concentration**

Microsoft Excel was used to simulate the growth of polymers from surfaces. Each term in equation 3 (see Chapter 3) was simulated from time = 0 seconds to approximately eight hours. Since some simulations required over three billion rows in the

spreadsheet, a Visual Basic macro was used to collect every 65532<sup>nd</sup> data point for graphing, and then restart the calculation. The simulation required the input of 5 variables:  $k_a$ ,  $k_d$ ,  $k_t$ , initiator concentration, and  $dt$ , the time between iterations.  $k_a$ ,  $k_d$ , and  $k_t$  were taken from values reported in the literature.<sup>3</sup> The initiator concentration was chosen to be 2 mol/L. The simulations included the range of Cu(I)/Cu(II) concentrations used for polymer film growth. The value of  $dt$  used in each simulation depended upon the Cu(I)/Cu(II) system that was being simulated, and was selected to allow the smallest number of iterations without causing the simulation to oscillate out of control. The radical concentration at the conclusion of each step was multiplied by  $dt$ , and then summed over the whole polymerization time. The radical concentration versus time was plotted at five different catalyst concentrations.

### **III. Synthesis of Triblock Copolymer Brushes**

#### **III-1. Preparation of Substrate Immobilized with Initiator**

Gold-coated Si wafers (200 nm of gold sputtered on 20 nm of Cr on Si (100) wafers) were cleaned in a UV/O<sub>3</sub> chamber for 15 min, immersed in de-ionized water for 15 min, and dried under a flow of N<sub>2</sub> just before use. A SAM of MUD was obtained by immersing the gold-coated Si substrate in a 1 mM MUD solution for 1 day, and the MUD SAM was washed with copious amounts of ethanol and de-ionized water, and dried under N<sub>2</sub>. The ellipsometric thickness of the MUD layer was  $12 \pm 1$  Å. To produce the initiator-anchored surface, **1** (**Scheme 3.1**), the MUD SAM was immersed for ~10 sec in 5 mL of 0.12 M triethylamine in dry THF at ~0 °C after which 5 mL of 0.1 M 2-bromopropionyl

bromide (2-BPB) in dry THF was added drop-wise while gently agitating the triethylamine solution. During the addition of 2-BPB, the reaction vial was tilted at different angles to ensure that the reaction surface was well exposed to the incoming 2-BPB solution. This initiator-immobilization reaction was carried out in a helium-filled drybox. Upon addition of 2-BPB, a white precipitate formed immediately, which presumably was triethylamine hydrobromide. After the reaction (~3 min), the surface was washed with fresh THF several times and allowed to dry. Once the substrate was taken out of the drybox, it was rinsed sequentially with EtOAc, EtOH, and de-ionized water, and dried under N<sub>2</sub>. Initiator immobilization was apparent from the appearance of a carbonyl peak at 1743 cm<sup>-1</sup> in the reflectance FTIR spectrum of this film.

### III-2. Procedures for Block Formation

The preparation of monomer solutions, polymerizations, and Q & R procedures were done in a drybox filled with helium. 2M solutions of MA, MMA, and HEMA were prepared in 1:1 (v/v) CH<sub>3</sub>CN:THF. Each solution contained monomer, Cu(I)Br/Me<sub>6</sub>TREN (2 mM), and Cu(II)Br<sub>2</sub>/2(dnNbpy) (0.6mM). Each block of the polymer brush was synthesized by dipping substrates 1, 2, or 3 (Scheme 4.2) in the appropriate monomer solution, and then quenching the polymerization as described below. Polymerizations were run at 25 °C for the first and second blocks (PMA and PMMA) and at 40 °C for the third block (PHEMA), and the reaction times for formation of each block were 20 min, 40 min, and 5 hrs, respectively. After polymerization, the substrate was removed from the solution and sequentially immersed in three vials of CH<sub>3</sub>CN-THF (1:1) and three vials of THF. This procedure avoids drying of the film and

consequent deposition of solids that are difficult to remove from the substrate surface. For the synthesis of heptablock copolymers, the polymerizations were carried out in a 2M solution of monomer in 1:1 CH<sub>3</sub>CN-THF, 1 mM CuBr/Me<sub>6</sub>TREN, and 0.3 mM of CuBr<sub>2</sub>/2dnNbpy at 24 °C. To compare Cu(II)Br<sub>2</sub> quenching with solvent washing, polymerizations were either quenched or solvent rinsed after 15, 25, 40, 60, 90, and 150 min of reaction time and then re-initiated.

### **III-3. Quenching Procedure**

To quench polymerizations, 3 vials of 0.02 M Cu(II)Br<sub>2</sub>/2(dnNbpy) in 1:1 CH<sub>3</sub>CN:THF were prepared, and substrates were transferred sequentially into the vials. The substrates were then washed in 3 vials containing the cosolvent to remove Cu(II)Br<sub>2</sub> from the surface. After examination by reflectance FTIR spectroscopy, substrates were immersed in a solution containing another monomer/catalyst mixture to form the next block. When simple solvent rinsing was used rather than Cu(II)Br<sub>2</sub> quenching, the substrates were sequentially immersed in six separate vials containing CH<sub>3</sub>CN:THF.

### **III-4. Detachment of Polymer Brushes from Gold Surfaces**

Polymer brushes were detached from gold surfaces by immersing the polymer-coated substrates in a 4 mM solution of I<sub>2</sub> in CH<sub>2</sub>Cl<sub>2</sub> for 15h at room temperature. After rinsing the surface with fresh CH<sub>2</sub>Cl<sub>2</sub> and drying under a flow of N<sub>2</sub>, the reflectance FTIR spectrum was measured to confirm that the polymer chains were detached from the surface. The initial CH<sub>2</sub>Cl<sub>2</sub> solution was collected and transferred to a pear-shaped flask

that was connected to a closed vacuum line. The solution was frozen in liquid N<sub>2</sub>, and after opening the vacuum line, the bath was withdrawn, and the solvent was slowly removed under reduced pressure. After evaporation of CH<sub>2</sub>Cl<sub>2</sub>, a purplish thin coating remained on the inside of the flask. The flask was kept at 60 ± 10 °C in an oil bath and as I<sub>2</sub> was removed by sublimation under vacuum, the thin film coating on the flask walls became pale yellow. For GPC measurements, all of the remaining material in the flask was dissolved in ~150 μL of THF and injected into the instrument. Assuming full recovery of the polymer from a 380 Å-thick PMMA film on ~8 cm<sup>2</sup> of gold surface, the concentration of detached polymer brushes in 150 μL of THF should have been ~0.2 mg/mL.

#### **IV. Synthesis of Biodegradable Nanometer Thick Films of PLA**

##### **IV-1. Preparation of Monomer Solution and Substrates**

A saturated solution of lactide was prepared in a drybox by stirring an excess of lactide in toluene (120 mL) at room temperature for one hour. The homogeneous solution was decanted from undissolved lactide, and the concentration of the lactide solution was determined by gravimetry to be ~0.13 M. Sn(Oct)<sub>2</sub> catalyst (0.0844 g) was added to the lactide solution (100 mL) to give a catalyst concentration of ~2.1 mM. PHEMA substrate **2** (Scheme 5.1), was synthesized by surface-initiated atom transfer radical polymerization. To prepare monomer solutions, Cu(I)Br (4.5 mg), Cu(II)Br<sub>2</sub> (1.6 mg), and Me<sub>6</sub>TREN (8.9 mg) were dissolved in 5 mL of CH<sub>3</sub>CN:THF (5:1, v/v) in a drybox. HEMA (15 mL, 0.123 mol) was added and the solution was diluted to 35 mL with the

cosolvent. The concentrations of each component were: Cu(I)Br/Me<sub>6</sub>TREN (0.9 mM), Cu(II)Br<sub>2</sub>/Me<sub>6</sub>TREN (0.2 mM), and HEMA (3.5 M). The initiator-immobilized substrates were immersed in the monomer solution and polymerized for one day at 40 °C. After polymerization, the samples were taken out of the monomer solution and immersed in anhydrous DMF to wash out catalyst and monomers. The sample surface was rinsed with EtOAc, EtOH, and de-ionized water, and then dried under a flow of N<sub>2</sub>. The PHEMA films were characterized by ellipsometry and surface reflectance FT-IR.

#### **IV-2. Ring-opening Polymerization from PHEMA Surfaces**

In a helium-filled drybox, PHEMA substrates, **2**, were immersed in the lactide (0.13 M) and Sn(Oct)<sub>2</sub> catalyst (2.1 mM) solution. Silanized glass vials (15 mL) with silicon rubber caps were used as reaction vessels to avoid polymerization from surface silanol groups. The vials were suspended in an oil bath from copper wires, and a hot plate was used to heat the bath to 95 °C. Vials were removed from the oil bath at various intervals, and the samples were removed from the vial and were sequentially immersed in a series of vials containing toluene, ethyl acetate, ethanol, and de-ionized water to clean the surface. The surface was dried under a flow of N<sub>2</sub> and characterized by reflectance FTIR and ellipsometry.

Acetylated PHEMA samples were prepared by reacting PHEMA with acetyl chloride in dry THF. A PHEMA substrate was placed in a 20 mL glass vial and 8 mL of dry THF were added. While the vial was gently shaken, 2 mL of acetyl chloride was added drop-wise. After completion of the addition of acetyl chloride, the surface was

washed with fresh THF and the process was repeated twice to ensure maximum blocking of the hydroxy groups on PHEMA side chains. The acetylated PHEMA sample was used as a substrate for ROP of lactide as describe above.

### **IV-3. Hydrolytic Degradation of PLA film**

To study the hydrolytic degradation of PHEMA-*g*-PLA on gold, substrates were immersed in phosphate buffer solution (pH 7.40) at  $55\pm 0.1$  °C. At predetermined times, the sample was removed from the buffer, washed thoroughly with de-ionized water, and dried under a flow of N<sub>2</sub>. The sample was characterized by surface reflectance FTIR and optical microscopy, and then the sample was returned to the proper buffer solution. We ran two sets of hydrolytic degradation experiments to test for an autocatalytic effect in the degradation. In the first, a PHEMA (174 nm)-*g*-PLA (464 nm) substrate was degraded in the same buffer solution throughout the degradation process. The second used a PHEMA (174 nm)-*g*-PLA (488 nm) substrate, and the buffer solution was replaced every 2 days. The degradation rate was measured by surface reflectance FT-IR to monitor the decrease of the PLA carbonyl peak with time.

### **IV-4. Observation of PHEMA-*g*-PLA Films During Hydrolytic Degradation**

Changes in surface roughness of the polymer films during the hydrolytic degradation of PHEMA-*g*-PLA were observed using a Nikon Optiphot2-POL polarizing optical microscope equipped with a video camera. Digital images of the dried polymer

surface and changes in the surface morphology during the drying process were captured as graphic files.

## V. References

- (1) Ciampolini, M.; Nardi, N. *Inorg. Chem.* **1966**, *5*, 41-4.
- (2) Matyjaszewski, K.; Patten, T. E.; Xia, J. *J. Am. Chem. Soc.* **1997**, *119*, 674-680.
- (3) Matyjaszewski, K.; Paik, H.-j.; Zhou, P.; Diamanti, S. J. *Macromolecules* **2001**, *34*, 5125-5131.

MICHIGAN STATE UNIVERSITY LIBRARIES



3 1293 02429 2413